Lawrence Berkeley National Laboratory

LBL Publications

Title

Building Reconfigurable Devices Using Complex Liquid—Fluid Interfaces

Authors

Forth, Joe

Kim, Paul Y

Xie, Ganhua

et al.

Peer reviewed

Building Reconfigurable Devices Using Complex Liquid–Fluid Interfaces

Joe Forth, Paul Y. Kim, Ganhua Xie, Xubo Liu, Brett A. Helms, and Thomas P. Russell*

Liquid–fluid interfaces provide a platform both for structuring liquids into complex shapes and assembling dimensionally confined, functional nanomaterials. Historically, attention in this area has focused on simple emulsions and foams, in which surface-active materials such as surfactants or colloids stabilize structures against coalescence and alter the mechanical properties of the interface. In recent decades, however, a growing body of work has begun to demonstrate the full potential of the assembly of nanomaterials at liquid–fluid interfaces to generate functionally advanced, biomimetic systems. Here, a broad overview is given, from fundamentals to applications, of the use of liquid–fluid interfaces to generate complex, all-liquid devices with a myriad of potential applications.

1. Introduction

The broken symmetry of a liquid–fluid interface is an ideal plat- form for the assembly and synthesis of dimensionally confined, functional nanomaterials with potentially useful properties, e.g., electronic, plasmonic, and magnetic. The individual and collective behavior of the assembled nanomaterials, in turn,

imparts novel mechanical and functional properties to the macroscopic interface itself. These properties include size- and charge-selective pathways for molecules and particulates, shear and compressive moduli, and selective binding and reaction sites. Complex interfaces can then be used to generate complex, mac- roscopic, all-liquid materials with very high surface areas that have unique prop- erties, such as compartmentalization, communication between compartments, and the ability to move and reconfigure. With the rapid growth in the study of complex materials made from inter- facially structured liquids, there is a need to review the field from the funda-

mental aspects, including anisotropic surface stresses and the behavior of nanoparticles (NPs) at interfaces, to applications, such as flow-through chemical reaction vessels and reconfig- urable 3D-printed materials, highlighting significant recent progress and open questions.

Many of these topics are covered individually in several, separate reviews of varying ages. The fundamental physics of particles at the liquid–liquid interface is already discussed in-depth in reviews and textbooks.[1,2] Likewise, the

and mechanics of complex interfaces has been discussed extensively in several recent reviews.[3–5] Thijssen and Vermant recently produced a review dedicated to the rheology of particles at liquid–fluid interfaces with an emphasis on micrometer-sized particles and bijel formation.[6] Shi and Russell focused specifically on nanomaterial assembly at liquid–liquid interfaces.[7] From an applications perspec- tive, Lach et al. produced an excellent materials-oriented review dedicated solely to droplet-based systems.[8] Our aim here is to show the connections between these fields, from the nanoscale to the macroscale and from fundamentals to applications.

In Section 2, we develop a coherent understanding of how the surface tension of a liquid–fluid interface can be used to assemble nanomaterials. We briefly discuss the interaction potentials between nanomaterials adsorbed at interfaces, paying particular attention to effects that are specific to the small size and low binding energy of NPs. Most importantly, we discuss the emerging field of in situ characterization of

rheology

Dr. J. Forth, Dr. P. Y. Kim, Dr. G. Xie, X. Liu, Dr. B. A. Helms, Prof. T. P. Russell
Materials Sciences Division
Lawrence Berkeley National Laboratory
1 Cyclotron Road, Berkeley, CA
94720, USA E-mail:
russell@mail.pse.umass.edu

Dr. G. Xie, Prof. T. P. Russell
Polymer Science and Engineering
Department University of Massachusetts
120 Governors Drive, Conte Center for Polymer
Research, Amherst, MA 01003, USA

X. Liu, Prof. T. P. Russell
Beijing Advanced Innovation Center for Soft
Matter Science and Engineering
Beijing University of Chemical
Technology Beijing 100029, China

Dr. B. A. Helms
The Molecular Foundry
Lawrence Berkeley National
Laboratory Berkeley, CA 94720,
USA

Prof. T. P. Russell
WPI—Advanced Institute for Materials Research
(WPI-AIMR) Tohoku University
2-1-1 Katahira, Aoba, Sendai 980-8577, Japan

nanomaterials at liquid–fluid interfaces.

In Section 3, we discuss how the collective behavior of nanomaterials at interfaces gives rise to changes in macroscopic observables. At the simplest level, this means a change in surface tension. We discuss how irreversibly

adsorbed interfacial assemblies give rise to anisotropic surface stresses that can be used to structure all-liquid systems into complex shapes. NPs provide a natural model system to understand the fundamental principles, but recent work on proteins and interfacially assembled polyelectrolyte coacervates prove both instructive on a fun- damental level as well as interesting from a materials sci- ence perspective. In Section 4, we discuss recent progress on the quantitative description of complex interfaces and experimental techniques that allow the mechanical proper- ties and rheology of viscoelastic interfaces to be directly and indirectly probed.

Section 5 affords an applications-oriented view of how com- plex interfaces can be used to construct simple devices, such as flow-through reactors and growth media for biological organisms. We discuss how self- assembly at interfaces due to macroscopic phase separation can be exploited in all-aqueous and all- nonaqueous systems. In this section, and throughout this Review, we discuss the wealth of different materials that can be assembled at liquid–fluid interfaces, from proteins, to polyelectrolyte–polyelectrolyte complexes, to nanocrystals and colloidal particles.

Finally, in Section 6, we look at stimulus-responsive, func- tional materials that can be assembled at the liquid–liquid interface and the complex, reconfigurable d evices t hat t hese interfaces can be used to build. We cover recent successes in generating highly controllable, reconfigurable, all-liquid struc- tures using molding and 3D printing. We show how complex interfaces can be used to drive preprogrammed self-assembly of droplet- based materials. Finally, we discuss how function- alizing liquid–liquid interfaces with components that are either derived from or inspired by biological materials, such as transmembrane pores, allows for communication between compartments in all-liquid structures, giving rise to the con- duction of ionic current and internal flows that drive macro- scopic reconfiguration o f t he s tructure i n a p redetermined manner.

We conclude by arguing that soft, interfacially structured, all-liquid systems hold enormous potential for a new generation of materials, with uses in chemical synthesis, chemical separations, and the design of a new generation of soft, reconfigurable devices. The key feature of these systems is the ease with which they can adapt and respond to changes in their external environment. Most important is the facile tunability of the energy scales governing the behavior of the systems and the ability to alter the composition and proper- ties of complex interfaces in situ. One of the most promising developments in this area is the ability to encapsulate active and living matter within an interfacially structured system. Further development of this concept would allow for the crea- tion of biomimetic, active, macroscopic structures that drive themselves from equilibrium and that can respond to, and even alter, their surrounding environment. Development of these concepts requires further fundamental understanding of the physics of complex interfaces and interfacial assemblies, as well as the development of new functional nanomaterials that draw inspiration from both synthetic chemistry and biology, enabling us to fully harness the potential of interfacially struc- tured, all-liquid

systems.

2. Assembly, Dynamics, and In Situ Characterization of Nanomaterials at the Liquid–Fluid Interface

2.1. Basic Principles

The interface between two liquids has an inherent surface stress or surface tension, γ, with corresponding units of a spring constant (N m^{-1}) or energy per unit area (J m^{-2}). It has

two complementary, equivalent interpretations. First, surface tension is the force per unit length that acts tangentially to the interface at the contact line between two (or more) phases. A number of excellent pedagogical articles exist in the litera- ture to discuss this rather unintuitive idea.[9–11] Second, surface tension is the free energy cost, G_γ, associated with creating a unit of contact area, A, between two immiscible liquids,[12-15] and can be defined both by its product with its thermodynamic conjugate variable, A, and as a partial derivative

$$G_\gamma = \gamma A = \left.\frac{\partial G}{\partial A}\right|_{T,V,N} \tag{1}$$

The energetic cost due to the existence of a liquid–liquid interface, G_γ, means there is an associated drive to minimize the amount of surface area between two liquids. Systems of immis- cible liquids therefore tend to adopt a geometry that minimizes the surface area to volume ratio, i.e., a sphere, while multiple, small spherical droplets will coalesce into larger droplets for the same reason. The interfacial tension of the system can also be reduced by the adsorption of a range of materials to the interface, resulting in a reduction in the amount of ener- getically expensive oil–water interface.[2,16] It is this mechanism that is the key driving force behind the assembly of almost all nanomaterials at the liquid–fluid interface. The simplest case of this is a spherical particle adsorbed at a liquid–liquid interface (**Figure 1**).

The reduction in interfacial energy associated with screening the oil–water interface, ΔE, by a single NP of radius, r, can be estimated by considering geometry and surface tension alone. For particles with homogeneous surface chemistry[1,18]
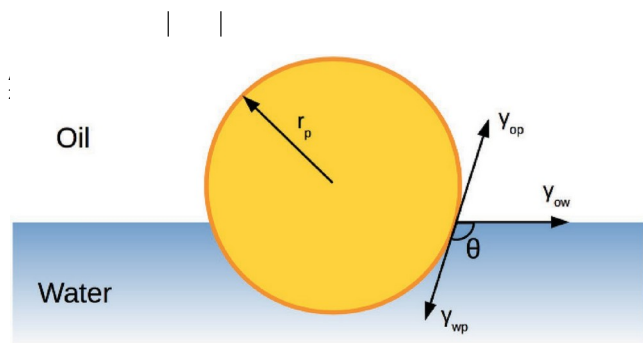
where γ_{ow} is the oil–water surface tension, and θ is the contact angle at the three-phase contact line (drawn through the polar phase by convention). θ can also be derived pictorially by performing a force balance on the three interfacial tensions drawn in Figure 1, yielding

$$\cos\theta = \frac{\gamma_{op} - \gamma_{wp}}{\gamma_{ow}} \tag{3}$$

where γ_{op} and γ_{wp} are the oil–particle and water–particle surface tensions, respectively. Typical values of ΔE vary from 1 to 10 kT for nanometer-sized particles[19,20] up to 10^6 kT for micrometer-sized particles.[12] The quadratic dependence of ΔE upon particle size means that as r increases, ΔE increases rap- idly and micrometer-sized particles can be treated as irrevers- ibly adsorbed, even at interfaces with extremely low surface tensions.[21,22] Note that Equations (2) and (3) hold for particles at the interface of any combination of immiscible liquids and fluids that have a well-defined surface tension, γ. A number

of modifications to Equation (2) can be made to account for particles having different geometries, surface roughness, and heterogeneous surface chemistries,[1,23] or the effects of line tension,[24–26] but the underlying quadratic dependence on particle size remains the same.

2.2. Interactions between NPs at the Liquid–Fluid Interface

Ensembles of particles that are adsorbed to the liquid–fluid interface behave somewhat like a 2D system that is distinct from the bulk, with their behavior governed by the areal density and interaction potentials of the particles. Interactions between particles adsorbed at a liquid–fluid interface differ from the interactions in a bulk liquid. The particles are confined to a fluc- tuating surface separating two phases that may markedly differ in density, permittivity, and ionic strength. This discontinuity in phase properties gives rise to effects intertwined with several physicochemical aspects, e.g., particle size, shape, wettability, electrical potential, and surface chemistry, operating synergis- tically in a way that can make them difficult to quantify.[27-31] These interactions are extensively covered, often quantitatively,

in a number of reviews and textbooks.[1,27,30–33] As such, we give a qualitative overview of the interactions between NPs at liquid–fluid interfaces, with an emphasis on phenomenology, self-assembly, and in situ characterization.

2.2.1. Electrostatic Dipole–Dipole Interactions between Particles at Liquid–Fluid Interfaces

Figure 1. A simplified picture of the adsorption of a NP of radius, r_p, to a liquid–liquid interface with contact angle, θ. This adsorption reduces the interfacial energy per unit area, $\gamma '$, of the system. Reproduced with permission.[17]

To stabilize particles in aqueous solutions, NP surfaces are often decorated with charged groups that dissociate under particular conditions, such as above or below a critical pH. The typical den- sity of these surface charges ranges from 0.1 to 1 e nm^{-2}. Ions in the polar phase that bear the opposite charge are attracted to the charged surface groups and significantly reduce (or "renor- malize") the effective charge by surrounding the particles. At the liquid–fluid interface, this can lead to an asymmetric charge distribution and, hence, strong electrostatic dipoles
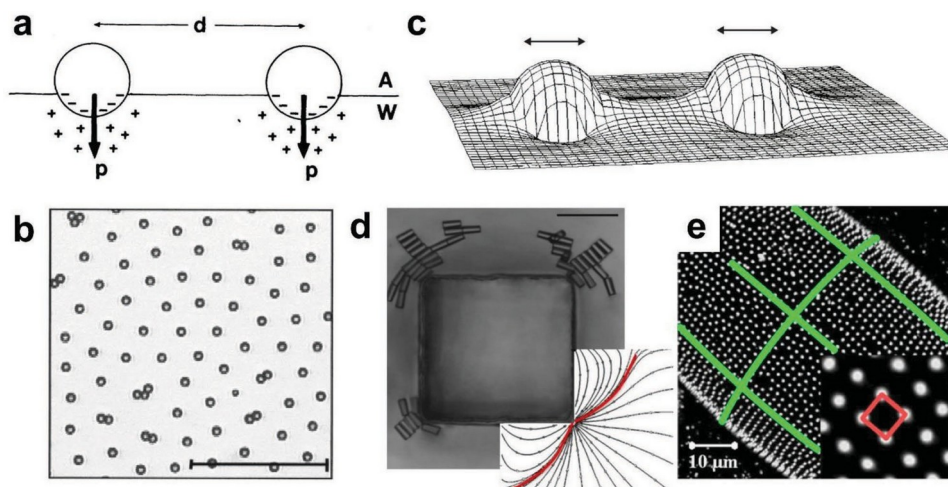
Figure 2. Interactions between particles attached to liquid–fluid interfaces. a) Dipole–dipole interactions between adsorbed particles due to asymmetric charge distributions near the surface of particles at interfaces. Reproduced with permission.[34] Copyright 1980, American Physical Society. b) Dipole–dipole interactions give rise to 2D colloidal crystals with large lattice spacings. Scale bar, 50 μm. Reproduced with permission.[36] Copyright 2000, American Chemical Society. c) Roughness or chemical inhomogeneities on the surface of a particle deform the liquid–fluid interface, resulting in capillary interactions. Reproduced with permission.[38] Copyright 2000, American Physical Society. d) Migration and assembly of rod-like particles by capillary interactions. Reproduced with permission.[39] Copyright 2011, The Authors. Published by the National Academy of Sciences.
e) Spherical microparticles arranged in a square lattice (characteristic of a quadrupolar potential) on a surface with differing principal radii of curvature. Reproduced with permission.[40] Copyright 2013, The Authors. Published by the National Academy of Sciences.

(**Figure 2**a). The resulting dipole–dipole interactions between adsorbed particles are strong and long-ranged, resulting in the formation of low-density, 2D colloidal crystals with lattice spacings as large as ten particle diameters (Figure 2b).[34]

While long-ranged, repulsive, dipole–dipole interactions between particles at interfaces are widely observed and conceptu- ally simple, the nature and origin of the dipole in some instances is complex and remains a source of controversy. The source of disagreement is what happens to charged groups on the non- polar (e.g., air or oil) side of the interface. Bare surface charges are very energetically expensive in media with a low dielectric constant and ion pairs in such media will, in principle, recom- bine to neutralize any bare charge. In the case of the air–water interface, the surface charges are apparently neutralized, and the system exhibits the expected behavior. For the case of particles at oil–water interfaces it remains an open question whether some charges may remain on the low-dielectric oil side.[27,35–37]

Several quantitative theories exist to describe the magnitude of the electrostatic dipole–dipole interactions that account for particle contact angle, surface charge density and location, and salt concentration in the aqueous phase. Pieranski was the first to connect crystallization of colloidal particles at the air–water interface with the formation of electrostatic dipole moments due to an asymmetric distribution of charge at the air–water–particle interface.[34] He further observed that, as the electric field prop- agates at least in part through the nonpolar side, the lower dielectric constant of the nonpolar side resulted in the electro- static interactions being extremely strong. Hurd built upon the work of Pieranski and Stillinger by developing a rigorous theory for the dipole–dipole interactions between two charged particles at an interface between fluids of different dielectric constants.[41,42] Danov and Krachelvsky derived an asymptotic expression of the electric dipole field near a colloidal particle.[43]

Frydel et al. showed that solving the nonlinear Poisson– Boltzmann equation results in a fundamentally different dependence of the effective dipole potential upon the surface charge density and Debye screening length.[44] A significant body of work also studies the various effects of changing ionic strength,[45] including ion-size-specific effects.[46] The effect of adding surfactant to the system, which can both neu- tralize charge groups and change the particle contact angle at the liquid–fluid interface has also been investigated.[47] In the simplest case, making the particles more hydrophilic, i.e., reducing the contact angle, or adding salt to the system reduces the strength of the repulsive interactions and causes particle aggregation.[48,49] There remain some disagreements over the finer points of the location of the charges and the exact scaling behavior of the particle pair-potential upon various quantities and the field remains a topic of active investigation.[50,51] Regard- less of these details, the fundamental observation that parti- cles adsorbed at liquid–fluid interfaces interact via long-ranged electrostatic dipole–dipole interactions remains valid.

2.2.2. Capillary Interactions between Adsorbed Particles

Deformation of the liquid–fluid interface is energetically expen- sive, and the system will tend to minimize any interfacial deformations. Liquid–fluid interfaces can be deformed by both particle attachment and the pinning of the droplet on a rough or textured substrate (Figure 2c). This produces a meniscus that mediates long-range particle–particle and particle–surface interactions, so-called "capillary interactions," that are a conse- quence of the thermodynamic drive for the system to minimize its surface area. Capillary interactions can propagate over distances much greater than particle size, producing directed

particle migration, the so-called Cheerios effect.[52] Under capil-lary interactions, particles at an interface attract or repel each other, reflecting the general principle that interfacially bound particles are driven up gradients of Gaussian interfacial cur-vature (Figure 2d).[53-56] As such, these interactions are absent with homogeneous isotropic particles, such as uniform spheres and disks, on an infinite planar liquid interface, i.e., one that is flat in the absence of particles, and only become significant due to anisotropy in the contact line around a particle's perimeter (Figure 2e).

On a planar interface, creation of a meniscus around an adsorbed isotropic particle requires that the particle impose a vertical force on the interface. This occurs, for example, when the particle and fluid densities are mismatched[57,58] or when the particle and interface are charged.[59,60] Even so, capillary inter-actions are negligible in the first situation if the particle is small, or in the second, if the electrostatic interactions are weak. Ver-tical forces can also arise from nonuniform particle wetting.[61] If the particle shape is not isotropic, the fluid–solid– liquid contact line distorts to satisfy the equilibrium contact angle condition, creating a nonuniform meniscus around the particle. A rod-like particle, for example, produces a meniscus of quadrupolar form, driving a collection of the particles to assemble variously into chains, loops, arrows, or orthogonal lattices.[39,53,54,62–68] For similar reasons, roughness or chemical inhomogeneities on the surface of a nonideal spherical particle can cause contact line undulations and directional interactions.[38,69] On curved inter-faces, both isotropic and anisotropic particles can be oriented in controlled directions and steered along predicted trajectories. Even slightly nonspherical (1% deviation from unity aspect ratio) particles can undergo dendritic aggregation because of nonuniform contact lines.[70]

2.2.3. NP-Specific Interactions at the Liquid–Fluid Interface

The previous two sections discussed two examples of interac- tions that are specific t o p articles a t i nterfaces a nd t hat h ave been historically investigated using particle sizes between
100 nm and 10 μm. Indeed, given that micrometer-sized particles can be studied optically, much of the fundamental physics of particle behaviors at the liquid–liquid interface has been obtained by adapting colloidal microparticles as a model system. However unique effects can be observed in NPs that arise from their nanoscopic size.

Several experiments have reported the formation of unusual 2D structures in systems of NPs adsorbed at liquid– fluid interfaces,[71,72] motivating new theories and micro- scopic models of NP interactions that go beyond traditional macroscopic considerations. NPs are weakly attached to the interface compared to microparticles, with adsorption ener- gies of 1–10^3 times thermal energy.[31] NPs are therefore more sensitive to thermal fluctuations,[73] and indeed the competi- tion between thermal fluctuation and interfacial energy leads to self-assembly that is dependent on particle size.[19] Further, by pinning or otherwise altering the thermally driven height fluc-tuations of the oil–water interface, NPs can be attracted to one another.[74,75] The adsorption of NPs also exhibits a dependence on the line tension,[76] which is the free energy cost associated

system can be obtained using ex situ methods. The characteristics of NP assemblies most often studied are their contact angle and their structure at the

with the presence of the three-phase contact line between the particle and the liquid–fluid interface. Line tension has been connected to NP interactions, but its effect is unknown and dif- ficult to measure.[31]

New phenomena can emerge if the particle size is reduced to the length scale of the interfacial region, i.e., ≈1 nm for an air–water interface, 4–6 Å for alkane–water interfaces, which contains high-energy solvent molecules.[77,78] Damodaran analyzed adsorption kinetics of proteins, in terms of formation of an interfacial protein solution and water displacement in the interfacial region, to understand protein binding and viscoe- lastic properties of adsorbed protein films.[78] The reduction in surface tension observed due to protein adsorption was attrib- uted to a decrease in the concentration of water (i.e., chemical potential) in the interfacial regions, which is more a function of protein size than lateral pressure generated by adsorbed molecules.

The interactions between NPs grafted with capping ligands or polymers can be dominated by the grafted layer, particularly when its thickness is comparable to the size of the NP core (**Figure 3**).[32] Molecular simulations predict that the conforma- tion of ligands grafted onto the NP surface can change upon adsorption to the interface due to the asymmetric environment surrounding the particles.[79–81] Yong characterized the adsorp- tion process, i.e., approaching and breaching of the interface, and subsequent change in conformation, of polymer-grafted NPs via molecular simulation.[82] They observed that grafted chains can undergo significant reconfiguration during adsorp- tion by spreading onto the interface to maximize the reduction in surface tension (Figure 3a–f), indirect evidence for which has also been seen experimentally.[83] The resulting particles exhibit a discoid or lens shape depending on the chemical prop- erties of the grafted layer. The interfacial behavior of polymer ligands can be tuned in situ by altering solvent properties, such as temperature and pH.[84] Soft particles composed of polymer gels have also been observed to deform upon adsorp- tion, where the extent of particle deformation at the interface is governed by a competition between particle elasticity and surface tension.[85–87] Through freeze–fracture shadow casting cryo-SEM, Geisel et al. observed spherical microgels stretched at the contact line, where particle diameters were much larger than those in the bulk (Figure 3g). This deformation of the par- ticles can increase adsorption energies by orders of magnitude relative to rigid particles. These particles form a 2D network of percolating aggregates with large voids at low surface coverage, reflecting the presence of attractive capillary forces between the particles (Figure 3h).[88–90]

2.3. Characterizing Static and Dynamic Properties of NPs at Interfaces

The challenges of optically observing NPs in situ mean that traditional methods of characterizing NPs are performed ex situ, requiring the sample be extensively manipulated before characterization. Under certain circumstances, however, useful information about the
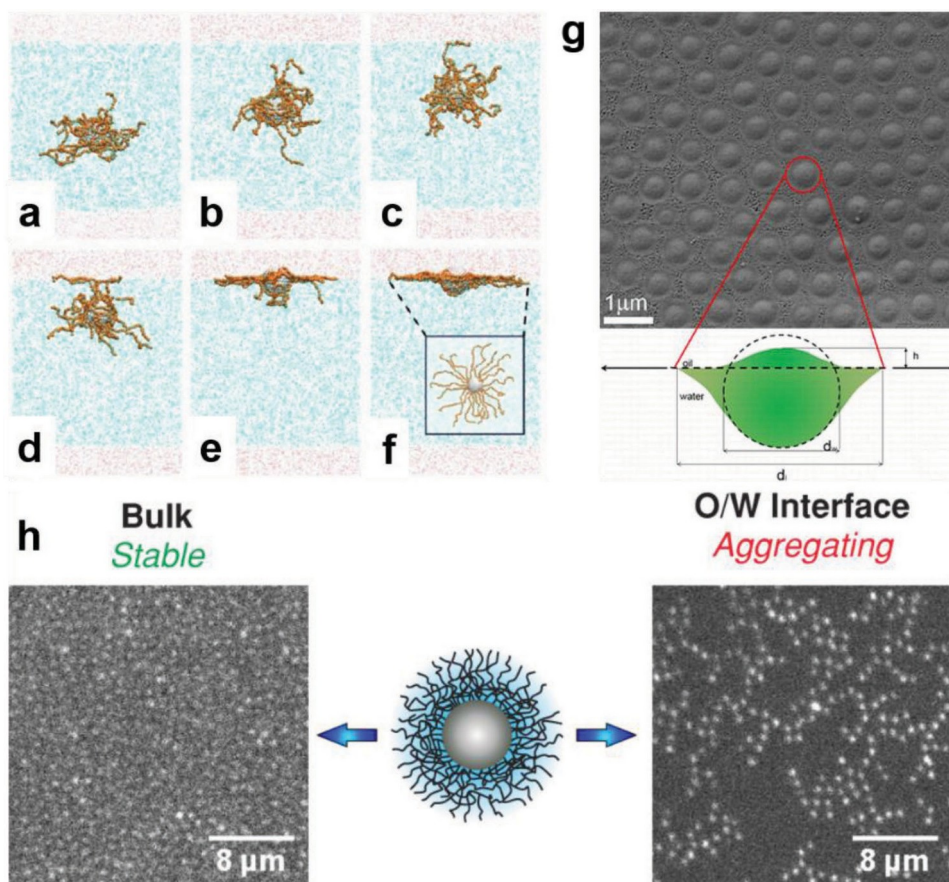
Figure 3. Reconfiguration and deformation of nanoparticles and their ligands at the liquid–fluid interface. a–f) Snapshots of adsorption simulation of a single NP grafted with hydrophilic polymer chains. Reproduced with permission.[82] Copyright 2015, American Chemical Society. g) Deformation of polymeric hydrogel particles at the liquid–fluid interface observed by freeze–fracture shadow casting cryo-SEM. Reproduced with permission.[87] Copyright 2012, American Chemical Society. h) Deformation of particles adsorbed to the liquid–fluid interface leads to strong capillary interactions, causing their aggregation. Reproduced with permission.[90] Copyright 2018, American Chemical Society.

interface. The assembly of NP monolayers and the resulting structure has traditionally been investigated ex situ by using electron microscopy on Langmuir–Blodgett films transferred to a solid substrate at constant surface pressure. However, this method cannot be used at low areal densities because the struc- tures can be significantly altered by capillary forces both during sample extraction and solvent evaporation, and distortion of even densely packed monolayers during transfer limits the use of quantitative analysis of the structure of the transferred film.

Traditional methods of measuring NP contact angle typi- cally measure it after the solidification of one of the phases that comprise the interface.[91,92] The height of the trapped NPs protruding from the solidified surface can be measured by electron microscopy or by atomic force microscopy (AFM), where the height image directly provides the topography of the interface and, hence, the contact angle.

Paunov developed the gel trapping technique (GTT), where particles are spread at the air–water or oil–water interface and the aqueous phase is subsequently gelled using a nonsurface- active polysaccharide.[93] The particles trapped on the gel surface where then replicated by a poly(dimethylsiloxane) elastomer, and the contact angle was extracted by imaging the replica using scanning electron microscopy (SEM). Isa et al.

presented another method based on freeze–fracture shadow casting (FreSCa).[94] In this technique, the oil–water interface, frozen instantly by a jet freezer, is fractured and unidirection- ally metal-coated at an oblique angle before being imaged in cryo-SEM. The contact angles of the particles can then be easily calculated from the protruded height of the trapped NPs from the solidified interface. The accuracy of this approach has been proven by cross-comparison with different techniques; how- ever the solidification of the liquid remains a concern, since this can change the vertical position of the NPs at the original interface. Further discussion of experimental studies related to NP contact angle, e.g., wetting dynamics, characterization techniques, effects on interfacial properties, can be found in a recent review.[92]

In situ characterization techniques are far more desirable, though challenging to realize with liquid–fluid interfaces (**Figure 4**). Beyond measuring static properties such as the contact angle, in situ measurements of particle structure and dynamics are key to understanding how collective NP behavior relates to macroscopically observable properties. In situ analysis of assembly structure, for instance, allows the pair interac- tion potential $U(r)$ to be measured, where r is the separation distance between the two particles. In a thermally equilibrated
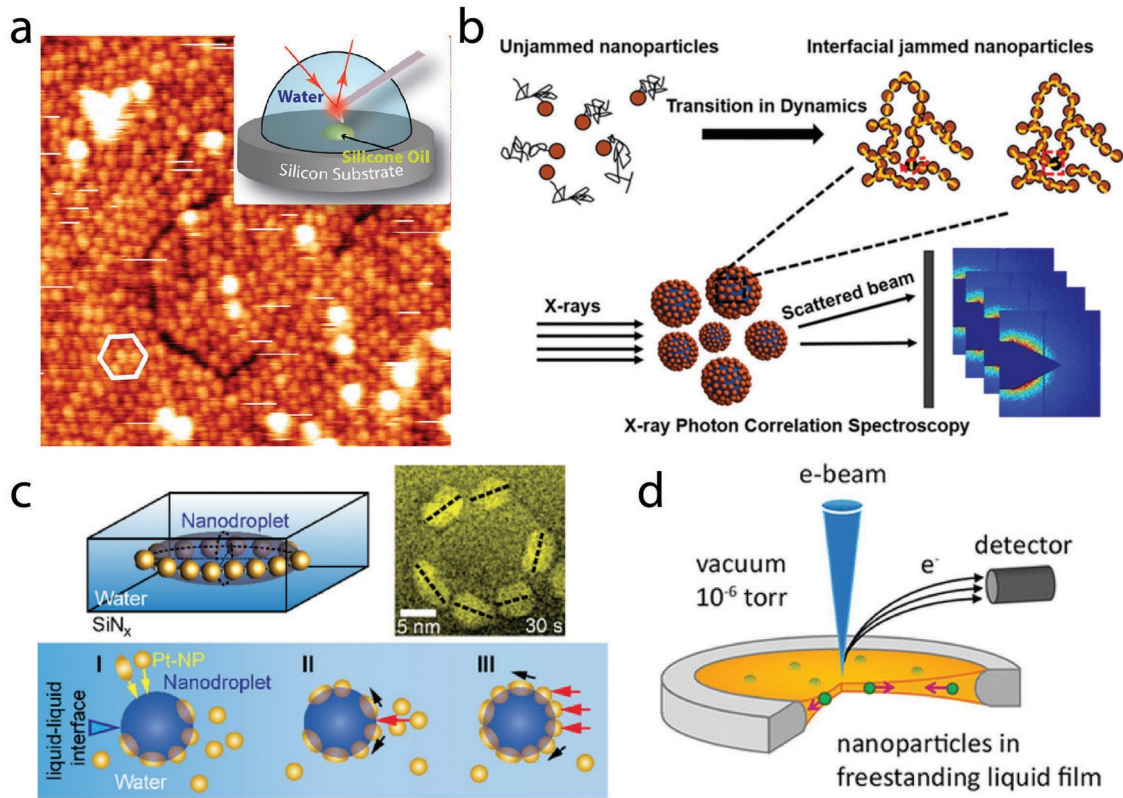
Figure 4. In situ characterization of NPs attached to liquid–fluid interfaces. a) Atomic force microscopy on silica NPs attached to water–silicone oil interface. Reproduced with permission.[95] Copyright 2017, American Chemical Society. b) X-ray photon correlation spectroscopy on CdSe–ZnS NPs at interfaces of water-in-toluene emulsion droplets. Reproduced with permission.[96] Copyright 2017, American Chemical Society. c) Liquid cell transmission electron microscopy on platinum NPs attached to interface between ethylenediaminetetraacetic acid nanodroplet and water. Reproduced with permission.[97] Copyright 2016, American Chemical Society. d) Scanning electron microscopy on polymer-grafted silica NPs at the vacuum–ionic liquid interface. Reproduced with permission.[98] Copyright 2016, American Chemical Society.

interfacial layer, direct measurement of the pair correlation function, $g(r)$, from micrographs can be used to calculate the interparticle potential[99]

$$\frac{U(r)}{kT} = -\ln[g(r)] \tag{4}$$

Some important caveats come with using this method. To exclude effects of multibody interactions, the samples should be measured at a dilute concentration.[100] When analyzed by direct imaging (e.g., optical microscopy), this method can be difficult to implement accurately when $U(r)$ varies by more than a few kT. This method has been effectively used to determine the interactions between colloidal particles attached to a fluid interface, but for NPs, the measurements remain a challenge as optical microscopy is diffraction limited. New imaging techniques with nanoscopic resolution have been developed for liquid samples, which allows for the direct study of NP micro- structure and pair potential.

Grazing incidence X-ray scattering (GISAXS) has been used to this end, where a finely collimated X-ray beam impinges on the liquid–fluid interface and the scattered X-rays provide infor- mation on the packing of the NPs averaged over the footprint of the beam.[101,102] If the characterize the in-plane dynamics of the NPs assembled at the interface.[96] GISAXS provides information not only about packing symmetry and interparticle spacing within the monolayer, but also about particle arrangement in the direc- tion normal to the interface. However, because the structural information is averaged over the size of the radiation beam, the technique may not effectively detect some structural details, incident X-rays are coherent, the time dependence of the X-ray speckle pattern can be used to

such as nonperiodic assemblies and defects. Recent develop- ments in atomic force microscopy have been successful in constructing real-space maps of the structure of NP assemblies. Costa et al. performed in situ AFM to support reciprocal space structures obtained from GISAXS.[103] Chai et al. used in situ AFM at the oil–water interface to relate pendant drop tensiom- etry measurements to adsorption kinetics and areal densities of NP surfactants (Figure 4a).[95] Recently, the latter group have further refined their technique and used it to interrogate the structure and mechanical properties of polyoxometalates and colloidal nanocrystals at the liquid–liquid interface.[104,105]

Several techniques have also been developed to understand the dynamics of interfacially assembled NP monolayers. Using X-ray photon correlation spectroscopy (XPCS), i.e., the X-ray analog of dynamic light scattering, Cui et al. recently studied NP-stabilized emulsions, observing a transition in NP dynamics from a liquid-like state to an interfacially jammed state (Figure 4b).[96] The limited timescale over which the

dynamics measured by XPCS can be complemented and signif- icantly extended by fluorescence recovery after photobleaching (FRAP).[106–108]

While scattering-based methods give a useful statistical measure of the behavior of NPs at the liquid–fluid interface, real-space imaging provides access to both the structure and dynamics of nanoparticle assemblies in localized regions. Many recent computational and experimental studies on the 2D packing of geometrically simple objects such as spheres and disks, and in the limits of jamming and crystallization, suggest this area holds a wealth of new physics.[109–122] This can only be investigated if the spatial location of each NP can be visualized and mapped as a function of time. Recent advances in in situ transmission electron microscopy (TEM) are bringing this to reality (Figure 4c,d). The structural aspects of NP dynamics can be best understood when visualized on a nanometer scale by electron microscopy. To study NP dispersions by TEM, the specimen can be encapsulated in a liquid cell with silicon nitride windows, to prevent evaporation in the high vacuum of the imaging environment.[123–125] Lin et al. performed in situ TEM to follow the dynamics of NP assembly on the interface of nanodroplets dispersed in solution (Figure 4c).[97] Attachment, rearrangement, and reorientation of NPs were observed at the interface.

A significant limitation of liquid TEM is that the handling of liquid cell is cumbersome, beam damage for organic mate- rials is inevitable, and interactions of the specimen with the cell walls can bias the dynamics. As an alternative method, Kim et al. developed an SEM technique combined with ionic liquids, displaying negligible volatility, to enable open- specimen, in situ, nonperturbative single-particle imaging of NPs on liquid interfaces (Figure 4d).[98] Positions and movements of individual particles could be determined with high spatial and temporal resolution, even for particles of asymmetric shape, mixed shapes and/or chemistry and for systems that packed close to their jamming point. Many phenomena associated with NPs at liquid interfaces were subject to single particle imaging, including diffusion-limited aggregation, triggered dissociation, jamming and unjamming, caged diffusion, rod rotary and anisotropic translational diffusion, binary mixing and mixtures, and ordering under interparticle interactions.

3. Studying NP Adsorption on Macroscopic Lengthscales

The adsorption of nanoscale materials to liquid–fluid inter- faces gives rise to macroscopically observable phenomena, from a reduction in interfacial tension to the deformation of the interface due to the presence of an elastic assembly. In prin- ciple, the discrete nature of NPs means that variations in these macroscopic variables allow us to extract physical properties of individual NPs from studies of macroscopic phenomena alone. In practice our ability to connect the pictures produced by studies of particle assembly on the nanoscale to the phenomena observed on the macroscale remains remark- ably limited, though some progress has been made in
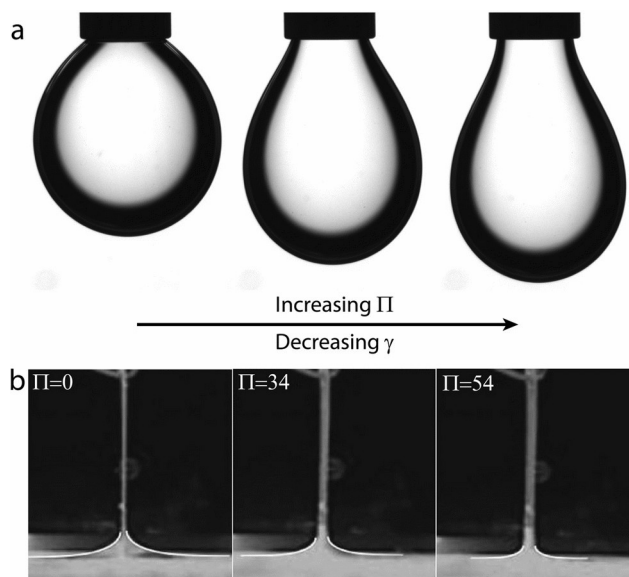

Figure 5. Measuring surface tension using two different methods. a) An aqueous pendant drop (in oil) sags under its weight as NP surfactants adsorb to the oil–water interface (see ref. [132]) b) The weight of the meniscus attached to a Wilhelmy plate in a Langmuir trough reduces as a particle-laden air–water interface is compressed and the surface tension decreases. b) Reproduced with permission.[133] Copyright 2009, American Physical Society.

3.1. The Effect of Nanomaterial Assembly upon Surface Tension

Perhaps the most widely studied macroscopic variable in the field of nanomaterial assembly at liquid–fluid interfaces is surface tension. Intuitively, one expects the reduction in surface energy given by Equation (2) to give rise to a reduction in the macroscopic surface tension of a liquid–fluid interface. The two most widely used tools to study the effect of NP adsorption are pendant drop tensiometry (**Figure 5**a) and the Langmuir trough used in conjunction with a Wilhelmy plate (Figure 5b).[3,6,126] The effect of adsorption on the liquid–fluid interfacial tension is typically given in terms of a measured interfacial tension, γ', or a surface pressure, Π, which can be defined by comparison with the surface tension of the liquid–fluid interface with no surface-active species present, γ_{clean}, such that

$$\Pi = \gamma_{clean} - \gamma' \qquad (5)$$

recent years.

The pendant drop method is particularly popular due to its affordability, relative ease of use (particularly with liquid–liquid interfaces), and suitability for use with small volumes of difficult- to-synthesize nanomaterials (as little as 50 μL vs 100 mL for a commercially available Langmuir trough). This popularity has resulted in several recent reviews dedicated to the method,[3,126] as well as simulations[127] and analysis software[126,128–130] written explicitly for the more challenging geometry of the pendant drop. For both pendant drop and Langmuir trough tensiometry, the shape of the oil–water interface is determined by gravita- tional and surface stresses and the boundaries that confine the system. Consideration of these factors leads us to the Young–Laplace equation

$$\Delta P - \Delta \rho \, gz = \gamma' \left(\frac{1}{R_1} + \frac{1}{R_2} \right) \tag{6}$$

where $\Delta \rho$ is the density difference between the internal and external fluids, R_1 and R_2 are the principal radii of curvature of the interface at a distance, z, from the apex of the droplet, and ΔP is the pressure difference between the internal and external fluids. This topic has been reviewed elsewhere, with extensive derivations and historical discussion.[3,131] Equation (6) can be numerically solved to give the shape of a liquid–fluid interface or, more usefully, the surface tension can be extracted from the measured shape of the liquid–fluid interface.

Note that Equation (6) supposes the existence of a single, isotropic surface tension. For the case of a solid interface or, more generally, in the presence of any anisotropic surface stresses, Equation (6) is clearly not valid as both the surface energy and the mechanical properties of the material formed at the liquid–fluid interface must be accounted for. Care must, therefore, be taken in measuring surface tension using both pendant-drop- and Langmuir-trough-based methods when studying systems with complex interfaces. In the case of drop shape analysis methods, integration of a pressure sensor on the droplet-side in a commercially available tensiometer allows for the properties of complex interfaces to be extracted (we discuss this more thoroughly in Section 4.2). In the case of Langmuir-trough-based methods, measuring surface tension by aligning the Wilhelmy plate both parallel and perpendicular to the direction of compression in principle allows the experimen- talist to account for the effects of a complex interface, however hysteretic effects as well as frictional interactions between the interfacial film and the edge of the trough, as well as the rapid increase in the surface pressure as solid-like assemblies are compressed, can limit the practical efficacy of this method. We return to these concepts in Section 4.1.

The overwhelming majority of surface tension measurements find that the adsorption of NPs onto the liquid–fluid interface causes a reduction in the macroscopic surface tension.[19,134,135] The major contribution to this reduction comes from the NPs screening the oil–water interface. For the case where particles are free to exchange between the bulk and the interface, i.e., small, reversibly bound particles, the system has a well-defined equilibrium concentration of particles at the interface, n, which is, in turn, determined by the total number of particles in the entire system, N. The effective surface tension of the oil–water interface, γ', is then given by

$$\gamma' = \left(\frac{\partial G}{\partial A} \right)_n = \left(\frac{\partial G}{\partial A} \right)_{T,V,N} \tag{7}$$

Adsorption of a particle to the liquid–fluid interface leads, in principle, to a reduction in γ' by an amount $\frac{\Delta E}{A}$ per particle. Macroscopically, this can be detected as a reduction in the interfacial tension, as measured by both

Despite several limitations, in particular a failure to account for both particle–particle interactions and the ener- getic cost of the creation of excess three-phase contact line at the oil–water interface, this relation appears to work reason- ably well. Du et al. found that Equation (8) gave physically reasonable estimates of particle binding energies for both micrometer- and nanometer-sized particles. This work assumed that the particles were near close packing ($\eta \approx 0.91$, where $\eta = \pi r^2 \frac{N}{A} = \pi r^2 n$ is the fraction of the oil–water interface occu- pied by the particles). Zhang et al. recently combined SEM (to measure particle density) and pendant drop tensiometry to show that Equation (8) allowed packing density of particles to be measured to within $\approx \pm$ 15%. Two important conclusions can be drawn from this latter study. First, it shows that the liquid– fluid surface tension can sometimes be used as an estimator of particle packing density, provided that one can perform the challenging measurements of contact angle but is unsuitable for a precise measure of η. Second, and most important, it shows that Equation (8) holds even up to near close packing of the interface, suggesting that in many cases particle–particle interactions do not contribute significantly to the reduction in surface tension of the oil–water interface. Equations (2) and (8) can then be combined to write an explicit relation for the packing density of the particles, η

$$\gamma' = \gamma_{clean} \left[1 - \eta \left(1 - \cos\theta \right)^2 \right] \tag{10}$$

Bizmark et al. recently showed that in systems with no barrier to NP adsorption, ΔE can be extracted from dynamic surface tension data at short timescales (approximately the first 10 s) using the relation[139]

$$\gamma'(t) = \gamma_{clean} - 2c\Delta E \sqrt{\frac{Dt}{\pi}} \tag{11}$$

where c is the bulk concentration of NPs (number per unit volume) and D is the diffusion coefficient governing their rate of adsorption onto the oil–water interface which, in this case, is equal to the diffusion coefficient given by the Stokes–Einstein relation. Furthermore, the adsorption barrier of the particle to a bare interface could be extracted from long timescale data, allowing two key quantities of interest to be extracted from a single dynamic surface tension measurement.

3.2. The Effect of Particle-Particle Interactions upon Surface Tension

Wilhelmy plate[133] and pendant drop tensiometry.[136,137] When n is small, i.e., particle– particle interactions can be neglected, then[138]

$$\Pi(n) = n\Delta E \tag{8}$$

All methods presented thus far depend on the validity of Equation (8) which, while it works well for NPs even up to rather high areal densities, fails to give a quantitative description of $\Pi(c)$ when particle–particle interactions affect surface tension.[127,140] A more

$$\gamma' = n\Delta E - \gamma_{clean} \tag{9}$$

physically insightful equation of state would relate the concentration of particles at the interface, n, and in the bulk, c, to the surface pressure. This requires us to consider how wetting of the oil–water interface and particle– particle interactions affect Π, as well as the chemical potentials of the NPs both in the bulk and at the interface.

Hua et al. recently made progress here by separately measuring the extent to which the screening of oil–water interface by the NPs and particle–particle interactions indi- vidually reduce surface tension, both in single and multi- component systems (**Figure 6**).[141,142] By directly measuring particle concentration at the interface, the contributions to Π from wetting, Π_{NP}, and the surface pressure of the 2D particle phase at the interface, $\Pi_{NP\text{-}NP}$, were separated under the assumption that the two contributions added linearly, i.e., $\Pi = \Pi_{NP} + \Pi_{NP\text{-}NP}$ (Figure 6a,b). Pendant drop tensiom- etry combined with UV–vis spectroscopy was then used to directly measure particle concentration at the interface by measuring the reduction in particle concentration in the bulk. By measuring the relation between $\Pi(c)$ and $n(c)$ at low concentrations, the wetting term (i.e., Equation (8)) could be measured. As the areal particle density was known for all bulk concentrations, the contribution to the surface pressure due to particle–particle interactions at high concentrations could then be directly extracted and further physical param- eters could then be calculated using the Frumkin model of adsorption[143,144]
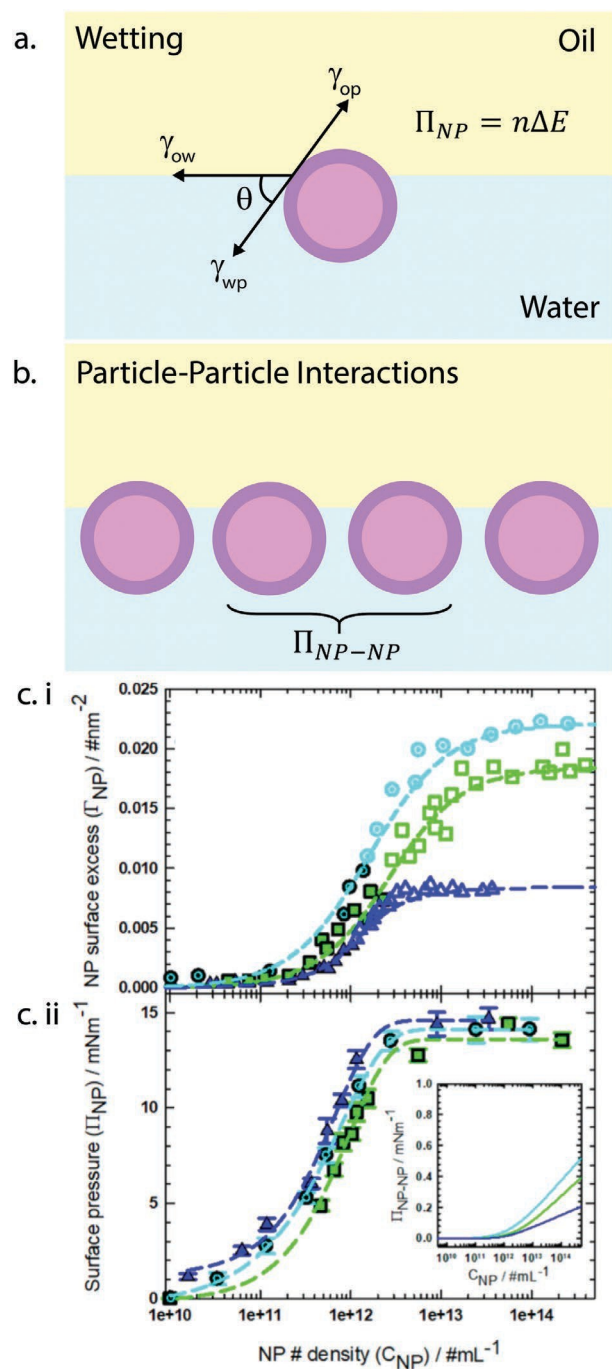
$$c(\theta) = a^{-\theta}\exp\left[\frac{K\theta}{1-\theta}\right] \tag{12}$$

$$\Pi_{NP\text{-}NP} = -kTn_{c\to\infty}\left[\ln(1-\theta) - 0.5K\theta^2\right] \tag{13}$$

where $\theta = \dfrac{n}{n_{c\to\infty}}$ describes the affinity of the particle for the interface, and K gives the interaction potential between the particles in units of kT, typically of order ±1 for NP systems. Positive K corresponds to repulsive interactions and, intuitively, an increase in the surface pressure; negative K corresponds to repulsive interactions and a decrease in surface pressure, while the special case of $K = 0$ corresponds to noninteracting particles giving the Langmuir model of adsorption. The resulting data prove rather compelling and the observations agree with findings elsewhere that particle–particle interactions contribute only a small reduction to the interfacial tension for many NP systems.

3.3. NPs May Not Always Reduce Measured Surface Tension

The description of how particle adsorption affects surface tension given so far is both simple and intuitive, which makes it appealing. However there exist a number of studies that explicitly disagree with it.[145,146] Both Zhang et al.[136] and Manga et al.[137] contain excellent reviews on the subject. The recent work by Manga et al.[137] is a useful case study. Manga et al. used pendant drop tensiometry and microtensiometry to study the effects of three different particles of differing sizes and surface chemistries upon the surface tension. The study, despite some limitations, contains some compelling observations. Dense, relatively large (density, ρ = 2200 kg m^{-3}, r = 400 nm) particles were found to cause a significant reduction in the "effective" interfacial tension of the system as measured by pendant drop tensiometry, while less dense, smaller (ρ = 1050 kg m^{-3}, r = 150 nm) particles did not affect oil–water

Figure 6. Different mechanisms by which NPs reduce the surface tension of an oil–water interface. a) Screening of energetically more expensive oil–water interface. b) Repulsive particle–particle interactions make it energetically favorable for interfacially bound particles to maximize their separation and, hence, expand the interface. c) The contributions of these two mechanisms can be separated by using tensiometry and a second technique that measures the concentration of particles at the interface, n. Adapted with permission.[141] Copyright 2017, American Chemical Society.

surface tension. When complementary measurements were performed using microtensiometry, no change in the interfa- cial tension due to the presence of either type of particle was observed. They attributed the "reduction" in interfacial tension

measured by pendant drop tensiometry to the weight of the particle shell adsorbed at the oil–water interface.

The extensive literature documenting the failure of some particles to reduce oil–water surface tension raises a number of interesting questions. It is not clear why adsorption of parti- cles to an oil–water interface should not reduce the free energy per unit area of an oil–water interface when it is measured on macroscopic lengthscales. Clegg et al. have identified a spe- cific case in Pickering emulsions that have undergone limited coalescence, in which all particles have adsorbed to the oil– water interface, and so further dilatation simply creates extra,

bare oil–water interface, i.e., the case in which $\frac{\partial G}{\partial A} = \gamma_{clean}$ [12]

However, the studies referenced here have significant excess particles in solution, and extra oil–water interface ought to be occupied by particles on the experimental timescale. The study of Manga et al. also has some limitations; the particle concentrations in the systems used with the two comple- mentary techniques differed by orders of magnitude and no attempts were made to estimate particle concentration at the interface (e.g., by measuring the compression of the interface required to induce buckling). Furthermore, the hypothesis that the pendant drop sagged under the weight of the particle shell is rather dubious and was not accompanied by quan- titative modelling of the effect of the weight of the particles upon the drop shape. Finally, the adsorption of the particles to the oil–water interface was not directly observed, but rather inferred from the ability of the particles to stabilize emulsions. This overlooks two key factors: i) in the case of emulsions, particle adsorption may be facilitated by turbulent eddies and ii) there are a number of cases where particles can stabilize emulsions even when they are not surface active.[35,147] Fur- ther comments have also been made elsewhere.[6] Regardless, the results do echo the findings of other studies that, in some instances, particle adsorption does not alter oil–water surface tension.[145,146]

One of the key challenges in this area is determining whether or not the particles have actually adsorbed at the inter- face at all. In many cases, there exists an energy barrier to the adsorption of particles, even when the binding of the particle to the interface corresponds to a local free energy minimum. The oil–water interface often bears an inherent charge, leading to repulsive electrostatic interactions between the particles and the interface that hinders the adsorption of NPs.[33,148,149] These repulsive electrostatic interactions may be due to image charges that arise at the interface of the two fluids that differ in permittivity,[150-152] or due to hydroxyl ions released from the water molecules adsorbing to the oil–water interface.[153] Like- wise, different types of interactions, i.e., hydrodynamic, van der Waals and hydration forces, have been found to act as a barrier to adsorption.[154-157]

The most obvious, brute-force resolution to the disagree- ments in the literature regarding the effect of NPs upon surface tension are studies that measure surface tension using complementary techniques, combined with direct observation of the adsorption of the

the effect of NPs upon surface-tension-mediated hydrodynamic instabilities using an appropriate model system.[162-165]

3.4. From Scalar Surface Tension to Tensor Surface Stress: Phenomenology

By assembling material at the interface, we impart the mechanical properties of that assembly upon the interface. Compressing an interface that contains adsorbed species, e.g., particles, lipids, or proteins, results in an increase in the density of the adsorbed species. If the surface-active species are reversibly adsorbed, then their concentration at the interface is particles at the interface (and their contact angle), using either confocal fluorescence microscopy for larger particles,[158,159] or freeze–fracture cryo-SEM[160] or gel-trapping.[161] More elegant approaches include the study of

determined by their concentration in the bulk, and compression leads to the species desorbing and surface tension relaxing to an area-independent equilibrium value.[142,166] More interesting is the case of materials that have a low solubility in either of the bulk phases, or are effectively irreversibly adsorbed. Some insoluble species, such as certain lipids, are driven through a rich range of phase behavior as their density at the inter- face increases.[4] Above a critical density further compression results in a collapse into a 3D structure, e.g., multilamellar, at the interface.[167,168] In the case of larger particles that are strongly bound to the interface, the particles typically remain a monolayer when compressed and exhibit fairly simple phase behavior,[169-174] but when compressed to the point of solidifi- cation rather than forming a multilayer the particle assembly buckles out of plane, forming wrinkles (**Figure 7**).

For simple, particle-based systems, the mechanical properties of the interface when it is compressed depend on the relative balance between the rate of compression (i.e., the strain rate), $\dot{\varepsilon} = \dfrac{dA/A}{dt}$, and the characteristic timescale of particle desorption, τ_{des}. If $\dot{\varepsilon} \gg \tau^{-1}$, the shape of the interface remains well described by Equation (6) during compression (Figure 7a).[166,175] In the case of larger particles ($r \approx 5 - 10$ nm), some polymers, proteins, and asphaltenes, $\dot{\varepsilon} \approx \tau^{-1}$, and contraction of the interface leads to buckling (i.e., wrinkling) of the interface, with wrinkles relaxing on the timescale of particle desorption (Figure 7b).[176] For irre- versibly bound particles wrinkles remain visible indefinitely (Figure 7c).[177]

The energies that constitute "reversible" and "irreversible" binding on the experimental timescale are unclear. When binding energy (ΔE) is of order 10 kT or less, NP binding to the interface is reversible and interesting kinetic effects can be observed in particles with differing binding energies. Lin et al. showed that r = 1.4 nm CdSe particles ($\Delta E \approx$ -5 kT, estimated using Equation (2)) were displaced by r = 2.3 nm CdSe particles ($\Delta E \approx$ -13 kT) at the oil–water interface.[19,108] The substitution of small particles for large ones is a purely kinetic effect; the smaller particles exchange more rapidly with their counterparts in the bulk, while the larger particles were adsorbed quasi- irreversibly on the experimental timescale. Bizmark et al. recently estimated the upper limit for "reversible" binding to be $\approx$20–50 kT,[139] however this contradicts observations by other groups that particles with binding energies as high as 100 kT are reversibly bound to the liquid–fluid interface.[166,175]

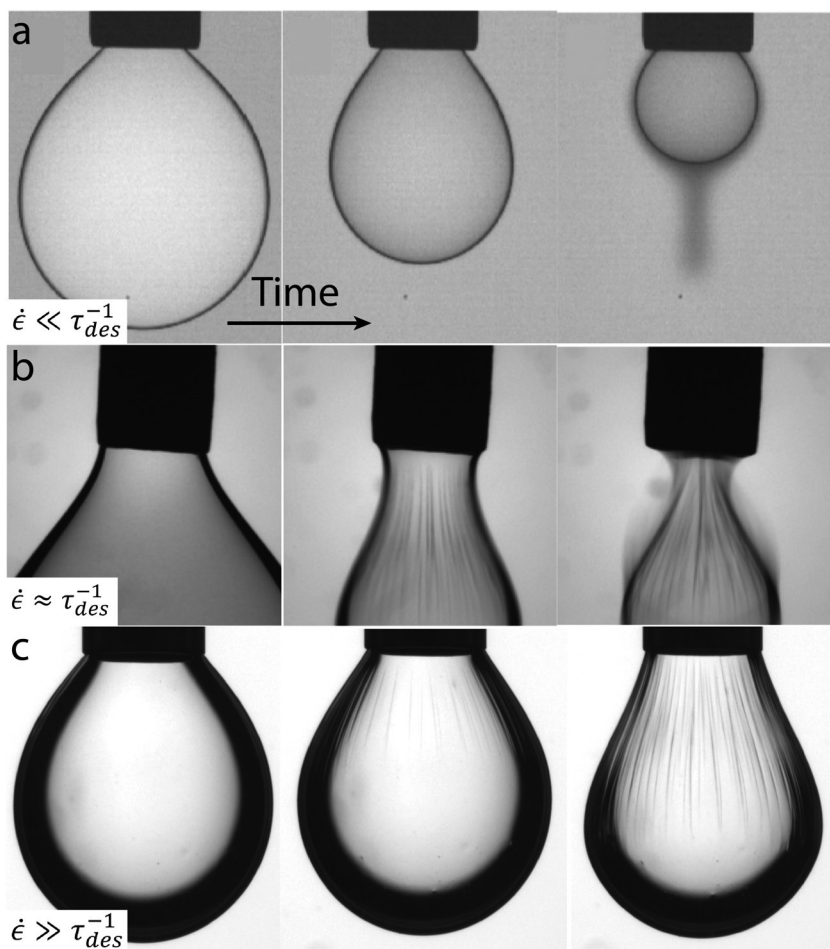In the case of particle desorption occurring on the experi- mental timescale, the desorption of particles leads to the

Figure 7. Desorption timescales and buckling of the oil–water interface. a) r = 2.3 nm Au particles are ejected from the oil–water interface in response to water being extracted from a pendant drop. Adapted with permission.[166] Copyright 2012, American Chemical Society.
b) Asphaltenes desorb from a pendant drop on a timescale comparable to the rate of compression. Small wrinkles form that relax within minutes, desorbed material can be seen to accumulate near the interface. Adapted with permission.[176] Copyright 2014, American Chemical Society. c) 14 nm Silica NP surfactants that are effectively irreversibly bound to the interface buckle in response to interfacial compression.[132]

properties of the interfacial film and the reversibility of its adsorption. While particles that interact via a purely repulsive potential will always attempt to maximize their separation, attractive in-plane inter- actions between surface-active species give rise to the formation of macroscopic constructs at the liquid–fluid interface with a large effective size and, hence, a large effective ΔE. These in-plane interac- tions can be controlled readily in NP sys- tems by crosslinking particle assemblies at the liquid–liquid interface,[178,179] many examples of which are covered in a recent review.[7] However, remarkably fine con- trol over this phenomenon can also be found in more complex biological nano- materials. Recent work on the surfactant- like protein BslA is a stand-out example of this.

The protein, in its wild-type strain, folds into a surfactant or Janus-like struc- ture that contains a hydrophobic cap and a hydrophilic tail (**Figure 8**a). Hobley et al. studied the effect of substituting single amino acids in the hydrophobic cap upon the tertiary structure and surface activity of the protein, as well as the biofilms in which it was present.[180] By identifying the hydrophobic leucine residues that could be replaced with more hydrophilic lysine without significantly disrupting the struc- ture of the hydrophobic cap, the group studied how minimal modifications to the amino acid sequence affected the binding of the BslA to the oil–water interface. Wild-type BslA was found to adsorb irreversibly, while modified BslA adsorbed reversibly, with the desorption timescale depending on the location of the substituted residue (Figure 8c).[180,181] It is important to note

accumulation of particles near the interface (Figure 7a,b),

allowing the concentration of the particles at the inter-face to be estimated by quantitative photometric methods. Garbin et al. applied this technique to measure ΔE for r = 2.3 nm (1-mercaptoundec-11-yl)tetra(ethylene glycol)- stabilized gold NPs. They found that $\Delta E \approx 111$ kT and that the particles desorbed upon interfacial compression (Figure 7b).[166,175] This is of a similar magnitude to value of $\Delta E = 60$ kT measured by Du et al. for the same particles using Equation (8),[138] though the disagreement is still significant, underscoring the limitations in using tensiometric methods to estimate particle density and binding energies.

adsorbed species also play a role in determining the mechanical

3.5. Physical Simplicity in a Complex Biological System: BslA Protein

Beyond geometry, in-plane interactions between

that, despite the amphiphilic structure of the BslA at the inter- face, adsorption of the BslA often did not reduce the inter- facial tension, even up to rather high areal protein densities ($\eta \approx 0.5$), as has been observed elsewhere with a variety of proteins.[182,183]

Bromley et al. then compared the reversibility of adsorption to the oil–water interface and tertiary structure of the modi- fied and unmodified BslA.[184] TEM images showed that the reversibly adsorbed species bearing lysine-substituted hydro- phobic caps formed disordered interfacial assemblies. In stark contrast to this, the irreversibly bound, wild-type BslA had strong, in-plane, anisotropic interactions at the oil–water inter- face, forming extended ordered regions with the individual pro- teins ordered into square crystals (Figure 8b). A consequence of these strong, in-plane interactions is the ability to generate interfacial wrinkling that does not relax on experimental time- scales and, hence to stabilize nonspherical emulsion droplets (Figure 8d).
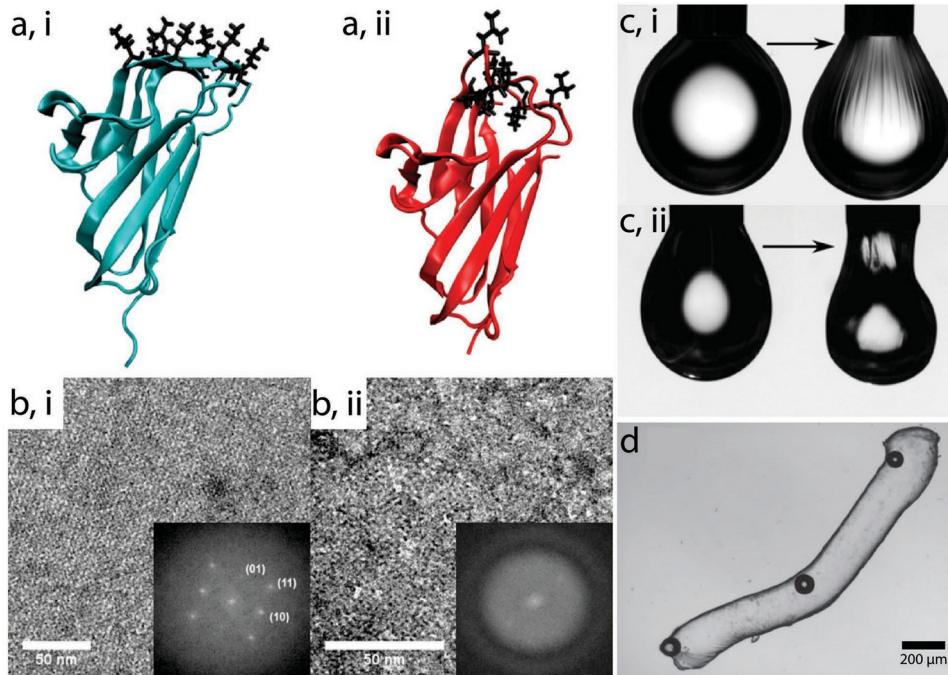
Figure 8. The interfacial behavior of BslA, from molecular-level control, to mesoscopic structure, to macroscopic function, to application. i) Unmodified and ii) modified structure of BslA, in which a single leucine residue has been replaced with a lysine. a) Structure of BslA, showing the distinctive hydrophobic cap (top of the image). b) TEM images of the interfacial assemblies of BslA after they had been transferred to a substrate. c) Irreversible and reversible binding of BslA upon interfacial compression. d) Nonspherical droplets of coconut oil in water stabilized by BslA. a–c) Reproduced with permission.[184] Copyright 2015, The Authors. Published by the National Academy of Sciences. d) Reproduced under the terms of the CC-BY 4.0 license (https://creativecommons.org/licenses/by/4.0/).[185] Copyright 2017, The Authors. Published by Royal Society Publishing.

4. Quantitative Descriptions of Complex Interfaces

4.1. The Surface Stress Tensor

In addition to the more qualitative, phenomenological treatment in the previous section, major progress has also been made in quantitatively describing the mechanics and rheology of interfaces.[5,186] When we deform an interface two things occur: the amount of liquid–fluid interface is changed and the material formed at the interface is deformed. Both of these processes have an energetic cost and, hence, determine the mechanical properties of the interface. Hermans et al. described this intuitively using the expression[187,188]

$$\sigma_{ij} = \gamma_{ow}' \delta_{ij} + \Gamma_{ij} \tag{14}$$

where, δ_{ij} is the Kronecker delta and σ_{ij} is the surface stress tensor (bold font corresponds to 2 × 2 tensors). The right-hand side of Equation (14) is broken into two terms that represent two different contributions to the surface stress. First is the isotropic, scalar, surface energy term ($\gamma_{ow}' \delta_{ij}$), which describes the energetic cost of deforming the liquid–fluid interface itself, as well as the effect of adsorption and desorption of material on the surface tension. Also included in this term are Marangoni stresses asso- ciated with spatial gradients in surface tension. The second ani- sotropic, tensor term (Γ_{ij}) describes the cost of deforming the material that is adsorbed at the interface. Rigorous definitions of this term and its physical origin can be found in Nagel et al. and a review

and the surface stress is exactly equal to the liquid–fluid surface tension as measured using pendant drop or Wilhelmy plate. In the presence of material that is quasi-irreversibly bound to the liquid–liquid interface Γ_{ij} becomes significant,[128,189-194] and gives rise to the complex shapes observed in Pickering emul- sions,[12,195] liquid capsules,[196] bijels,[21,22,197] and, most recently, printed and molded liquids.[163,198,199]

The elastic moduli of the interface are then given by the deriva- tive of Equation (14) with respect to the appropriate strain. The shear response of the interface is more physically intuitive than its dilatational response, as $\gamma' \delta_{ij}$ does not change in response to a shear deformation. As such, interfacial shear rheology allows us to directly probe the mechanical properties of the adsorbed (pro-

tein, particle, polymer, etc.) layer. Note, also, that the existence of

by Sagis.[3,5] For the case of liquid–fluid interfaces and interfaces wetted by reversibly adsorbed components, $\Gamma_{ij} = 0$

a shear modulus is characteristic of the presence of quasi-irrevers- ibly adsorbed material at the interface. This shear modulus can be viscous or viscoelastic, as with lipids, or elastic-dominated, as is often the case with particle assemblies;[200] soluble surfactants, by contrast, possess negligible (possibly zero) shear viscosity.[201]

4.2. Commercially (and Freely) Available Methods to Study the Rheology of Complex Interfaces

As more complex interfaces have attracted both academic and industrial interest, several commercially or freely available tools have emerged that allow the mechanical properties and rheology of complex, viscoelastic and elastic interfaces to be quantitatively probed. For systems in which structure and functionality are
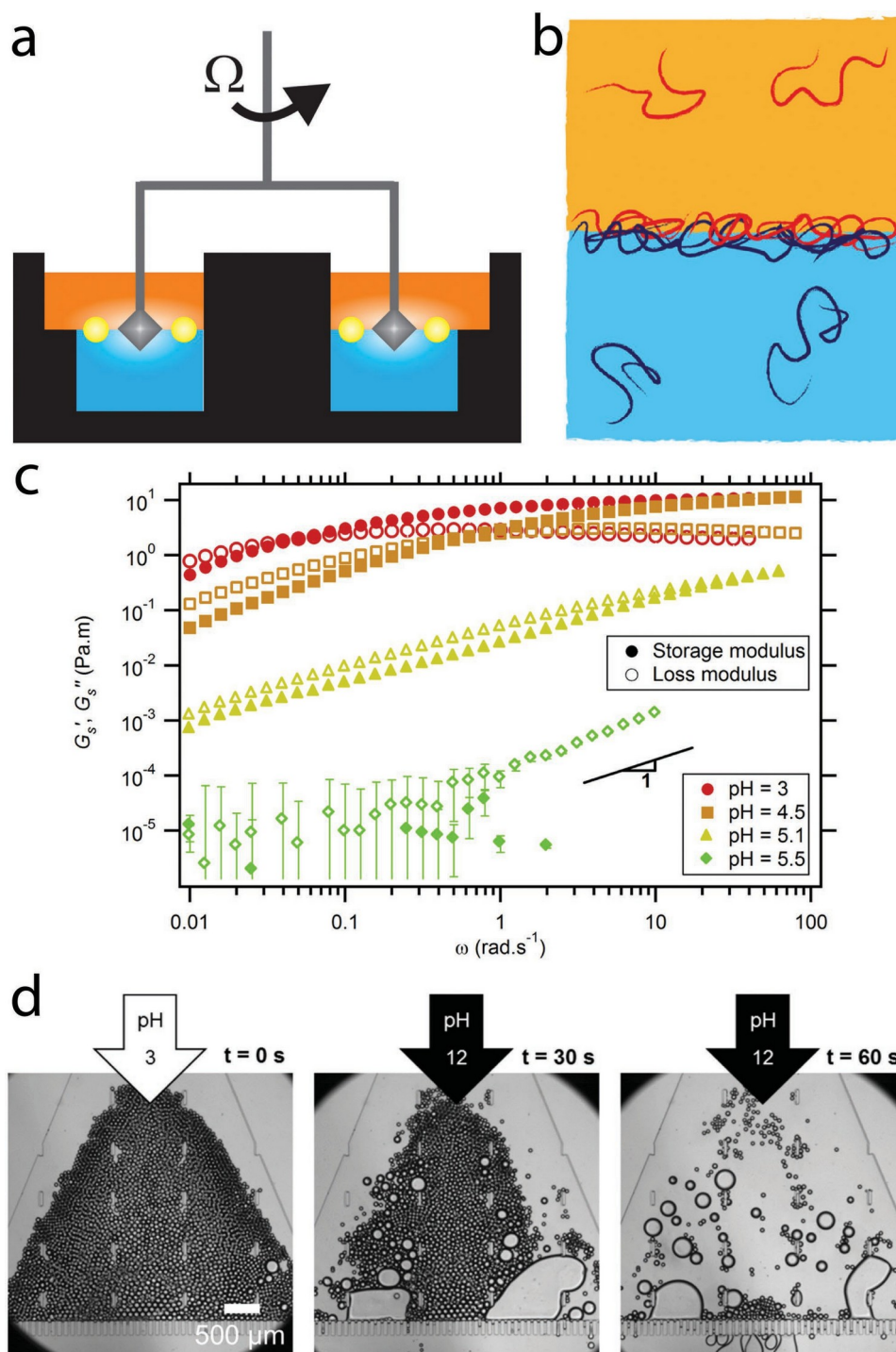
Figure 9. From molecular interactions to interfacial shear rheology to functionality. a) The Double Wall Ring geometry, which can be mounted on a commercial rheometer and used to probe solely the material properties of the adsorbed species. Reproduced with permission.[202] Copyright 2017, American Chemical Society. b) Schematic showing the formation of viscoelastic polyelectrolyte–polyelectrolyte complexes at the oil–water interface. c) pH- dependent interfacial shear rheology of PMAA–PPO coacervates. d) Droplets stabilized by PMAA–PPO coalesce in response to a pH change. Reproduced under the terms of the CC-BY 4.0 license (https://creativecommons.org/licenses/by/4.0/).[203] Copyright 2017, The Authors. Published by Springer Nature.

derived from complex interfaces, studying the mechanical prop- erties of an interface (viscoelastic moduli, yield stresses, etc.) and their response to external stimuli (e.g., temperature and pH changes) allows for rational design and formulation of a system.

Interfacially assembled polymer–polymer coacervates provide a highly controllable system that exhibits a rich range of phase behavior and interfacial rheology (**Figure 9**). Recently, Monteux and co-workers have studied how reactions at the molecular level

in polymer coacervates formed at the oil–water interface relate to the interfacial rheology of the coacervates and, ultimately, the function of the structures they stabilize. Le Tirilly et al. used the Double Wall Ring geometry of Vandebril et al. (Figure 9a) to study interfacially assembled polymer coacervates of a range of thicknesses (Figure 9b).[204,205] Layer-by-layer assembly was used to produce a number of interfacial coacervates based on hydrogen-bonding polymers, in which a H-bond-donating polymer, e.g., poly(methacrylic acid) (PMAA) or poly(acrylic acid) (PAA), binds to a H-bond-accepting polymer, e.g., poly(vinylpyrrolidone) (PVP) or poly(propylene oxide) (PPO). De Baubigny et al. then studied the same system but, rather than using layer-by-layer assembly, the polymers were initially separated in immiscible phases (i.e., oil and water) and interacted with one another at the liquid–liquid interface, [203] in a manner similar to that used by Kaufman et al.[206] Interfacial shear rheology showed that the mechanical moduli of the H-bonded polymer coacervates could be tuned over four orders of magnitude by varying pH (G_s' ≈ 10^{-3} - 10^{1} N m^{-1}, note that the upper limit may underestimate film strength due to the compliance of the DWR geometry).[202] In combination with microscopy and profilometry to measure film thickness and capsule behavior, the rheological properties of the film could then be related to capsule and emulsion structure and stability as a function of pH (Figure 9c,d). The pH-response of the cap- sules also suggests the interesting possibility of being able to tune the mechanical properties of the capsules in situ, leading to reconfigurable, interfacially structured liquid materials.

The dilatational response, which is typically more important from an applications perspective, is rather more complex. Significant insight into these complexities has been given in recent years by Vermant and co-workers.[3,187–190,207] A number of commercially available methods exist for the study of the response of interfaces to dilatational and compressive stresses (i.e., their Gibbs elasticity, bending modulus, and elastic modulus).[3,128–130,208] Measuring these properties, however, can be extremely challenging for at least three reasons: i) sepa- rating contributions from surface tension and material proper- ties, ii) measurement of the initial stress in the system, and iii) the application of a shear-free strain field. This third problem is particularly significant in rectangular-Langmuir-trough-based methods, where the limitations are so significant that we do not cover them here. A recent review contains critiques of most existing methods, as well as providing a number of cautionary tales for the experimentalist starting out in this discipline.[3]

Several methods exist to extract the mechanical properties of pendant drops coated with solid-like interfaces in response to dila- tational stresses. All methods work in one of two regimes (either before or after the interface has buckled) and rely on varying assumptions. Danov et al. modified a pendant drop tensiometer by attaching a pressure sensor to the droplet-side of the apparatus, allowing them to directly measure the Laplace pressure and, hence the surface stress.[129] Applying a method they called "cap- illary meniscus dynamometry," they combined image analysis and pressure measurements to directly measure the stress field at the oil–water interface and its degree of

anisotropy. As well as providing a technical-yet-accessible guide to workers interested in the field, the review by Nagel et al.[3] also includes a refined, freely available MATLAB implementation of the method of Danov et al.

As an interface is compressed, interactions between adsorbed particles (that contribute to the Γ_{ij} term in Equation (14)) grow rapidly as the particles are brought into contact with one another. When these stresses become comparable to γ', the interface buckles out of plane.[127,129,209] Knoche et al. have been successful in using a pendant drop tensiometer to extract mechanical parameters from the structure of the wrinkles formed at buckled interfaces.[128,130] The method uses image analysis, requiring only an off-the-shelf, entry level tensiometer; software to perform the analysis is freely available online and provided in Hegemann et al.[130] By comparing an undeformed reference shape to obtain surface tension, a deformed shape to obtain the 2D Young's modulus, Y_{2D}, and the Poisson ratio, ν_{2D}, the bending modulus, B, of a solid interfacial film could be obtained from the wrinkles of buckled pendant drops (**Figure 10**a). They applied this method to study the mechanical properties of poly- merized octadecyltrichlorosilane and HFBII, a hydrophobin sim- ilar in tertiary structure to the BslA that is the subject of indus- trial interest.[210,211] It should be noted, however, that a major limi- tation of the method is the requirement that the initial state of the system be stress-free, a questionable assumption in many cases.

More interestingly from a materials perspective, Salmon et al. used the pendant drop elastometry method of Kierfeld et al. to study drying capsules coated with a supramolecular complex of cucurbit[8]uril and stilbene-functionalize poly(vinyl alcohol), in which an elastic interface film is assembled via a host–guest interaction (Figure 10b,c).[212,213] The group attributed the observed behavior to the novel 2D phase behavior of the interfa- cial supramolecular complex, in which the buckling strain of the system was determined not by a jamming transition (as in repul- sive or hard-sphere particle monolayers),[214] but rather a 2D gelling transition. While the work highlights the application of easy-to-use interfacial rheology tools in materials science, it also points to the growing diversity of materials used in liquid–liquid systems. The oil–water interface in this work acts as a platform for synthesizing a material with novel functional and mechanical properties. Feedback between the ability to interrogate the mate- rial properties of the interface in response to stimuli and syn- thesize novel materials at the interface provides a platform for the design of new materials with new and useful properties. We return to these concepts later, in which we discuss the complex liquid–liquid interfaces can be used to generate materials with reconfigurable mechanical and functional properties.

4.3. Custom-Built Interfacial Rheology Apparatus

There also exist several homemade interfacial rheology methods that offer greater sensitivity than their commercial counterparts, or that can be used in tandem with advanced characterization equipment. Pepicelli et al. confronted the experimental difficul- ties in applying a pure dilatational strain to the interface by con- structing what is, in effect, a circular Langmuir trough.[189] Thus far, the system has only been applied to model systems, but the marked difference in the rheology of systems measured on the circular versus a typical rectangular Langmuir trough were sig- nificant, suggesting it has significant promise as a platform for studying viscoelastic interfaces. Measurements performed on this circular trough are affected differently by frictional interactions
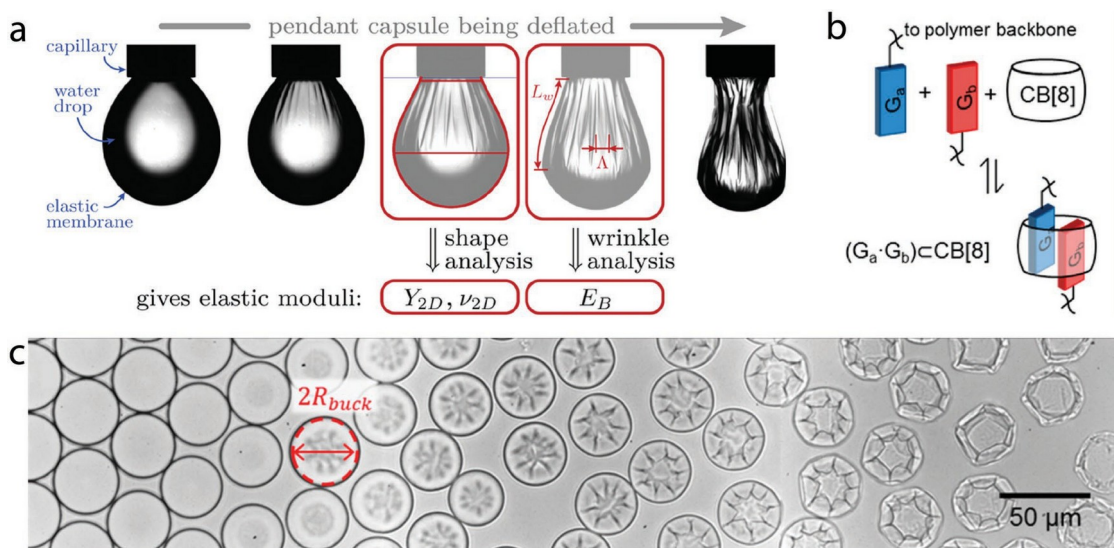
Figure 10. Interfacial dilatational elastometry as a tool for rational design. a) Extraction of the mechanical parameters of the elastic interface of a pendant drop. Reproduced with permission.[128] Copyright 2013, American Chemical Society. b) Assembly of an elastic interfacial film via the host–guest interaction between stilbene-functionalized poly(vinyl alcohol) and CB[8]. c) Phase change-induced buckling of oil-in-water capsules due to evapora- tion of water. Reproduced under the terms of the CC-BY 4.0 license (https://creativecommons.org/licenses/by/4.0/).[213] Copyright 2016, The Authors. Published by the American Chemical Society.

between the interfacially formed material and the trough wall, [133] meaning it will be of significant use in measuring the mechan- ical properties of solid-like films both pre- and post-buckling.

The magnetic button of the Squires and co-workers (**Figure 11**),[215] which represents an evolutionary improvement over the older magnetic rod rheometer, [216,217] is more suitable for softer interfaces (G_s', $G_s'' \approx 10$ mN m^{-1} or less). Zell et al. used this setup to argue that not only do monolayers of soluble surfactants, e.g., sodium dodecyl sulfate, have zero shear viscoelasticity, they further have zero interfacial shear viscosity.[201] The facility with which the magnetic button rheometer can be coupled with a microscope is a major ben- efit; Buttinoni et al. used this to perform a rheo-imaging study on well-defined monolayers of repulsive colloidal particles. [218] The method has also proven to be remarkably effective at probing biologically and industrially relevant systems, such as the rheo-imaging study of Choi et al. on phase-separated phos- pholipid monolayers,[215] the study of Williams and Squires on the impact of fibrinogen on the interfacial rheology of a model lung surfactant,[219] and the study of Chang et al. on rheology

and structural heterogeneity in asphaltenes at the oil–water interface.[220]

4.4. Mechanics of a Model System: The Case of CTAB-SiNP

The rheology and mechanical properties of nanomaterial assemblies are extremely rich and depend on the structure of the assembly and, hence, the interparticle potential. However, for many systems consisting of assemblies of weakly attrac- tive NPs, some rather general observations have been made. The model system developed by Ravera et al., is perhaps most representative of these properties (**Figure 12**).

This system consists of a mixture of CTAB (a surfactant) and commercially available silica NPs. The positively charged CTAB partitions strongly to the surface of the silica NPs, meaning the concentration of the CTAB at the liquid–fluid interface is low (but nonzero),[221,222] forming a NP-surfactant complex (CTAB- SiNP, Figure 12a). The result is a system of surface-active, quasi-irreversibly adsorbing particles whose contact angle and
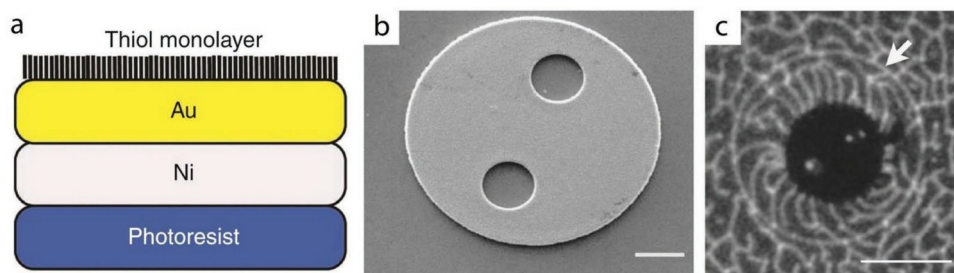

Figure 11. a) Schematic, b) SEM image, and c) fluorescence microscopy image of the magnetic button shear rheology apparatus of Squires et al. and the effect of shear deformation on phase-separated phospholipid monolayers at the air–water interface. Reproduced with permission.[215] Copyright 2011, Springer Nature.
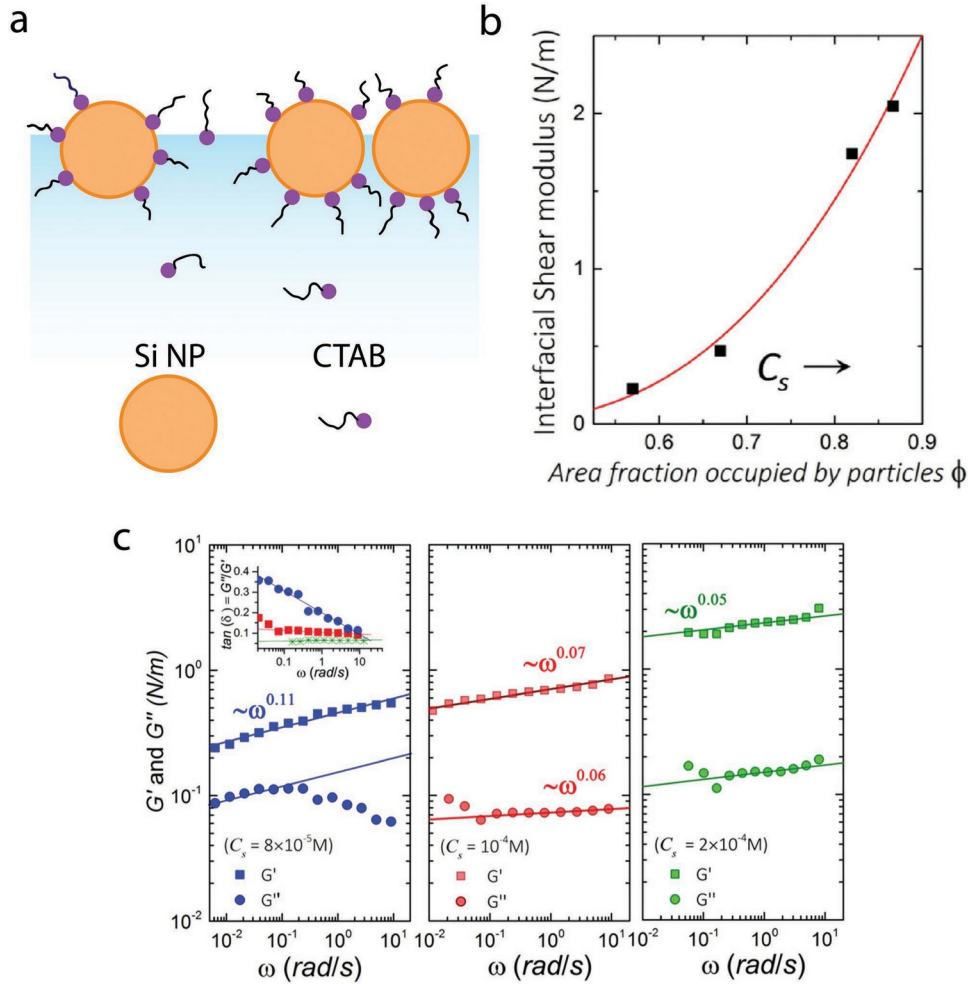
Figure 12. CTAB-SiNP assemblies at liquid–fluid interfaces and their interfacial rheology. a) Schematic of the model CTAB-SiNP. b) Power-law increase of G'_s with η. c) Power-law increase of rheological moduli with oscillation frequency. Lines of fit reflect interpretation of data using Soft Glass Rheology model. Reproduced with permission.[225] Copyright 2015, American Chemical Society.

concentration at the interface can be tuned, though not inde- pendently of one another. Over the last decade, the surface tension, dilatational and shear moduli (both in the isotropic and anisotropic stress regime), surface tension during continuous compression, contact angle, and particle density as a function of CTAB concentration of CTAB-SiNP have all been studied.[223,224] Maestro et al. recently performed both shear rheology meas- urements, coupled with imaging ellipsometry, to measure particle density and complemented these studies with modelling of the rheology of CTAB-SiNP (Figure 12b,c).[225,226] The shear modulus of CTAB-SiNP monolayers was found to be in the range 0.1–1 N m⁻¹, comparable to most values found elsewhere in the literature for silica NPs.[227–229] The low frequency shear modulus, G'_s, was found to follow a power-law dependence on the interfacial particle density, η, identical to a system undergoing a gel transition. Below a critical particle density, η_c, the shear modulus is negligible, while above η_c it grows rapidly as the system approaches close packing, i.e.

The yield stress, τ^*, of weakly attractive nanoparticle assem- blies is also strongly dependent on η. Maestro found that the yield stress of CTAB-SiNP exhibited power-law behavior, i.e., $\tau^* \sim \eta^\alpha$.[225] This was in agreement with trends observed in work by Beltramo et al. and Reynaert et al. on attractive, micrometer-sized particles, and simulations by Roy and Tirum- kudulu, where α was found to vary between 4 and 8.4.[230–232]

Both G'_s and G''_s show power-law dependence on the oscillation frequency of the applied shear, ω (Figure 12c). This frequency- dependence in the solid-like films was interpreted in terms of the soft glassy rheology (SGR) model of Sollich et al.,[233] with more in-depth modelling performed in follow-on work.[226] Zhang et al. also studied a silica-NP-based system to study the response of particle monolayers to both large- and small-amplitude oscillatory shear, also finding a soft, glassy response to the applied shear.[234]

It is interesting to note that G'_s in all of these systems is of a similar magnitude regardless of particle size, which raises an interesting general question about the dimensionality (i.e.,

$$G'_s \sim \left| \frac{\eta}{\eta_c} - 1 \right|^\beta \qquad (15)$$

the effective $\left(_c \right)$ thickness) of particle monolayers. For instance, similar behavior to that seen in CTAB-SiNP has been seen in the rheo-imaging work of Reynaert et al. on micrometer-sized,

repulsive particles.[230] In general, β is in the range 2–8, and η is typically 0.2–0.4. Similar behavior was seen by Beltramo et al. and Cicuta et al. for micrometer-sized particles,[190,235] while Maestro et al. observed similar values for G_s' for silica NPs. In all cases G_s' is between 0.1 and 1 N m^{-1}, even though the par- ticle size ranged from 14 nm up to 3 μm. This goes against the prevailing convention of treating these systems as continuum materials with a thickness, $d \approx r$, where one would expect $G_s' \propto r$

, and compels us to consider whether a more accurate model for these systems is as a set of point contacts between nonover- lapping particles, i.e., a force chain-type description. We treat these two ideas in the next section on interfacial buckling.

4.5. The Bending and Buckling Behavior of Interfacially Assembled Films

The emergence of the large shear modulus of NP monolayers in Figure 12 is a consequence of the assemblies ceasing to behave like individual NPs and, instead, behaving like a contin-

uous material. In the simplest case, for linear, homogeneous, isotropic materials, one expects the 2D shear, compression, and Young's moduli (G_s, E_s, and Y_s, respectively, all of which have units of force per unit length) to be related by[3,236]

$$E_s = \frac{Y_s}{2(1-v)} \quad (16a)$$

$$G_s = \frac{Y_s}{2(1+v)} \quad (16b)$$

$$Y_s = \frac{4G_sE_s}{G_s + E_s} \quad (16c)$$

$$v_s = \frac{E_s - G_s}{E_s + G_s} \quad (16d)$$

$$-1 < v_s < 1 \quad (16e)$$

where v_s is the 2D Poisson ratio.

In addition to resistance to shear and compression, interfacial assemblies exhibit resistance to bending. The origin of this resistance to bending is varied and complex and, as we will see, does not typically obey continuum relations in the case of NP monolayers. Regardless of the physical origin of the resistance to bending, the behavior of an interfacial film with some bending modulus, B, buckling out-of-plane in response to small compressions can be well described by a simple model. By neglecting self-adhesion of the film, the energy required to buckle a film into a specific, arbitrary shape can be modelled as the sum of the bending energy, U_B, which favors long-wavelength buckling, and the gravitational energy, U_G, due to vertical

Here $\kappa(r)$ is the spatially varying local curvature of the film and $\Delta\rho$ is the density difference between the liquids, g is the acceleration due to gravity, and $h(r)$ is the spatially varying vertical displacement field of the film. It is important to note that the film itself is effectively incompressible (the particles that make up the assembly are not deformed); applying a compressive stress to a film of area, A, results in a film of the same area being confined within some smaller area.

For small, uniaxial confinement, the interfacial assembly buckles with a single, well-defined wavelength, λ. Milner et al. were the first to observe that the continuum description given by Equation (17) could be applied to solid-like films and monolayers at the liquid–fluid interface. Minimizing Equation (17) yields a simple relationship between B and λ in the small deformation regime[237]

$$\lambda = 2\pi \left(\frac{B}{\Delta\rho g} \right)^{\frac{1}{4}} \quad (18)$$

As the film is confined further, stress in the system becomes concentrated into a small number of highly curved folds, and regions of sinusoidal wrinkling flatten out (**Figure 13**a).[238-241] Changing geometry and topology adds further complexity to the
system, but for small compressions the behavior of the system
can be captured by physically intuitive models (Figure 13b). [242,243] The wealth of the theoretical and fundamental experimental work performed in this area means that the buckling of well-
characterized, interfacially assembled thin films can be used as colloidal- and cell-scale stress gauges (Figure 13c).[244,245]

4.6. NP Monolayers Do Not Buckle Like Thin, Homogeneous Films

Particle monolayers have anomalously small bending moduli relative to their shear moduli. While this idea makes intuitive sense (it is not obvious why a NP monolayer should offer any resistance to bending), it warrants discussion. Materials assem- bled at the liquid–fluid interface typically have thicknesses of

displacement of the liquids by the out-of- plane buckling of the film (which favors small-wavelength buckling)

1 μm or less; in the case of particle monolayers, it is not clear whether the system can be said to have a well-defined thickness at all. One consequence of this is that the bending stiffness of the interfacial assemblies is not trivially related to the moduli governing in-plane deformations. In linear, homogeneous, anisotropic, 3D systems, a simple set of equations similar to those in Equations (16a–e) relate the shear, compressive, and Young's modulus to the bending modulus (Equation (20)). While this relation is known to hold for polymer films down to film thicknesses of order 10 nm,[249] for

$$U = U_B + U_G = \frac{B}{2}\int_A \kappa^2(r)\, d^2r + \frac{\Delta\rho g}{2}\int_A h^2(r)\, d^2r \tag{17}$$

most materials that are assembled at the liquid–fluid interface resistance to bending in the system has an entirely different physical origin to the resistance to compression. This anisotropy, which is inherent to any quasi-2D material, leads to a rich range of behavior.

For particle monolayers made of large particles ($r > 5$ μm), Vella et al. observed that the bending modulus of the monolayer depends not on the material properties of the particles, but

upon surface tension and particle size.[250] They argued that, for large particles, capillary interactions give rise to particle
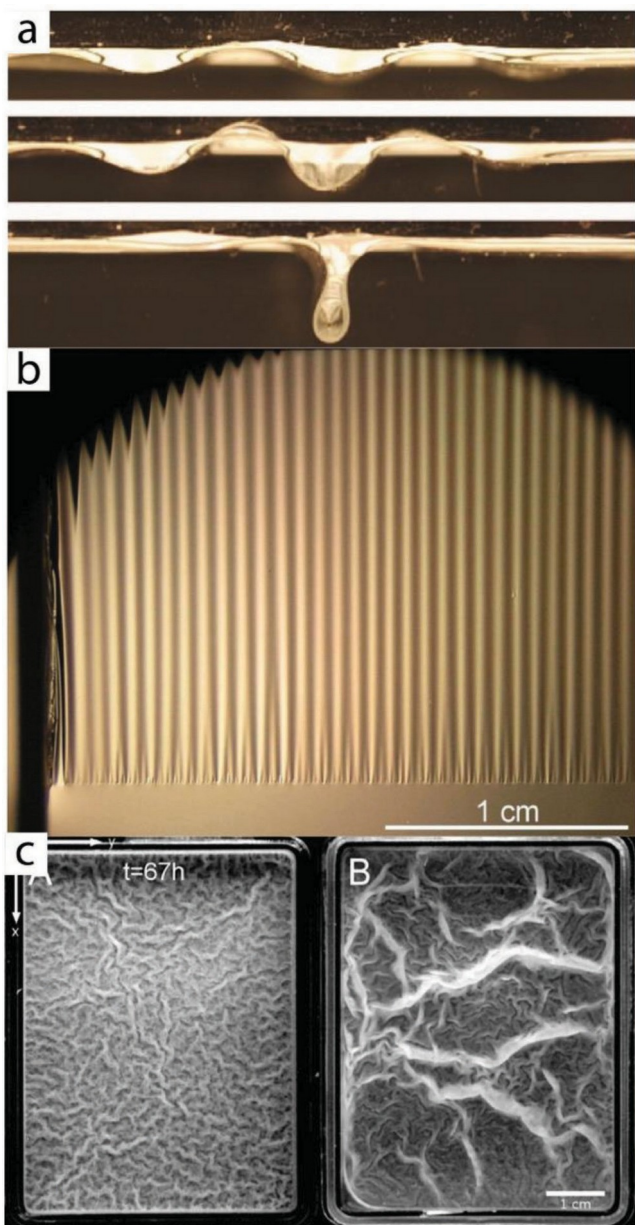
Figure 13. Buckling of thin films at the liquid–liquid interface in response to confinement. a) Thin, homogeneous films buckle sinusoidally at small compressions before concentrating stresses into a small number of highly curved folds at larger compressions. Reproduced with permission.[246] Copyright 2008, American Association for the Advancement of Science.
b) Competition between surface tension and bending energies result in a cascade of wrinkles of shrinking wavelength at the edges of a thin polymer film

sat on top of water. Reproduced with permission.[247] Copyright 2009, American Physical Society. c) Different strains of bacteria give rise to biofilms with

different wrinkling patterns, the mechanical properties of which can be quan- tified using Equation (21). Reproduced with permission.[248] Copyright 2011, The Authors. Published by the American Academy of Sciences.

$$Y_{3D} = 4.54 \frac{\gamma'}{2r} \tag{19}$$

Extending this continuum treatment further by treating a particle monolayer as a homogeneous film of thickness, $d \approx 2r$, where r is the particle radius, they related the Young's modulus and the bending modulus of the system

$$B = \frac{Y_{3D}d^3}{12(1 - \nu^2)} \tag{20}$$

In principle, combining Equations (18)–(20) allows Y_{3D} to be calculated from the wavelength of the wrinkles of the film and the liquid–fluid surface tension. While the Young's modulus of the interfacial assembly was not measured in the work, the group did show that, for monolayers of large particles, the bending modulus of the monolayer did exhibit a trivial scaling behavior that was largely independent of the material from which the particles were made. Remarkably, this relation was shown to hold for particle diameters ranging from 2.5 μm up to 7 mm.

It is worth noting that, in contrast with some other models, the bending modulus predicted by Vella et al. is independent of the wetting properties of the particles. A treatment by Kralchevsky et al. predicts significant dependence of the bending modulus of the monolayer upon the contact angle of the particle with the liquid–fluid interface.[251] Experimental measurements by other groups have not shown any depend- ence of bending modulus upon particle hydrophobicity.[252] It may be that measuring the bending modulus via buckling wavelength is an insufficiently sensitive method for the detection of contact-angle-dependence; the $B \sim \lambda^4$ dependence, combined with the rather nonergodic nature of solid particle monolayers, means error bars in measurements of bending moduli and wrinkle wavelengths are always large. As discussed below, it may also be the case that a continuum model is inap- propriate for describing particle monolayers in many instances, as discussed in the next paragraph.

For smooth particles smaller than 10 μm capillary interac- tions become vanishingly small and the treatment of Vella et al. becomes incorrect (**Figure 14**). This effect becomes remark- ably pronounced in the case of NPs. Leahy et al. were the first to notice this in their experiments on Au NP mono- and trilayers spread at the liquid–air interface. Applying a uniaxial compression to the Au NP assemblies on a Langmuir trough, they observed wrinkles of $\lambda \approx$ 1-4 μm, implying $B \approx 0.1$ kT. Complementary, direct measurements of the Young's modulus gave $Y_{3D} \approx 40$ MPa, implying $B \approx 250$ kT were a continuum treatment to hold for NPs. While the method used to measure Y_{3D} (i.e., the use of a Wilhelmy plate to measure the gra-

monolayers having continuum-like mechanical properties and, as such, standard continuum relations could be used to relate the Young's modulus and the bending modulus. They thus predicted a scaling relation for the Young's modulus of the particle monolayer

dient of the Π-*A* isotherm near buckling) has a number of deficiencies,[133,255,256] the value is within an order of magnitude of that observed elsewhere in the literature.[257] More impor- tantly, a bending modulus of 0.1 kT implies that coherent wrinkling ought to be destroyed by thermal fluctuations and that the system possesses an unphysically small $Y_{2D} \approx 0.1$ mN m^{-1}, almost three orders of magnitude smaller than the liquid–fluid surface tension. Note, also, that while direct measurements of the shear modulus of gold NP monolayers have not been
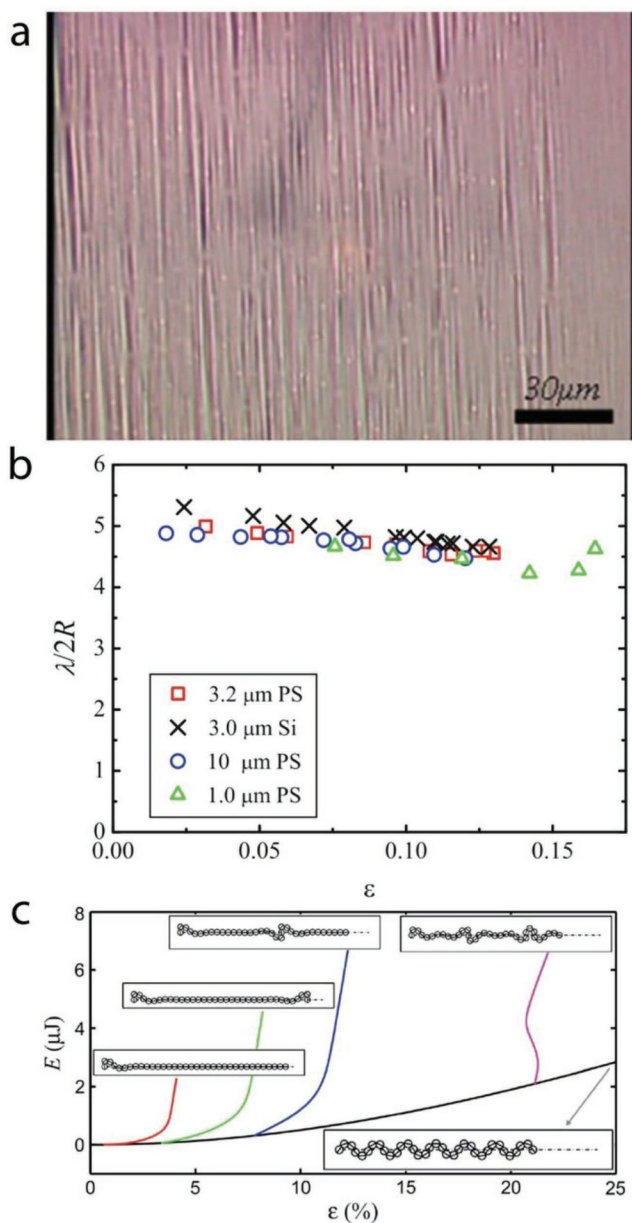
Figure 14. Noncontinuum behavior in buckling particle monolayers.
a) NP monolayers and trilayers at the liquid–fluid interface give bending moduli significantly smaller than would be expected from continuum relations. Reproduced with permission.[253] Copyright 2010, American Phys- ical Society. b,c) Tordesillas et al. found that buckling behavior in monolayers of colloidal PS and Si particles was best described by a force chain model. b,c) Reproduced with permission.[254] Copyright 2013, Springer Nature.

performed, shear measurements on solid-like particle mono- layers (e.g., Figure 12) find $G_{2D} \approx 0.1$-10 N m^{-1}, with this value typically being particle-size-invariant, inconsistent with any possible continuum mechanical treatment.

At the very least, the observations of Leahy et al., and the subsequent independent observations of similar phenomena by other groups,[246,258,259] show that there exist enormous anisotropies in the mechanical properties of NP monolayers when comparing in-plane and out-of-plane deformations.

This anisotropy naturally begs the question of the origin of the bending modulus in NP monolayers; it is not intuitively obvious why the resistance to bending of NP films is not, in most cases, zero. As observed by Mueggenburg et al., and other groups, the ligands bound to the NP surface clearly play a major role in governing the mechanical properties of the assemblies.[257,260] Ligands and polymer groups bound to the NP surface could, in principle, also be a source of the spontaneous curvature and bending modulus in these systems. The extreme anisot- ropy of the mechanical properties of NP monolayers also bring into question the validity of Equation (18) when describing the buckling behavior of small particles at liquid–fluid interfaces. Indeed, it is not clear if the wrinkles shown by these systems, e.g., Figure 14a, could even be reasonably described as sinusoidal.

One of the most compelling recent observations is that of Tordesillas et al.,[254] where the buckling behavior of a monolayer of micrometer-sized particles embedded in soft, elastic PDMS was investigated. Particles made of two different materials (polystyrene and silica) of three different sizes ($r = 0.5$, 1.5, and 5 μm) were studied. The wavelength of the buckling of the particle monolayers was found to scale linearly

with particle size, rather than the $\lambda \sim d^{\frac{3}{4}}$ scaling predicted by the continuum theory (Figure 14b). Further, λ was found to be independent of the material parameters of the particles used.

Taken together, these results led to a description of the buck- ling in terms of a force chain, rather than a homogeneous film. Here, the configuration of the chain is determined by the con- tacts between the individual particles and the condition that the particles cannot overlap one another when compressed. The buckling behavior predicted by their force chain model allows for single-wavelength, sinusoidal buckling, and also a range of different buckling behaviors (Figure 14c), more akin to that seen in NP monolayers.

To summarize, there are two major shortcomings in the existing descriptions of the buckling behavior of particle monolayers assembled at liquid–fluid interfaces. First, cur- rent theories do not give a satisfactory description of the phys- ical origin and magnitude of the bending modulus of particle monolayers, and how it relates to the shear and Young's moduli of the system. Existing theories currently only describe the behavior of particles that are large enough to generate strong interparticle capillary interactions via interfacial deformation ($r \gtrsim 5$ μm), in which case a simple model considering only particle geometry and surface tension describes the bending modulus of the monolayer. As particle size is reduced below this lengthscale, this model breaks down. Second, it is unclear whether, and under what circumstances, it is appropriate to model buckled particle monolayers as a continuum. The anoma- lously low measured bending modulus of nanoparticle mono- and trilayers, taken together with the particle-size independence of shear modulus seen in many particle assemblies, as well as the observations of Tordesillas et al., provide compelling evidence that using a continuum mechanical treatment to describe par- ticle monolayers is not, in many cases, a valid approach.

A number of experiments may prove insightful in this
area. There exist few, if any, measurements of the bending moduli of particle monolayers of intermediate size, i.e., in

the 0.05–1 µm range. Observations of the size dependence of the bending modulus of particle assemblies in this size regime would prove invaluable in understanding the physics of these systems. A study of the bending modulus of rough nanoparticle assemblies such as those investigated by Isa and co-workers, [90,261,262] which generate strong capillary interactions regardless of their size, would prove insightful to the role capillary interactions in governing the bending modulus of the monolayers. The nanoparticle surfactant system of Cui et al.,[213] in which particles are bound to the interface by polymer ligands of arbitrary size and structure, may prove an insightful system in helping us to understand the physical origins and magnitude of the bending moduli of par- ticle monolayers. Most simply, one would expect significantly different buckling behavior depending on whether the polymer ligands were significantly larger or significantly smaller than the particles to which they are bound.

5. Simple, All-Liquid Devices

Regardless of the finer points of binding energetics and the timescales of particle desorption, the assembly of nanomaterials at the liquid–fluid interface makes for a compelling route to change both the functional and mechanical properties

of the liquid–liquid interface. In addition to this, interfacial assemblies also impart structural metastability upon macro- scopic, all-liquid materials. These three properties allow us to construct devices made solely from liquids and complex liquid– liquid interfaces. In this section, we review several relatively simple systems that apply this principle, which also provides an opportunity to discuss the how the very general mechanism of surface tension–driven assembly of materials can be exploited using a broad range of phase separating systems.

5.1. Flow-Through, Biphasic, Particle-Stabilized Reactors

Perhaps the easiest-to-construct devices in this area are those based on Pickering emulsions. Pickering emulsions consist of one liquid dispersed within another, where colloidal par- ticles (typically, though not necessarily, micrometer-sized) are adsorbed to the liquid–liquid interface. The particles at the interface of these droplets are often (though not always) closely packed and irreversibly adsorbed, giving rise to non-spherical, physically robust droplets that are highly resistant to coalescence and Ostwald ripening.

Yang and co-workers have successfully developed a Pickering emulsion system with applications in biphasic chemical synthesis (**Figure 15**).[263–267] Silica microparticles, optionally
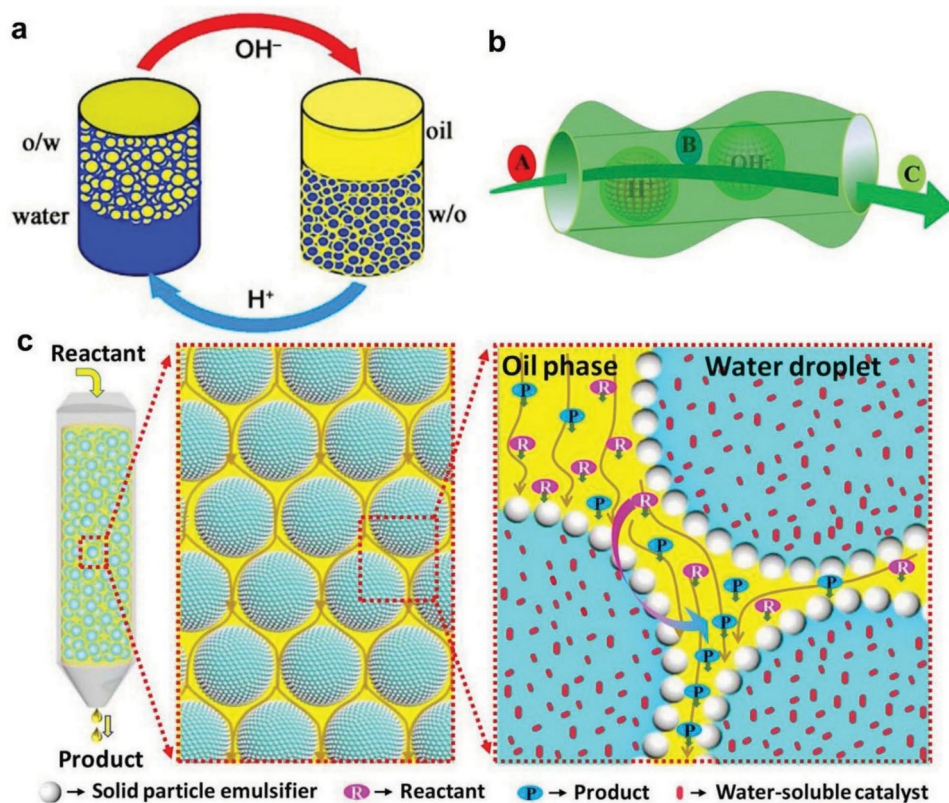

Figure 15. Catalyst-containing Pickering emulsions as flow-through chemical reactors. a) Catalyst separation and recycling using pH-responsive emulsion inversion. Reproduced with permission.[263] Copyright 2013, Wiley-VCH. b) One-pot cascade reaction system based on a Pickering emulsion (A is the substrate, B is the intermediate and C is the product). Reproduced with permission.[264] Copyright 2015, American Chemical Society.
c) A flow-through Pickering Emulsion system for catalytically accelerated oil–water biphasic reactions. Reproduced with

permission.[265] Copyright 2016, American Chemical Society.

coated with Pd NPs, were used to structure an emulsion that could be both oil-in-water and water-in-oil depending on the pH of the aqueous phase (Figure 15a).[263] Fundamentally, this required the particles to be switchable between hydrophobic and hydrophilic. Successful implementation of this allowed them to separate and recycle the sub-micrometer catalytic particles via triggered phase transfer and improved the efficacy of the catalysts. They further performed one-pot cascade reactions using a Pickering-emulsion-based system (Figure 15b).[264] Two parent, water-in-oil Pickering emulsions in which the aqueous phase was either acidic or basic, and in which the acid and base acted as either reactant or catalyst, were layered on top of one another. Reagent A (in the oil phase) could then be catalyzed stepwise into products B and C by diffusion between the alternating layers of droplets. In subsequent work, they then developed a flow-through Pickering emulsion reactor to process biphasic reactions under continuous flow (Figure 15c).[265] The group immobilized a catalyst inside silica NP-stabilized water droplets, and the droplets are in-turn immobilized within a column reactor. They then flowed an organic phase through the system that contained an oil-soluble reactant, demon- strating that H_2SO_4-catalyzed addition, HPA-catalyzed ring opening, and *Candida antarctica* lipase B-catalyzed reactions could all be performed at the oil–water interface, with reactant molecules and reaction products continuously flowed through, replenished, and extracted. A major benefit of such a system is the significantly reduced down-time that would typically be required in a batch process; the group also showed the droplets in their reaction vessel were remarkable durable, remaining usable for over 2000 h, and that the system exhibited greater- than-expected reaction rates compared to a batch reactor.

5.2. Aqueous Two-Phase Systems

The presence of a surface tension is not unique to immis- cible systems of oil and water. This phenomenon can also be observed in all-aqueous systems, in which pairs of hydro- philic polymers become immiscible with one another above a critical concentration. When the polymer concentration exceeds a threshold value, two immiscible aqueous phases that are enriched in either polymer are formed.[268] Typical properties of these systems are relatively high viscosities (1–100 mPa s), low surface tensions (0.1 mN m^{-1} or less) and excellent biocompatibility.[268–273]

Since Beijerinck first noted the phase separation of aqueous polymer solutions in 1896, aqueous two-phase systems (ATPS) have attracted significant attention in the physical, chemical and biological sciences.[276] Due to the different affinities of (bio)molecules toward the two aqueous phases, ATPS has become an important platform for the recovery and purifica- tion of specific materials such as plant and animal cells, fungi and their spores, proteins and nucleic acids. In the 1950s, Albertsson utilized ATPS to concentrate and separate different biomolecules.[277] In practice, the specificity of the partitioning of the desired molecule and contaminants between the two immiscible aqueous phases is often not high-enough to be useful from an applications stand-

point.[273] By modifying at least one of the phase-separating polymers with a functional

group that shows a high affinity for specific (bio)molecules, selective separation with better performance can be achieved by the ATPS.[273] In addition, free aptamer ligands can be added into ATPS to induce the partitioning shift for efficient, specific separation.[268]

The excellent biocompatibility of the system means that single-celled organisms can readily be cultured in ATPS. Recently, Takayama and co-workers used ATPS to culture cells in predetermined, printed patterns, providing a new platform for spatially defined delivery of molecules to living cells (**Figure 16**).[274,275,278–281] They used polyethylene glycol (PEG) and dextran as the immiscible components in their ATPS (perhaps the most widely used and well-characterized ATPS). They then generated a cell monolayer in a petri dish and covered the cells by printing the denser dextran solution within the PEG-rich phase (Figure 16a).[274] Appropriate formulation of the media ensured that reagents of interests were confined to the patterned dextran-rich phase without significant diffusion into the PEG-rich phase. The same principles were then used to pattern microbubbles in the dextran phase to disrupt the cell membrane by ultrasound, and to successfully generate cultured tissue structures within their ATPS (Figure 16b).[275]

The immiscibility of the two aqueous phases, combined with their potential applications in separations and the ability to assemble complex materials at the water–water interface also make ATPS attractive platforms for generating functional emulsions (**Figure 17**).[272,285] The low interfacial tension between the two aqueous phases (order 0.1 mN m^{-1}) is advan- tageous in some contexts but makes the generation of stable water-in-water capsules challenging, particularly when using microfluidics.[271,285,286] The recent work by Shum and co-workers makes for an extremely instructive basis for a discussion of the challenges in this field, as well as their solutions.[282,285,287–290]

One challenge in generating ATPS emulsions is driving the break up of the liquids into droplets; due to the low surface tension of the system, liquids in ATPS emerge from nozzles as threads even at low flow rates and Plateau–Rayleigh instabilities develop extremely slowly. To facilitate droplet formation in a microfluidics setup, Shum et al. used mechanical shaking at a controlled frequency (between 0 and 20 Hz) to successfully generate monodisperse water–water emulsions or water– water–water emulsions.[285,287–290] They further studied the effect of the assembly of material at the water–water interface on encapsulation efficiency and the structure of the materials their microfluidics setup produced. An interfacial precipitation reaction between calcium chloride and sodium carbonate and an interfacial gelation reaction using calcium chloride and alginic acid were studied. The elastic interfacial assemblies gave rise to greatly increased encapsulation efficiency, as well as the formation of complex, nonspherical droplet geometries and even elastic threads depending on the formation rate of the interfacial film and its resulting elastic properties.

The second major challenge in working with ATPS is that the low interfacial tension of the system and, hence,

low ΔE, makes assembling irreversibly adsorbed material at the interface extremely difficult, even when using micrometer-sized particles. As an alternative to surfactants or particles, polyelectrolytes bearing opposing charges, dispersed in opposing phases, can be used. The polyelectrolytes interact at the water–water
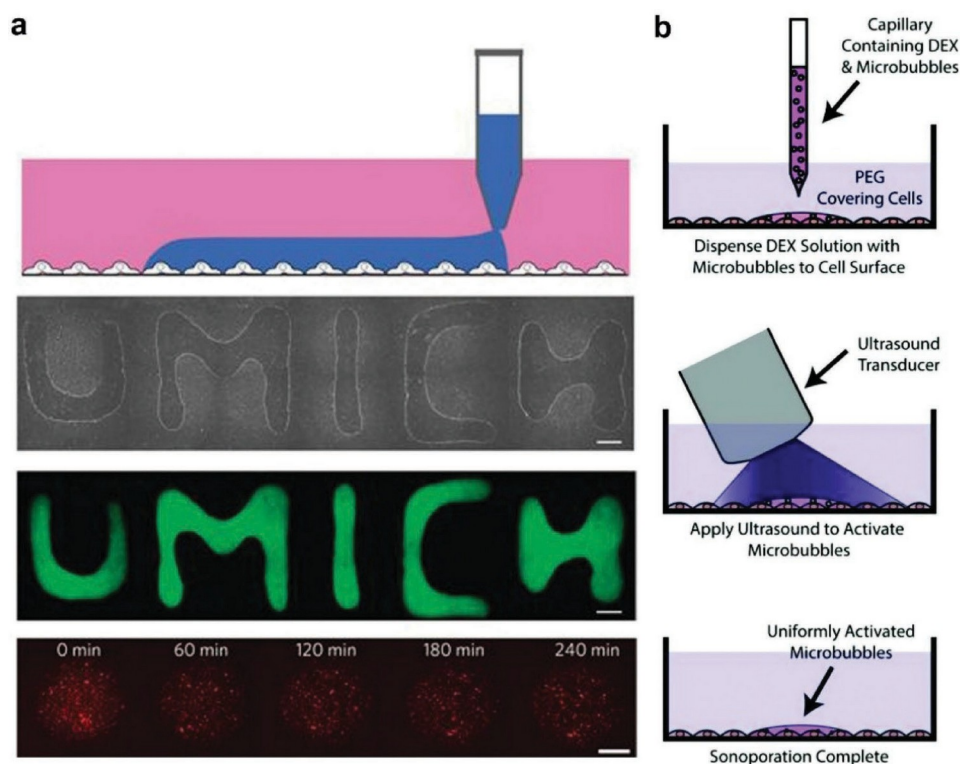
Figure 16. Aqueous two-phase systems as a platform for 3D printing and patterned cell culture. a) User-defined patterns of a reagent dispersed in a dextran-rich aqueous phase is deposited inside of a PEG-rich aqueous phase in a user-defined pattern on a cell monolayer using a 3D printer. Reproduced with permission.[274] Copyright 2009, Springer Nature. b) Patterned sonoporation is achieved by depositing microbubbles on cells in the dextran phase of the ATPS. The microbubbles are then activated by ultrasound to burst/shrink the cell. Reproduced with permission.[275] Copyright 2013, Wiley-VCH.

interface, forming a membrane-supported microcapsule (Figure 17a).[282] More complex polyelectrolytes, such as pro- teins and DNA strands, have also been successfully used as stabilizers to obtain stable microdroplets (Figure 17b).[291] Song et al. studied the interesting case of protein nanofibers that assemble at the water–water interface generating a colloi- dosome-like, 2D, crosslinked network.[290] Layer-by-layer growth of the crosslinked protein networks made it possible to control the thickness of the stabilized layer and thus the stability of the ATPS emulsions.[289] By modulating the fibril concentration and chemical properties of the network, budding and even division of the all-aqueous emulsion droplets was observed. Furthermore, release of encapsulated components in the ATPS emulsions could be triggered by changing the pH value or ionic strength of the surrounding environment.[289]

Several other groups have been successful in harnessing ATPS to generate bio-compatible, all-aqueous capsules. Zhang et al. used polyelectrolytes in an ATPS to fabricate tran- sient water–water–water double emulsions and found attractive electrostatic interactions between the polyelectrolytes and oppo- sitely charged, encapsulated molecules (in this case strepta- vidin) can delay the release of the molecules.[292] Hann et al. demonstrated that cells could be cultured in polyelectrolyte- stabilized ATPS microcapsules that were produced in relatively large volumes using a novel-yet-simple electrospray technique.[293] This ability to culture living matter in meta- stable capsules (or the complex geometries of

Tavana et al.), surrounded by a selectively permeable membrane, suggest

potential for ATPS as growth media with novel geometries that allow controlled exchange of metabolites between capsules containing colonies of different of organisms.

Recently, numerous groups have been successful in gener- ating aqueous two-phase Pickering emulsions. Hann, again with Stebe and Lee, used a positively charged polyelectrolyte ligand (PDADMAC) to anchor negatively charged silica NPs to the interface in a PEG-Dextran ATPS (Figure 17b).[283] The polyelectrolyte in their system binds electrostatically to the NPs, overcoming the negligible adsorption energy of the NPs and forming a rather brittle interfacial membrane that contrasts with the highly flexible polyelectrolyte–polyelectrolyte complexes. They further studied a complex system composed of a polycation with a mixture of a polyanion and a negatively charged NP in ATPS to tune the properties of the all-aqueous capsules. Douliez et al. crosslinked the particles at the inter- face of an ATPS Pickering emulsion to form hydrogelled drop- lets (Figure 17c).[284] They found that the hydrogel droplet was capable of reversible swelling and selective molecular uptake and exclusion. Combining the ability to tune geometry and mechanical properties of water-in-water droplets, combined with emerging 3D-printing technologies (discussed in Section 6.3), suggest the interesting potential to generate stimulus-responsive, all-liquid materials with heterogeneous mechanical, chemical, and even biological properties.

Most recently, O'Reilly and co-workers have leveraged a clever in-plane tiling of uniformly sized 2D poly(lactide) (PLA) platelets with tunable dimensions and differentiated coronal
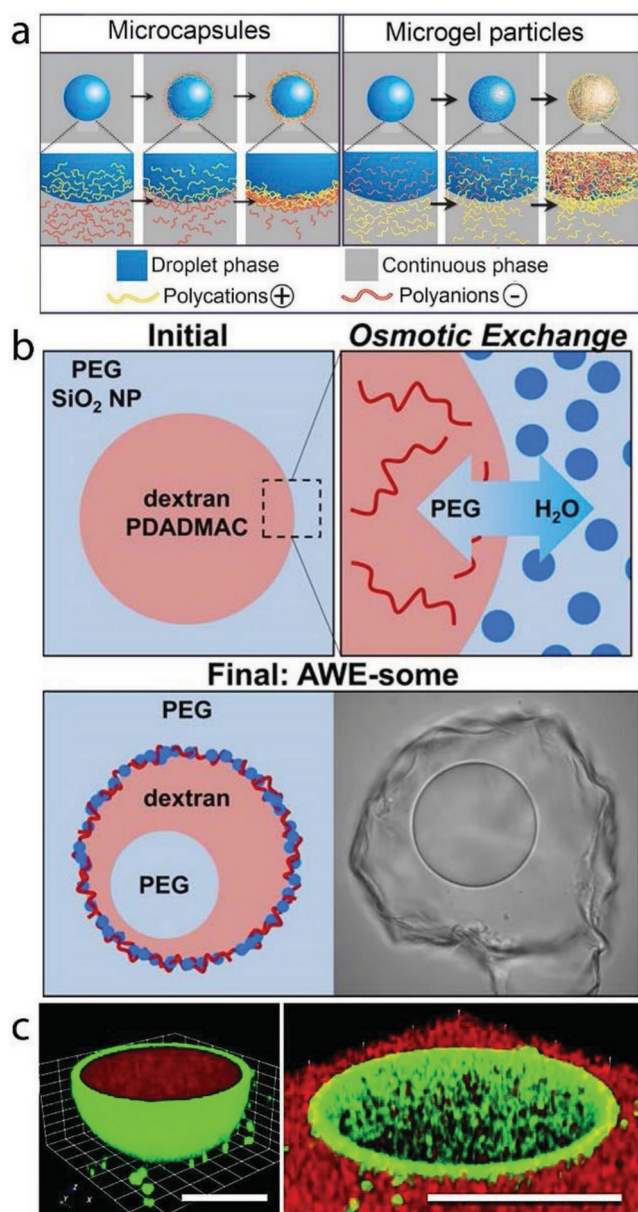
Figure 17. Stabilizing a range of different structures in aqueous two-phase systems. a) ATPS microcapsules and microgel droplets stabilized by a polyelectrolyte–polyelectrolyte complex formed at the water–water interface. Reproduced with permission.[282] Copyright 2016, American Chemical Society. b) ATPS emulsion stabilized by a polyelectrolyte-NP complex. Reproduced with permission.[283] Copyright 2017, American Chemical Society. c) Swellable hydrogel-containing ATPS Pickering emulsion droplet. Reproduced with permission.[284] Copyright 2018, Wiley-VCH.

chemistry to stabilize water-in-water emulsions consisting of immiscible solutions of poly(ethylene glycol) (PEG) and dextran (**Figure 18**).[294] Remarkably, the size of the self-assembled PLA platelets was deterministic in the dimension and stability of the emulsion, with the larger platelets yielding the most stable droplets with sizes ≈200 nm in diameter, regardless of the platelet's coronal chemistry. In future schemes, it is antici- pated that varying the chemistry presented by the platelets in either aqueous phase can be differentiated to manipulate their

physical properties and interactions in various settings, e.g., to meet stringent regulatory demands for safe pharmaceuticals, agrochemicals, cosmetics, and food.

5.3. Structured Oil-in-Oil Systems

Immiscible, nonaqueous solvents can also be used in the sepa- ration and purification of more hydrophobic materials with different affinities (**Figure 19**). Arguably the main application of oil-in-oil emulsions is to produce polymer (nano)particles by emulsion polymerization.[295] To reduce undesirable side reactions, water-sensitive or moisture-sensitive monomers can be encapsulated in an all-oil two-phase system. Lu et al. produced robust oil-in-oil capsules using a scalable process based on Pickering emulsification (Figure 19a).[296,297] Including guanidinium chloride (GuHCl) in the droplets as a partitioning inhibitor enabled them to achieve high encapsulation efficiency. Polyisobutylene was added to the continuous phase to act as a viscosity modifier, enhancing emulsion stability against coales- cence. The polymer shell was formed by interfacial polymeri- zation of isocyanates delivered through the continuous phase and polyamines from the droplet core. The components were first encapsulated within an oil-in-oil Pickering emulsion, before an interfacial polymerization reaction was used to yield GuHCl-containing, oil-in-oil capsules that were stable against coarsening via coalescence for 3 weeks. Binks and Tyowua used fumed silica particles to stabilize oil-in-oil Pickering emulsions.[298] By systematically varying the hydrophobicity of the particles in immiscible systems of (more polar) vegetable oil and (less polar) silicone oil, they found that relatively hydrophilic particles produced silicone-oil-in-vegetable-oil (S/V) emulsions, while highly hydrophobic particles produced V/S emulsions. This is consistent with the principle that the liquid that wets the particles less becomes the dispersed phase, as found in more familiar oil–water–particle systems.[299]

Zhang et al. further modified the continuous flow-through Pickering emulsion shown previously (Figure 15) by adapting it for use in nonaqueous systems (Figure 19b).[300] Droplets of micrometer-sized, catalyst-containing ionic liquid ([BMIM]PF$_6$) were dispersed in a nonaqueous continuous phase (octane) in a column reactor. The entirely nonaqueous nature of the system means that, rather than reactions taking place solely at the liquid–liquid interface, ionic-liquid-soluble reactant molecules can also access enzymes and catalysts dispersed within the droplet. The group then performed enzymatic enantioselective trans-esterification and CuI-catalyzed azide-alkyne cycload- dition as a proof-of-concept. As with the oil-in-water system, the nonaqueous emulsion flow-through system was found to be durable, functioning after 4000 h of use. The group also observed an 8 to 25-fold enhancement relative to batch processing methods.

Pentzer and co-workers recently studied oil-in-oil emulsions stabilized by 2D graphene oxide (GO) particles.[301] Through their coordination to both the edges and basal plane of graphene oxide, various primary alkyl amines can be chosen to establish which liquid will serve as the continuous phase of oil-in-oil emulsions

(i.e., nonpolar-in-polar or polar-in-nonpolar). Such emulsions were used to compartmentalize various reagents
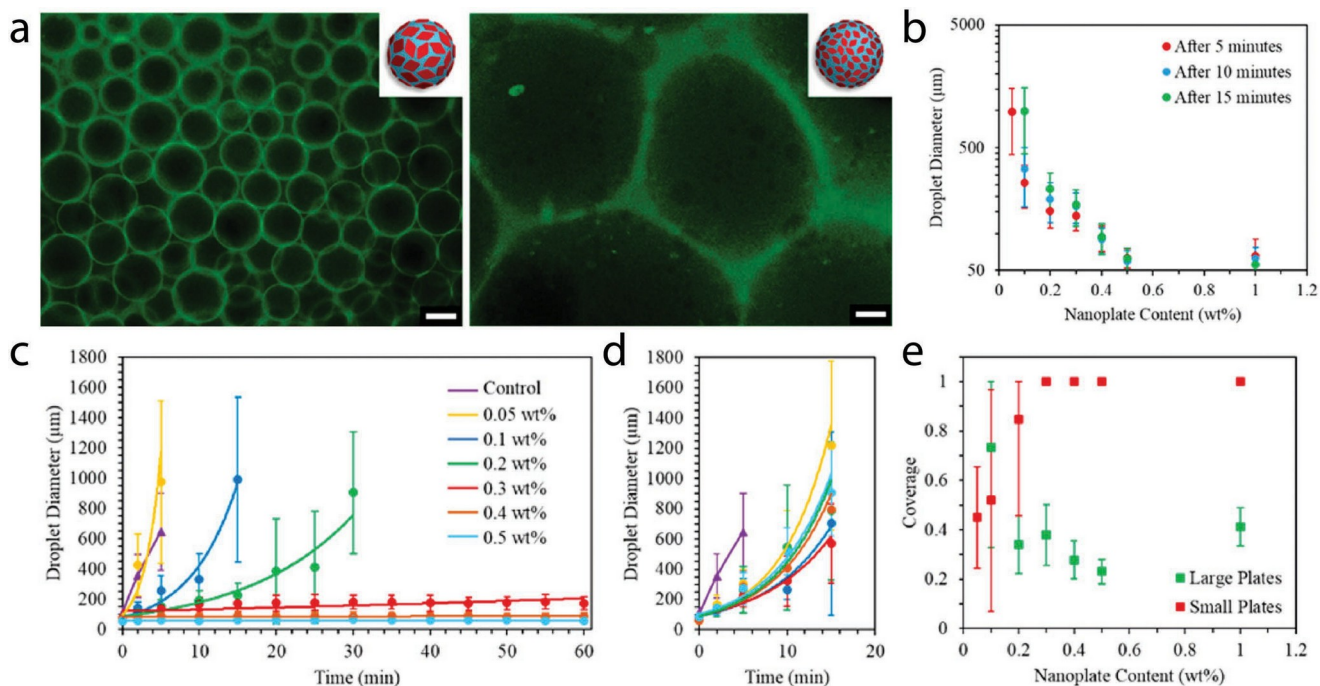
Figure 18. Water-in-water emulsions stabilized by PLA platelets of tunable dimensions. a) Fluorescence microscopy image of emulsion droplets prepared with large (left) and small (right) PLA platelets using 0.01wt % fluorescein-labeled dextran, where the green color indicates the dextran-rich phase. Scale bar = 200 μm. b) Emulsion droplet diameter as a function of nanoplate concentration and emulsion age. c,d) Emulsion droplet diameter using: c) large diamond platelets (prepared with 12% THF) and d) small diamond platelets (prepared with 0% THF) as a function of emulsion age. e) Mean areal density of platelets at the droplet surface as a function of nanoplate concentration. Reproduced under the terms of the CC-BY 4.0 license (https://creativecommons.org/licenses/by/4.0/).[294] Copyright 2018, The Authors. Published by the American Chemical Society.

of a chemical reaction, such that reaction occurred only upon physical agitation. The ability to switch continuous phases in such emulsions simply by switching the small-molecule amine surfactant interfacing with the GO came as a surprise, given prior work from Al-Lohedan and co-workers using 2D nano- clays and reactive surfactants that did not allow for a fine tuning of the interfacial interactions needed to invert oil-in-oil emul- sions.[302] GO-surfactant stabilized oil-in-oil emulsions have also been used for carrying out polymerizations, yielding in turn hierarchically complex and functional materials, including foams, capsules, and particulates.[303]

Such control over materials hierarchy has emerged as a powerful new design tool for generating functional materials for energy storage devices. Cai et al. carried out multistep macrosynthesis in a bijel to yield biphasic and hybrid electrolytes for Li-ion or Li-metal batteries, reminiscent of block copolymer electrolytes.[304] Luo et al. generated electrode– electrolyte hybrids comprised of an ionic liquid (as the elec- trolyte) encapsulated within a shell of reduced graphene oxide NPs (as the embedded electrode), making use of an interfacial polymerization of polyureas to bind the nanosheets together as a cohesive shell. Proof-of-concept experimentation led to determinations of their specific capacitances (80–127 F g^{-1}, depending on the temperature) in symmetric coin cells.[305] To enhance the capacitance of such devices, pairing the strategies of Pentzer and Clegg is likely a next step forward, particularly considering the availability of higher capacitance electrode

materials such as MXenes that can be integrated into the different materials architectures (although this has not yet been demonstrated for MXenes in oil-in-oil system).[306]

6. Reconfigurable, Time-Evolving, All-Liquid Materials

The simple devices in the previous section harnessed phase separation and assembly of material at the liquid–liquid interface to generate useful effects. However, they exploit the full capabilities of complex liquid–liquid interfaces to only a limited degree. Beyond simple functionality, complex interfaces are simultaneously highly deformable and can impart complex functionality, such as size- and charge-selective passage of molecules, plasmonic and magnetic response, and complex mechanical properties and structure. More interestingly still, the properties of the interface and, hence, the materials they stabilize and structure, can be altered in situ in response to any number of external stimuli. In the past few years, several groups have successfully exploited this principle to generate systems that time evolve, either in a preprogrammed manner or in response to external manipulation, and that contain com- partments that communicate with one another. These systems constitute a new class of materials that, if properly harnessed, will possess complex properties not offered by the existing, solid-based materials currently in use.
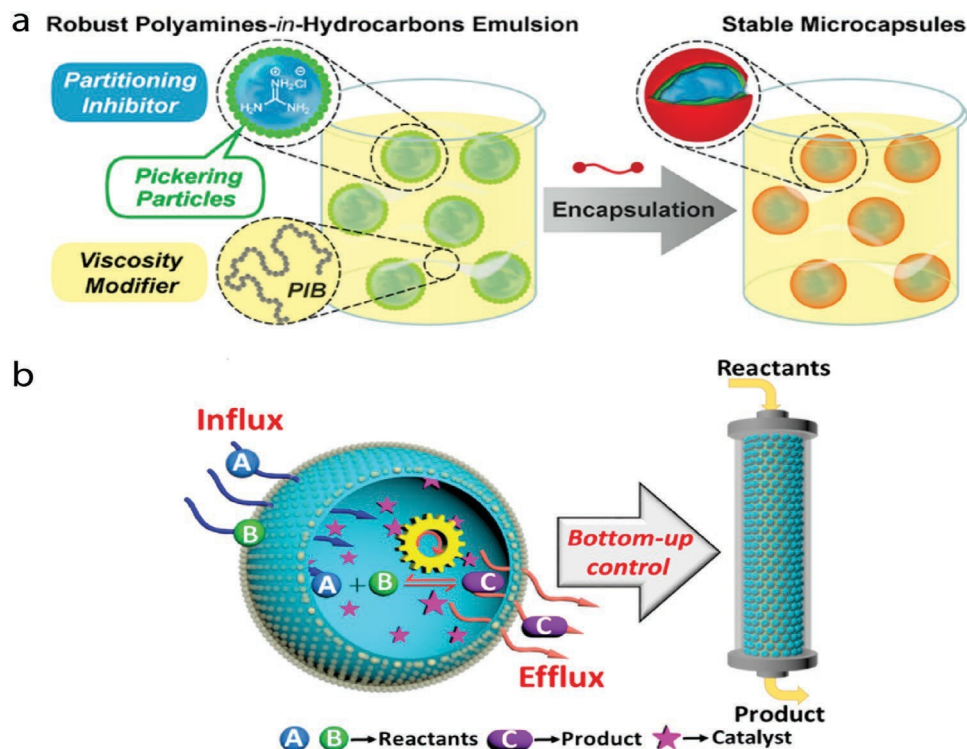
Figure 19. Nonaqueous Pickering emulsion systems for encapsulation and chemical synthesis. a) Hydrophopic compounds, such as diethylenetriamine can be encapsulated in oil-in-oil Pickering emulsions by using guanidinium chloride as a partitioning enhancer. High encapsulation efficiency and stability against coalescence and can then be achieved via an interfacial polymerization reaction, resulting in oil-in-oil capsules. Reproduced with permission.[296] Copyright 2018, American Chemical Society. b) A continuous flow catalysis system of Yang et al. can be adapted for use with wholly nonaqueous systems, using ionic liquid in oil Pickering emulsions as building blocks. Reproduced with permission.[300] Copyright 2017, American Chemical Society.

6.1. Assembling Reconfigurable Nanomaterials at the Liquid–Fluid Interface

Reconfigurability can be imparted upon complex liquid–fluid interfaces, and the systems they structure, by substituting one surface-active component for another, changing the binding energies of the materials that are adsorbed to the interface, or applying an external field. Proteins can be displaced from interfaces by low molecular weight surfactants.[307,308] In situ alteration of particle surface chemistry or solution conditions, e.g., pH, can result in a change of contact angle, desorption and, even phase transfer of particles.[263,309] External fields, e.g., electric and magnetic, can also drive the motion of particles at interfaces and, given sufficiently strong forces, their desorption.[309-311]

Nanoparticle surfactants (NPS), first developed by Cui et al., are a particularly promising set of reconfigurable, interfacially assembled nanomaterials with diverse functional properties.[213] This system consists of NPs and polymer surfactants that are initially dispersed in and confined to differing, immiscible phases, e.g., water and oil. The NPs and polymer surfactants, which bear complementary functional groups, interact with one another only at the oil–water interface, rendering the NPs irreversibly bound to the interface. The adsorbed NPs can be in both a liquid or a solid-like phase, with the corresponding surface stresses in the system being tunable from isotropic to anisotropic. NPs of arbitrary composition can be used as the

binding of the NP to the interface requires only that the surface groups of the particle be complementary to the functional group of the polymer (e.g., ion pairing). [312,313] Furthermore, mechanical and functional properties of the interface can be readily switched using any number of external triggers, such as light exposure and chemical triggers.[314]

In a recent work that advanced the material novelty and functional properties of NP surfactants, Zhang et al. generated magnetically responsive nanocrystal surfactant assemblies (**Figure 20**).[104] Fe_3O_4 nanocrystals that had been stripped of their coordinating ligands, leaving the underlying crystal-line structure of the nanocrystals intact ("naked" nanocrystals, NNCs) were dispersed in dimethylformamide (DMF).[315] The NNCs were attached to the DMF–oil interface using PDMS-NH_2 polymer surfactant ligands, which attached to the open metal coordination sites on the NNC surface, rendering the interface magnetically responsive (Figure 20a,b). The group imparted chemical tunability on the system by including a zwitterionic ligand in the nonpolar phase, which bound competitively to the NNCs' surface groups. As the concentration of zwitterionic ligand was increased, the desorption time of the particles in response to a compression decreased, allowing both the mechanical and mag-netic response of the interface to be controlled (Figure 20c).

Despite their negligible thickness, metallic NPs can impart optical properties upon interfaces due to plasmonic effects (**Figure 21**). Au NPs spontaneously adsorb to the interface formed between water and mixtures of hydrocarbons and
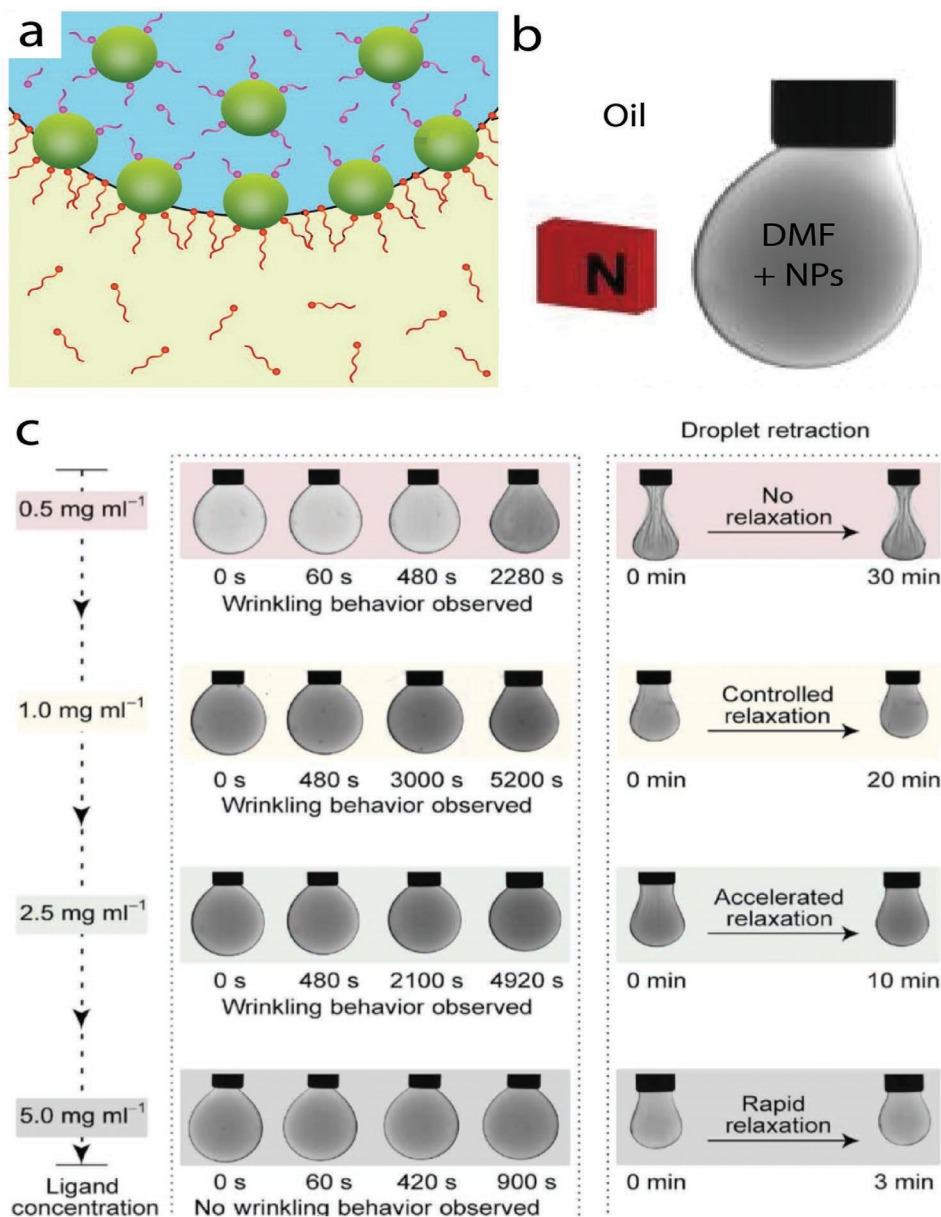
Figure 20. Reconfigurable mechanical properties and magnetic response in a NP surfactant monolayer. a) NP surfactants formed by the interfacial interaction between PDMS-NH$_2$ (red) and Fe$_3$O$_4$ naked nanocrystals (NNC, green). b) Solid NNC films render the interface magnetically responsive.
c) Introduction of a zwitterionic molecule that binds to the surface of the NNC, competing with the PDMS-NH$_2$, tunes the reversibility of the NNC adsorption and, hence, the mechanical and magnetic properties of the system. Reproduced with permission.[104] Copyright 2018, The Authors. Published by the American Association for the Advancement of Science.

1,2-dichloroethane (DCE), without requiring a binding ligand to be added to the nonpolar phase. At sufficiently high areal particle densities, surface plasmon resonance renders the Au NP assembly reflective (Figure 21a). Fang et al. used this effect to prepare a 2D liquid mirror by self-assembly of gold NPs at the interface between water and a mixture of heptane and DCE.[316] Here, particle size and the surface coverage of gold NPs binding at the interface deter- mined the mirror reflectivity, which reaches a maximum value when using 60 nm Au NPs to form the monolayer. In addition to possessing interesting optical properties, the assembled mono- layers are electronically conductive, exhibiting a transition from

insulating to conducting when the surface coverage becomes suffi- ciently high. Montelongo et al. recently used electric fields to tune the binding energy of the particles to the interface (Figure 21b). The group could then control the density and, hence, photonic response of gold NPs assembles at the oil–water interface in situ, producing a unique, reconfigurable, plasmonic NP liquid mirror (Figure 21c).[317] The paper and its extensive accompanying sup- porting information, as well as a recent review by the group,[318] also give a useful and fairly comprehensive summary of the fac- tors determining the binding energetics of particles at liquid– liquid interfaces.
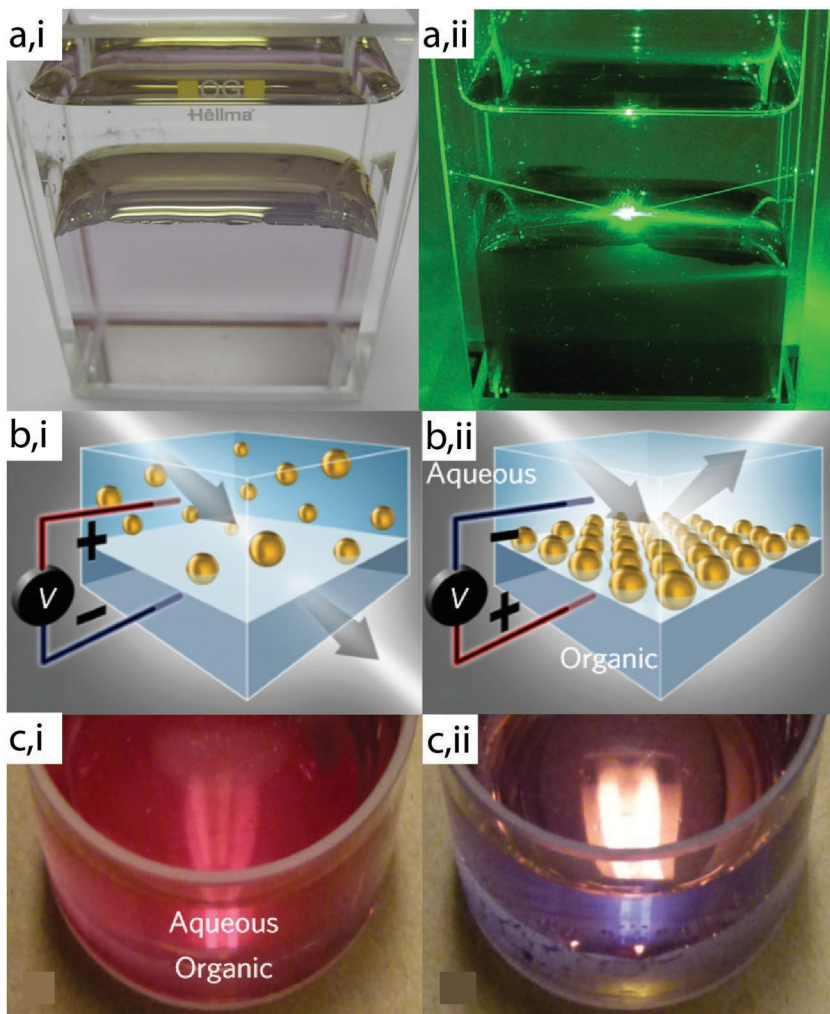
Figure 21. Reconfigurable, conductive, Au NP mirrors at liquid–fluid interfaces. a) Photographs of the monolayers prepared using 60 nm Au NPs at a [heptane + DCE]/water interface taken: i) in the absence of and ii) irradiated with laser light (λ = 532 nm). Reproduced with permission.[316] Copyright 2013, American Chemical Society. b) Schematic and c) implementation of changing NP areal density at the oil–water interface by using an electric field to control adsorption energy.
i) At low areal densities the interface transmits light, ii) while at high real densities surface plasmon resonances make it reflective. a–c) Reproduced with permission.[317] Copyright 2017, Springer Nature.

6.2. Molded and Printed Liquids Structure

by Reconfigurable Interfaces

Russell and co-workers have made significant progress in generating all-liquid systems with highly controlled macroscopic structure and interfacial components. Forth et al. adapted the nanoparticle surfactant system of Cui et al. to generate 3D-printed aqueous structures in a high viscosity (60 000 cSt at 25 °C) silicone oil (**Figure 22**a–d). They were able to produce aqueous threads in

The physical principle underlying the generation of 3D-printed water is ability of the jammed 2D assembly of NP surfactants to support anisotropic surface stresses.[319] Successful generation of 3D-printed liquid structures requires three criteria to be satis- fied. First, the binding energy holding the NPSs at the interface must be large suffi- ciently large that the particles are irreversibly bound to the liquid–liquid interfaces. This is achieved in nanoparticle surfactant systems by using a large, hydrophobic polymer sur- factant as a ligand to bind the particles to the interface. Second, the printed phase must emerge from the printhead as a thread. In a low-viscosity continuous phase, this requires the flow rate to be sufficiently high such that the liquid emerges from the needle as a jet. In a high-viscosity continuous phase, the needle must be dragged through the continuous phase sufficiently quickly such that capillary forces overcome surface ten- sion.[320,321] Finally, assembly of a high areal density of NPS onto the oil– water interface must be fast in comparison to the timescale of thread break up due to Plateau–Rayleigh instabilities. This timescale is given by

$$\tau = \frac{\alpha \mu r}{\gamma} \approx 0.01 - 100 \text{ s},$$ where μ is the viscosity of the external phase, r is the thread diameter, γ is the oil–water surface tension, and α is a numerical factor of order 10 that depends on the viscosity ratio between the internal and external phases.[322,323]

This final timescale makes 3D printing of liquids in a low viscosity oil rather chal- lenging, however there has been some success in this area. Toor et al. showed that NPS formation retarded the Plateau– Rayleigh instability of aqueous jets in toluene.[162] Liu et al. studied the stabilization of aqueous threads in toluene using cellulose nanocrystal surfactants (CNCSs).[163] CNCSs, which are notable for their extremely rapid interfacial assembly, were shown to be able to arrest the PR-instability completely even in oil with a range of diam- eters (10–1000 μm) and thread lengths up to several meters in length. Complex patterns, such as aqueous spirals, words, and branched structures such as T-junctions could all be produced this way (Figure 22b).[199]

low viscosity liquids (i.e., toluene), resulting in the formation of printed aqueous tubules in toluene. Shi et al. also applied the rapid interfacial assembly of CNCSs to develop a simple technique to produce all-liquid objects via molding. As with the printed tubules, the rapid assembly of a solid CNCS film at the oil–water interface arrested Plateau–Rayleigh instabilities, jamming the aqueous structures into the shape of a predesigned cavity with high fidelity (Figure 22c).[198]

The interfacial assemblies that stabilize these printed and molded liquid structures are inherently stimulus-responsive, most obviously to changes in pH.[314] This stimulus-response of the interfacial assembly renders the macroscopic liquid objects themselves reconfigurable. Both Shi et al. and Forth et al.
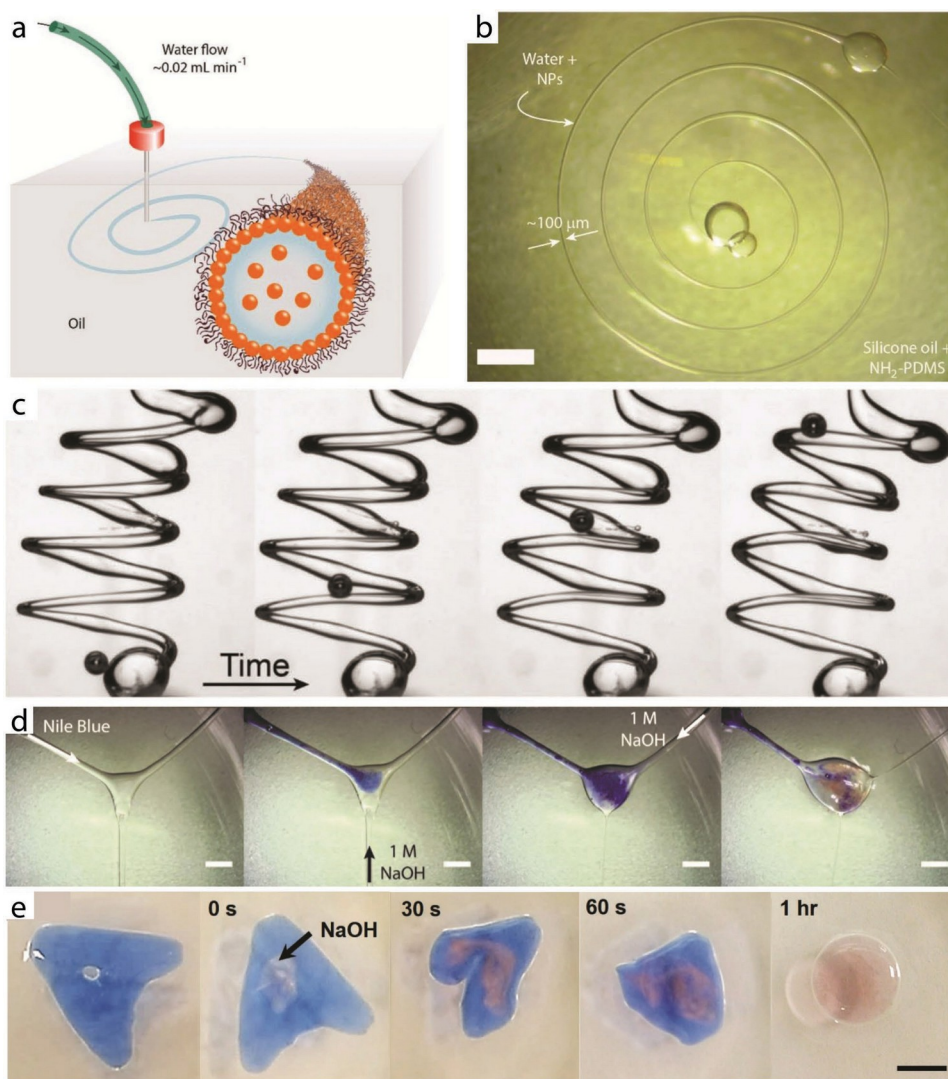
Figure 22. Printed and molded liquids structured by NP surfactant assembly at the oil–water interface. a) Schematic illustration of all-liquid 3D printing.
b) A 3D-printed aqueous spiral in silicone oil. Scale bar is 2 mm. c) An air bubble rises through a slowly sedimenting printed aqueous coil. d) An additively produced, branched aqueous thread has its structure and pH locally modified by the addition of NaOH. Scale bar is 5 mm. e) Aqueous letters made by all-liquid molding, buoyant in the CCl4 oil, is reconfigured by the addition of NaOH. Color in the system in d) and e) comes from Nile Blue dye, which turns red in response to an increase in pH. a–d) Reproduced with permission.[199] Copyright 2018, Wiley-VCH. e) Reproduced with permission.[198] Copyright 2018, Wiley-VCH.

showed that this allows the structures to be destructively and additively modified in situ (Figure 22d,e),[198,199] while Liu et al. showed how the pH of the aqueous phase could be used to tune the rate of NPS assembly at the oil–water interface in these systems.[163] The printed and molded liquids also possess a number of other interesting properties: the aqueous phase in the structures is biocompatible and, as discussed in previous sections, the mechanical properties of the NPs assemblies are highly tunable, meaning they are a promising platform for studies of the effects of geometry and interfacial interactions upon single-celled organisms. The liquid-biphasic nature of the constructs combined with their ability to guide the flow of pumped liquids in a manner reminiscent of vasculature suggest potential applications in chemical separations and as flow-through chemical reactors.

6.3. Reconfigurable Droplet-Based Materials with Complex Interfaces

Droplets also provide a platform for the generation of interface- rich, liquid-based, materials in which each droplet can form a communicating compartment within a macroscopic material. Relative to vascular printed and molded structures, cellular struc- tures of droplet-based materials are more robust and easier to manipulate but sacrifice the rate at which material can be flowed through the system. More precisely, the flow rate, V, through an emulsion is related to the droplet volume fraction, ϕ, and mean

droplet diameter, D, as $V \frac{(1 - \ ^3}{\phi^2} D^2$,[265] while the elastic modulus

of a cellular solid, E, increases rapidly with ϕ and, furthermore, cellular solids can undergo extensive plastic deformation without
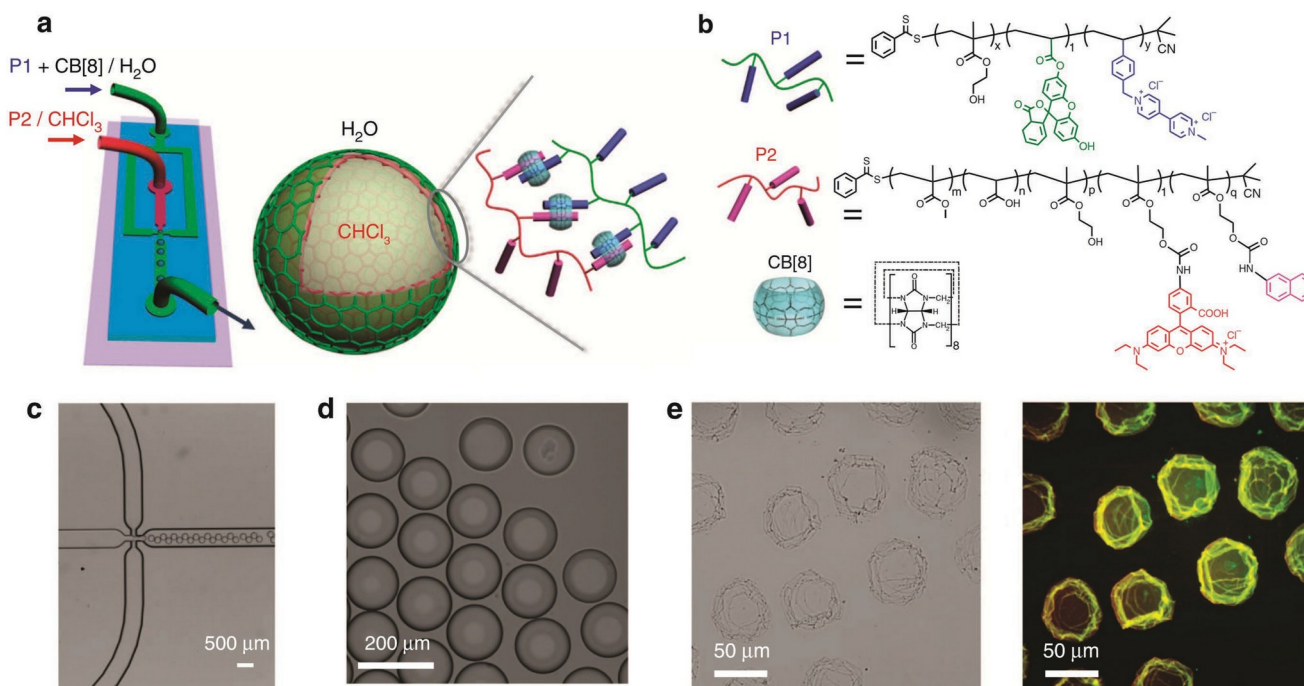
Figure 23. Microdroplet generation process using a microfluidic flow-focusing device. a) An aqueous phase containing CB[8] and copolymer P1. P1 is functionalized with methyl viologen (MV) and fluorescein o-acrylate (FOA). The aqueous phase intersects an immiscible chloroform phase containing copolymer P2, which is functionalized with naphthol (Np) and Rhodamine B. b) The chemical structures of P1, a hydrophilic poly(HEMA-co- StMV-co-FOA); P2, a hydrophobic poly(MMA-co-AA-co-HEMA-NP); and CB[8]. c) Formation of oil-in-water microdroplets generated at the microfluidic flow-focusing channel junction. d) The resulting monodisperse microdroplets ($d = 102.4 \pm 0.5$ μm). e) Bright field left) and fluorescence right) images of microcapsules formed after evaporation of the chloroform droplet, resulting in a collapsed capsule-like structure. Reproduced with permission.[326] Copyright 2014, Springer Nature.

failing structurally.[324,325] Droplet-based systems also have far greater surface area, allowing the functional properties of a com- plex interface to be exploited more readily.

Zheng et al. used microfluidic devices to fabricate mono- disperse water droplets of a controlled size in chloroform (**Figure 23**). The oil–water interface in this system was used to direct the co-assembly and crosslinking of a highly novel interfacial assembly. Polymeric materials P1 and P2 (Figure 23a) were bound to cucurbit[8]uril (CB[8]) at the chloroform–water interface via a supramolecular host–guest interaction ((Figure 23a,b), which in turn formed an encap- sulating skin at the droplet surface (Figure 23c–e).[326] The resulting elastic copolymer bilayer was responsive to the external UV light stimuli and able to assemble and disas- semble reversibly and could uniquely control the loading and release of cargos (i.e., drug molecules) encapsulated inside the droplets.

Selectively functionalized interfaces can also be used to guide the macroscopic self-assembly of droplets, allowing for the pre- programmed growth of droplet-based materials. Zhang et al. developed a simple system to allow for the sequential assembly of microdroplets, the surface of which were functionalized with DNA strands prehybridized in pairs (**Figure 24**).[327] Active strands on initiator droplets then displaced one of the paired strands and then released its complementary strand, which in turn activated the next droplet with the relative DNA sequence, akin to living polymerization (Figure 24a,b). This programmed

sequential self-assembly of microdroplets was shown to produce metastable nonequilibrium structures (Figure 24c–e). More importantly, the time and logic of the assembly process offers a new perspective on the synthesis of complex, soft materials.

Yang et al. recently investigated the manipulation, assembly, and triggered exchange of reagents between liquid droplets covered by a layer of jammed, nanoparticle surfactants (**Figure 25**).[328] The NPS consisted of amphiphilic nanocrystal heterostructures, such as Au/Fe$_3$O$_4$ or Au/PbS where the Au tip was selectively functionalized with 11-mercaptoundecanoic acid (MUA) to render it hydrophilic and with native oleic acid ligands on iron oxide or PbS establish to complementary hydrophobicity (Figure 25a). The droplets could be assembled into hierarchical structures and were addressable by mag- netic, optical, and electric fields (Figure 25b). Interestingly, a light beam could easily heat the local point of the droplet, both powering the rapid rotation of the droplets to turn it into a mechanical gear and triggering arrested coalescence allowing for exchange of reagents between droplets (Figure 25c). The flexibility of carrying different chemicals and designing morphological droplet clusters could be used to control the orientations of the droplets, interdroplet transport, mixing of contents and, ultimately, sequences of chemical reactions. Here, the interfacial jamming of the nanoparticle surfactants at the droplet surface was both the origin of metastability, triggered release, and response to external fields.
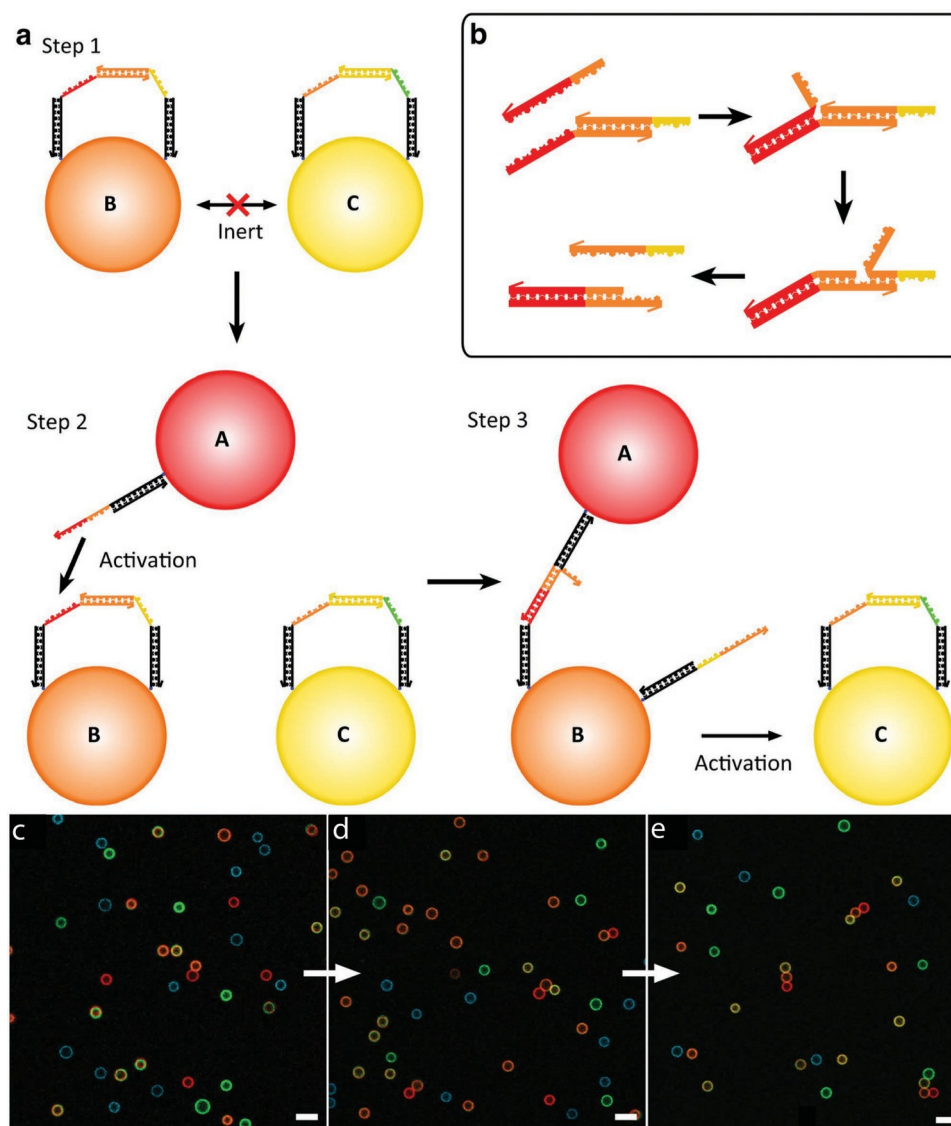
Figure 24. Preprogrammed self-assembly of DNA-functionalized droplets. a) Step 1: two droplets, B and C, with partially hybridized pairs of DNA strands are inert. Step 2: a droplet with an initiator strand, A, is introduced. Step 3: the initiator strand fully hybridizes to the protection strand on B through toehold strand displacement and frees the protected strand, leading to the activation of droplet B. The freed strand on B can then hybridize with the protection strand on C making a BπC bond and activating C for further binding. b) Schematic of the toehold displacement reaction showing details corresponding to the activation process of a). Representative confocal images of sequentially self-assembled structures. In the experiment, droplets A–E were false colored red, orange, yellow, green, and blue, respectively. Images taken after c) 10 h, d) 26 h, e) 74 h of incubation, respectively, showing the growth of triggered sequential self-assembly. Reproduced under the terms of the CC-BY 4.0 license (https://creativecommons.org/licenses/by/4.0/).[327] Copyright 2017, The Authors. Published by Springer Nature.

The stand-out development in the area of droplet-based materials, both from a conceptual and technical standpoint, is the work of Villar et al. (**Figure 26**).[329,330] The building blocks of their system are water droplets in oil, which are 3D printed into the desired structure (Figure 26a,b). The droplets are stabilized by a phospholipid monolayer (1,2-diphytanoyl-*sn*- glycero-3-phosphocholine), which renders the structures metastable against coalescence for several weeks. A notable feature of this system is the strongly attractive interactions between the hydrophobic tail groups of the adsorbed phospho- lipids, which drive the formation of bilayers (termed "droplet interface bilayers" or "DIBs").[331] DIB formation connects the

interfaces of the droplets and renders the droplets themselves faceted. The interfaces of the droplets were further func- tionalized by the addition of α-hemolysin pores, heptameric transmembrane protein pores that permit the size-selec- tive passage of ions and small molecules (Figure 26c). DIB formation combined with presence of α-hemolysin within the DIBs allows for communication between droplets. At the simplest level, this allows the flow of water due to gradients in osmotic pressure (leading to macroscopic evolution in the structure) and the conduction of ionic currents (Figure 26d,e). More complex implementations have since harnessed this capability to perform complex, multistep chemical reactions
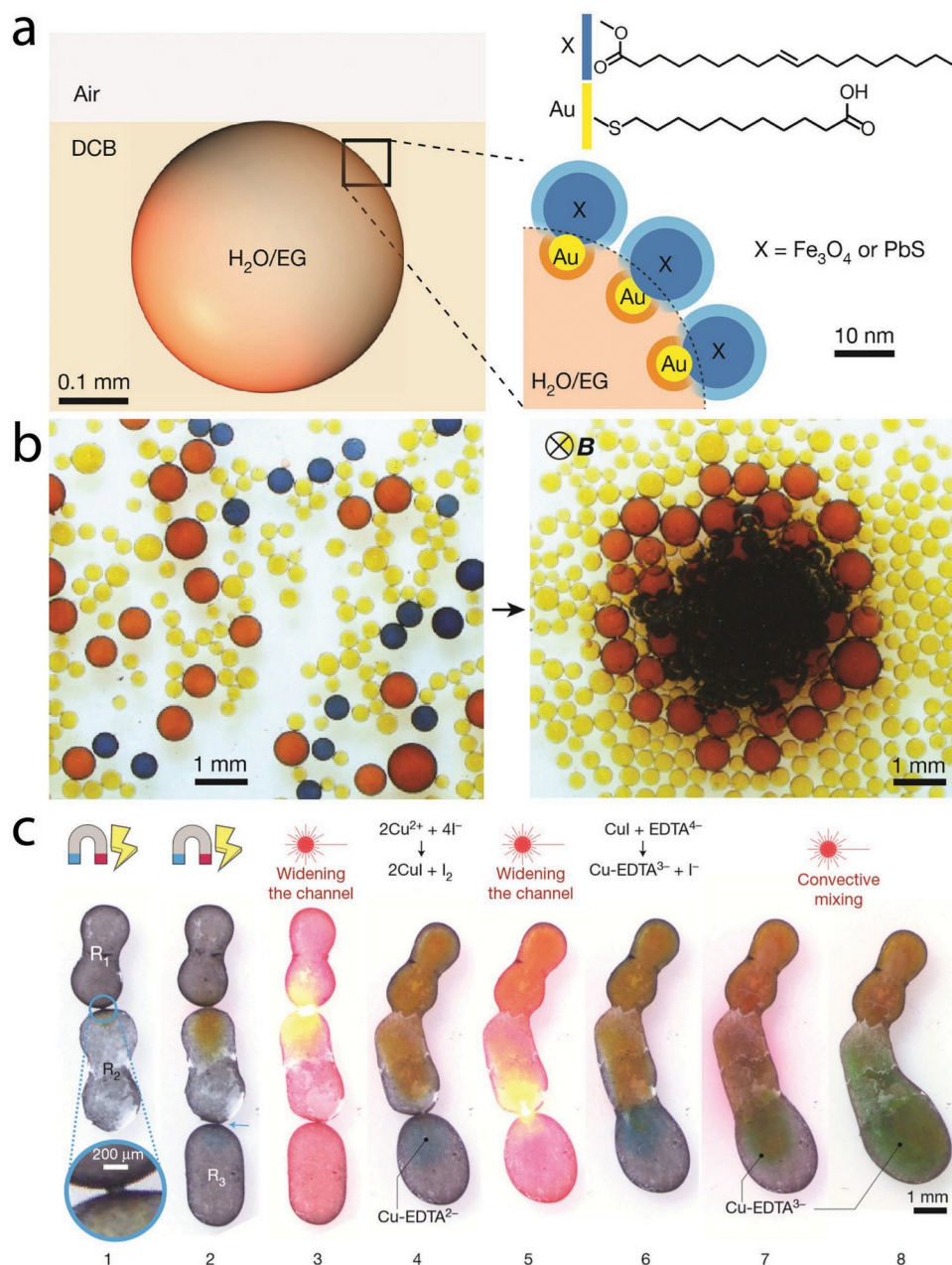
Figure 25. Multifunctional, multi-responsive NP surfactant stabilized droplets and interactions between them. a) Schematic of a H$_2$O/EG droplet covered with MUA–Au/X–OA surfactants and suspended near the 1,2-DCB–air interface (EG, ethylene glycol; MUA, mercaptoundecanoic acid; X, diamagnetic PbS or magnetic Fe$_3$O$_4$; OA, oleic acid; DCB, dichlorobenzene). b) Hierarchical assembly of three types of droplet that differ in magnetic susceptibility. A magnet is placed below the plane of the image. c) A sequence of reactions, $2Cu^{2+} + 4I^- \rightarrow 2CuI + I_2$ and $CuI + EDTA^{4-} \rightarrow Cu\text{-}EDTA^{3-} + I^-$. All three dumbbell-shaped reactors are filled with 1:1 v/v mixture of EG/H$_2$O. Reactor R_1 carries 1 μMol CuSO$_4$; R_2, 2 μmol KI; and R_3, 1 μmol Na$_4$EDTA. Reactors are oriented by the external magnetic field (magnet symbol; which is kept on for all frames 1–8 to keep the reactors in place) and electrostatically welded to one another via channels ≈200 μm wide (steps 1 and 2; connecting channel shown in the inset of 1). The channels are widened and the contents mixed by laser light (R_1–R_2 in steps 3 and 4; R_2–R_3 in steps 5–7). The yellow-brown color is due to I$_2$ produced in the first reaction; green is due to the mixing of I$_2$ with the Cu-EDTA^{3-} complex produced in the second reaction. Reproduced with permission.[328] Copyright 2018, Springer Nature.

is compartmentalized systems.[332,333] The encapsulation of living matter within these systems promises to add further complexity to the system, allowing for selective and spatially organized chemical communication between communities of microorganisms.[334]

7. Perspective and Conclusion

Herein, we have attempted to produce a coherent picture as to how complex liquid–liquid interfaces can be used to build all-liquid systems that have advanced functionality not offered by
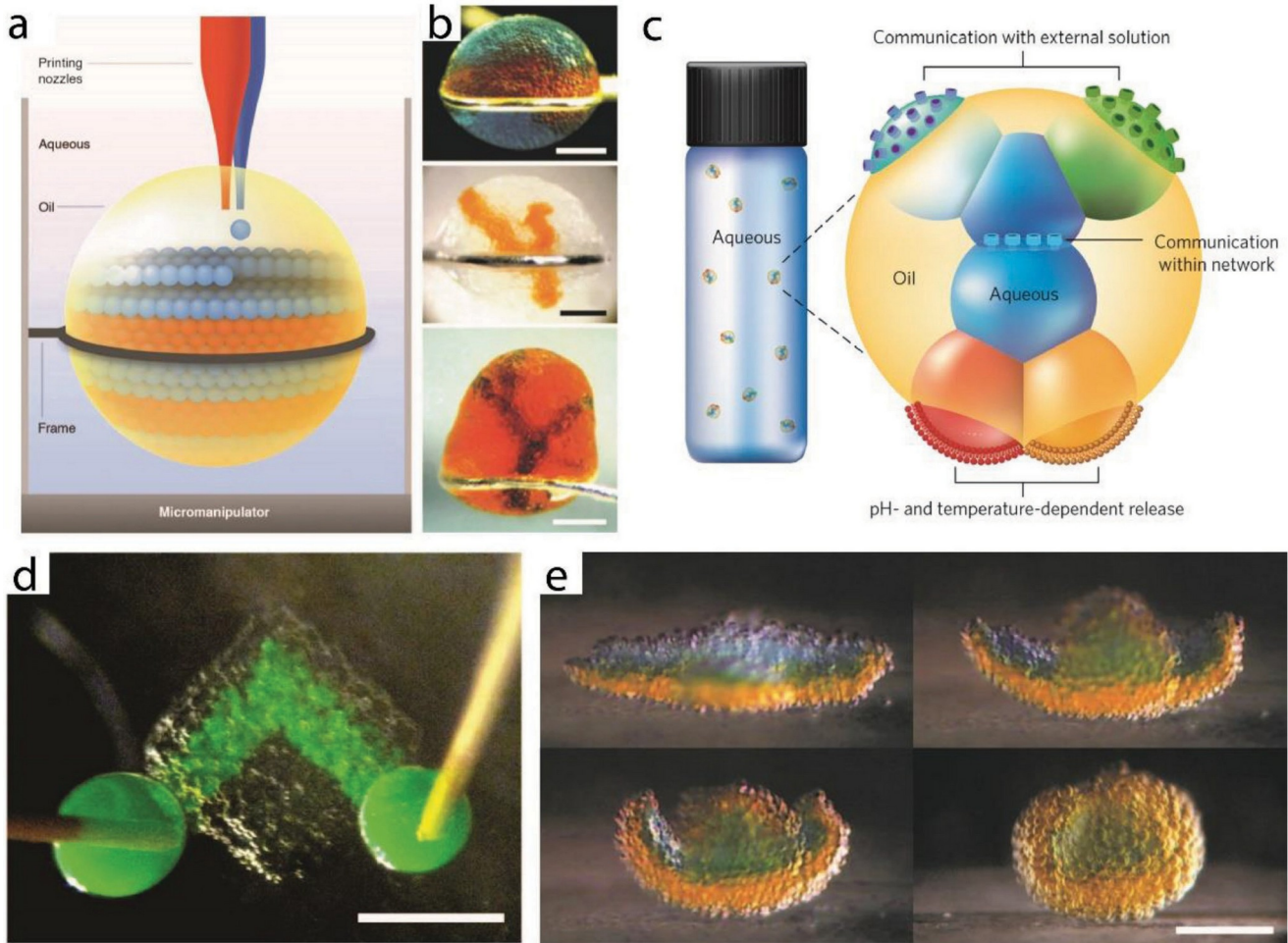
Figure 26. 3D-printed, tissue-like networks of communicating droplets. a) Phospholipid-stabilized aqueous droplets are 3D printed into complex structures. b) Photographs of the resulting printed tissue-like structures showing patterning of heterogeneous droplets. c) α-hemolysin pores adsorb to the oil–water interface, allowing for communication between droplets. This permits conduction of d) ionic currents and e) water between the droplets on macroscopic lengthscales, resulting in a material that exhibits programmable time evolution. a,b,d,e) Reproduced with permission.[329] Copyright 2013, American Association for the Advancement of Science. c) Reproduced with permission.[330] Copyright 2011, Springer Nature.

their solid counterparts. This requires an understanding of the nanoscale components that adsorb to liquid–fluid interfaces, the methods by which these interfaces can be characterized, how the collective behavior of the adsorbed materials alters the mechanical properties of the liquid–fluid interface and gives rise to complex macroscopic phenomena, and how these complex macroscopic phenomena can be harnessed towards a practical end.

The review is by no means exhaustive and there is a significant body of research in progress on systems with direct relevance to the topics discussed here. The bijel fibers of Haase et al., in which solvent transfer–induced phase separation (STRIPS) is used to produce macroscopic fibrils of bicontinuous interfacially jammed emulsions, show significant promise as flow-through chemical reactors.[335–337] The emulsion system of Swager et al. constitutes a compelling strategy for the development of reconfigurable, all-liquid materials.[338,339]

There also exist many potential synergies between synthetic biology and the materials sciences in this area. A striking

example of this is the water-in-water system of Cooper et al., in which injecting aqueous solutions of polyoxometalates into aqueous solutions of organic cations results in the formation of aqueous capsules in water surrounded by a selectively permeable, metallic membrane.[340] The phagocytosis-like process observed by Rodríguez-Arco et al. in Pickering emul- sions presents a promising strategy for the generation of complex reaction networks in emulsion-based systems. [341] All-liquid systems are also ideal platforms for the encapsulation of living and active matter,[342,343] such as the active gel systems that are the basis of an entire discipline of study.[342-348] Encap- sulating them within a complex structured liquid system has the potential to generate a new class of motile materials that drive themselves from equilibrium.

Systems built around unilamellar vesicles, be they polymer- or lipid-based, share a great many fundamental physical properties with droplets stabilized by complex interfaces, but introduce several practical and functional benefits. Recent work by Elani et al.,[334,349–351] as well as several others,[352,353] have shown how giant unilamellar phospholipid vesicles (and

droplet-based materials) can be manipulated into complex structures with tunable mechanical properties, in which com- partmentalization and communication between compartments gives rise to complex behavior. Polymer-based vesicles, which offer a number of practical advantages over their lipid-based counterparts, also show potential in generating active, soft, reconfigurable, materials.[354–357]

Complex interfaces are not the only method by which systems of immiscible liquids can be shaped into complex structures. Endoskeletal droplets, such as those studied by Spicer and co-workers, provide a compelling strategy to generate advanced liquid structures.[358–361] There is also huge scope for the applica- tion of novel physical effects. The rough particles of Zanini et al., which lack a well-defined contact angle and so impart spontaneous curvature upon a system in a history-dependent manner, are a particularly noteworthy example of this.[261,262]

This final section underscores a key point: there are myriad ways in which liquid-based systems can be structured, func- tionalized, and harnessed towards useful ends. Likewise, there is enormous potential in the field of structured liquids for new ideas, new science, and new technologies. It is in this final part that perhaps the need for progress is greatest. Nature already exploits complex liquid structures to generate constructs with functionality far beyond our current capabilities. However, many of the most scientifically e xciting d evelopments i n t he field o f s tructured l iquids r emain c onfined to th e la boratory. One of the stand-out shortcomings of the field is the absence of a "killer app" in the form of a commercially realizable product that lives up to the promise of the field. T his b eing s aid, t he sector is already starting to attract interest from venture capital; it may be that progress in this area is just around the corner.

Acknowledgements

[1] B. P. Binks, T. S. Horozov, *Colloidal Particles at Liquid Interfaces*, Cambridge University Press, Cambridge, UK **2008**.
[2] B. P. Binks, *Curr. Opin. Colloid Interface Sci.* **2002**, *7*, 21.
[3] M. Nagel, T. A. Tervoort, J. Vermant, *Adv. Colloid Interface Sci.* **2017**, *247*, 33.
[4] G. G. Fuller, J. Vermant, *Annu. Rev. Chem. Biomol. Eng.* **2012**, *3*, 519.
[5] L. M. C. Sagis, *Rev. Mod. Phys.* **2011**, *83*, 1367.
[6] J. H. J. Thijssen, J. Vermant, *J. Phys.: Condens. Matter* **2018**, *30*, 023002.
[7] S. Shi, T. P. Russell, *Adv. Mater.* **2018**, *30*, 1800714.
[8] S. Lach, S. M. Yoon, B. A. Grzybowski, *Chem. Soc. Rev.* **2016**, *45*, 4766.
[9] A. Marchand, J. H. Weijs, J. H. Snoeijer, B. Andreotti, *Am. J. Phys.* **2012**, *999*, 1705800.
[10] L. Gao, T. J. McCarthy, *Langmuir* **2009**, *25*, 14105.
[11] L. Gao, T. J. McCarthy, *Langmuir* **2006**, *22*, 6234.
[12] P. S. Clegg, E. M. Herzig, A. B. Schofield, S. U. Egelhaaf, T. S. Horozov, B. P. Binks, M. E. Cates, W. C. K. Poon, *Langmuir* **2007**, *23*, 5984.
[13] J. N. Israelachvili, *Intermolecular and Surface Forces*, Academic Press, Oxford, UK **2011**.
[14] D. F. Evans, H. Wennerström, *The Colloidal Domain: Where Physics, Chemistry, Biology, and Technology Meet*, Wiley-VCH, New York **1999**.
[15] G. Barnes, I. Gentle, *Interfacial Science: An Introduction*, Oxford University Press, Oxford, UK **2011**.
[16] S. Tcholakova, N. D. Denkov, A. Lips, *Phys. Chem. Chem. Phys.* **2008**, *10*, 1608.
[17] J. Forth, *Ph.D. Thesis: Insoluble Lipids and Colloidal Particles at the Oil-Water Interface*, University of Edinburgh, **2016**.
[18] A. F. Koretsky, P. M. I. Kruglyakov, *Izv. Sib. Otd. Akad., Nauk SSSR Ser. Khim. Nauk* **1971**, *2*, 139.
[19] Y. Lin, H. Skaff, T. Emrick, A. D. Dinsmore, T. P. Russell, *Science* **2003**, *299*, 226.
[20] M. Reeves, A. T. Brown, A. B. Schofield, M. E. Cates, J. H. J. Thijssen, *Phys. Rev. E* **2015**, *92*, 032308.
[21] E. M. Herzig, K. A. White, A. B. Schofield, W. C. K. Poon, P. S. Clegg, *Nat. Mater.* **2007**, *6*, 966.
[22] K. Stratford, R. Adhikari, I. Pagonabarraga, J.-C. Desplat, M. E. Cates, *Science* **2005**, *309*, 2198.
[23] K. D. Danov, P. A. Kralchevsky, *Adv. Colloid Interface Sci.* **2010**, *154*, 91.
[24] R. Aveyard, J. H. Clint, T. S. Horozov, *Phys. Chem. Chem. Phys.* **2003**, *5*, 2398.
[25] H. S. Wi, S. Cingarapu, K. J. Klabunde, B. M. Law, *Langmuir* **2011**, *27*, 9979.
[26] R. Aveyard, J. H. Clint, *J. Chem. Soc., Faraday Trans.* **1996**, *92*, 85.
[27] M. Oettel, S. Dietrich, *Langmuir* **2008**, *24*, 1425.
[28] M. Girotto, A. P. dos Santos, Y. Levin, *J. Phys. Chem. B* **2016**, *120*, 5817.
[29] D. F. Williams, J. C. Berg, *J. Colloid Interface Sci.* **1992**, *152*, 218.
[30] F. Bresme, H. Lehle, M. Oettel, *J. Chem. Phys.* **2009**, *130*, 214711.
[31] F. Bresme, M. Oettel, *J. Phys.: Condens. Matter* **2007**, *19*, 413101.
[32] V. Garbin, J. C. Crocker, K. J. Stebe, *J. Colloid*

      Interface Sci. **2012**,
      387, 1.

[33]   R. McGorty, J. Fung, D. Kaz, V. N. Manoharan,
      Mater. Today **2010**,
      13, 34.

[34]   P. Pieranski, *Phys. Rev. Lett.* **1980**, *45*, 569.

[35]   M. E. Leunissen, A. van Blaaderen, A. D.
      Hollingsworth, M. T. Sullivan,

P. M. Chaikin, *Proc. Natl. Acad. Sci. USA* **2007**,
                                   104, 2585.

[36]   R. Aveyard, J. H. Clint, D. Nees, V. N. Paunov,
      Langmuir **2000**, *16*, 1969.

[37] G. V. Bossa, K. Bohinc, M. A. Brown, S. May, *J. Phys. Chem. B* **2016**, *120*, 6278.

[38] D. Stamou, C. Duschl, D. Johannsmann, *Phys. Rev. E: Stat. Phys., Plasmas, Fluids, Relat. Interdiscip. Top.* **2000**, *62*, 5263.

[39] M. Cavallaro, L. Botto, E. P. Lewandowski, M. Wang, K. J. Stebe, *Proc. Natl. Acad. Sci. USA* **2011**, *108*, 20923.

[40] D. Ershov, J. Sprakel, J. Appel, M. A. Cohen Stuart, J. van der Gucht, *Proc. Natl. Acad. Sci. USA* **2013**, *110*, 9220.

[41] A. J. Hurd, *J. Phys. A: Math. Gen.* **1985**, *18*, L1055.

[42] F. H. Stillinger, *J. Chem. Phys.* **1961**, *35*, 1584.

[43] K. D. Danov, P. A. Kralchevsky, *J. Colloid Interface Sci.* **2006**, *298*, 213.

[44] D. Frydel, S. Dietrich, M. Oettel, *Phys. Rev. Lett.* **2007**, *99*, 118302.

[45] C. L. Wirth, E. M. Furst, J. Vermant, *Langmuir* **2014**, *30*, 2670.

[46] K. Masschaele, B. J. Park, E. M. Furst, J. Fransaer, J. Vermant, *Phys. Rev. Lett.* **2010**, *105*, 048303.

[47] B. J. Park, J. P. Pantina, E. M. Furst, M. Oettel, S. Reynaert, J. Vermant, *Langmuir* **2008**, *24*, 1686.

[48] D. Robinson, J. Earnshaw, *Phys. Rev. A* **1992**, *A46*, 2045.

[49] D. Robinson, J. Earnshaw, *Langmuir* **1993**, *9*, 1436.

[50] A. D. Law, D. M. A. Buzza, T. S. Horozov, *Phys. Rev. Lett.* **2011**, *106*, 128302.

[51] A. D. Law, M. Auriol, D. Smith, T. S. Horozov, D. M. A. Buzza, *Phys. Rev. Lett.* **2013**, *110*, 138301.

[52] D. Vella, L. Mahadevan, *Am. J. Phys.* **2005**, *73*, 817.

[53] L. Botto, E. P. Lewandowski, M. Cavallaro, K. J. Stebe, *Soft Matter* **2012**, *8*, 9957.

[54] E. P. Lewandowski, J. A. Bernate, A. Tseng, P. C. Searson, K. J. Stebe, *Soft Matter* **2009**, *5*, 886.

[55] L. Yao, N. Sharifi-Mood, I. B. Liu, K. J. Stebe, *J. Colloid Interface Sci.* **2015**, *449*, 436.

[56] N. Sharifi-Mood, I. B. Liu, K. J. Stebe, *Soft Matter* **2015**, *11*, 6768.

[57] H. H. Wickman, J. N. Korley, *Nature* **1998**, *393*, 445.

[58] M. M. Nicolson, R. C. Evans, *Math. Proc. Cambridge Philos. Soc.* **1949**, *45*, 288.

[59] H. Mollis Wickman, J. N. Korley, *Nature* **1998**, *393*, 445.

[60] M. M. Nicolson, *Math. Proc. Cambridge Philos. Soc* **1949**, *45*, 288.

[61] P. A. Kralchevsky, N. D. Denkov, K. D. Danov, *Langmuir* **2001**, *17*, 7694.

[62] H. Lehle, E. Noruzifar, M. Oettel, *Eur. Phys. J. E: Soft Matter Biol. Phys.* **2008**, *26*, 151.

[63] J. C. Loudet, A. G. Yodh, B. Pouligny, *Phys. Rev. Lett.* **2006**, *97*, 018304.

[64] A. B. D. Brown, C. G. Smith, A. R. Rennie, *Phys. Rev. E* **2000**, *62*, 951.

[65] E. P. Lewandowski, M. Cavallaro, L. Botto, J. C. Bernate, V. Garbin, K. J. Stebe, *Langmuir* **2010**, *26*, 15142.

[66] E. P. Lewandowski, J. A. Bernate, P. C. Searson, K. J. Stebe, *Langmuir* **2008**, *24*, 9302.

[67] J. C. Loudet, B. Pouligny, *Europhys. Lett.* **2009**, *85*, 28003.

[68] J. C. Loudet, A. M. Alsayed, J. Zhang, A. G. Yodh, *Phys. Rev. Lett.* **2005**, *94*, 018301.

[69] K. D. Danov, P. A. Kralchevsky, B. N. Naydenov, G. Brenn, *J. Colloid Interface Sci.* **2005**, *287*, 121.

[70] E. A. van Nierop, M. A. Stijnman, S. Hilgenfeldt, *Europhys. Lett.* **2005**, *72*, 671.

[71] R. Sear, S.-W. Chung, G. Markovich, W. Gelbart, J. Heath, *Phys. Rev. E* **1999**, *59*, R6255.

[72] W. M. Gelbart, R. P. Sear, J. R. Heath, S. Chaney, *Faraday Discuss.* **1999**, *112*, 299.

[73] S. Cheng, G. S. Grest, *J. Chem. Phys.* **2012**, *136*, 214702.

[74] H. Lehle, M. Oettel, *J. Phys.: Condens. Matter* **2008**, *20*, 404224.

[75] H. Lehle, M. Oettel, S. Dietrich, *Europhys. Lett.* **2006**, *75*, 174.

[76] D. L. Cheung, S. A. F. Bon, *Phys. Rev. Lett.* **2009**, *102*, 066103.

[77] D. M. Mitrinovic´, A. M. Tikhonov, M. Li, Z. Huang, M. L. Schlossman, *Phys. Rev. Lett.* **2000**, *85*, 582.

[78] S. Damodaran, *Curr. Opin. Colloid Interface Sci.* **2004**, *9*, 328.

[79] R. J. K. Udayana Ranatunga, R. J. B. Kalescky, C. Chiu, S. O. Nielsen, *J. Phys. Chem. C* **2010**, *114*, 12151.

[80] K. A. Tay, F. Bresme, *J. Am. Chem. Soc.* **2006**, *128*, 14166.

[81] L. Isa, E. Amstad, K. Schwenke, E. Del Gado, P. Ilg, M. Kröger, E. Reimhult, *Soft Matter* **2011**, *7*, 7663.

[82] X. Yong, *Langmuir* **2015**, *31*, 11458.

[83] Y. Jiang, T. I. Löbling, C. Huang, Z. Sun, A. H. E. Müller, T. P. Russell, *ACS Appl. Mater. Interfaces* **2017**, *9*, 33327.

[84] E. Guisasola, A. Baeza, M. Talelli, D. Arcos, M. Moros, J. M. de la Fuente, M. Vallet-Regí, *Langmuir* **2015**, *31*, 12777.

[85] F. Pinaud, K. Geisel, P. Massé, B. Catargi, L. Isa, W. Richtering, V. Ravaine, V. Schmitt, *Soft Matter* **2014**, *10*, 6963.

[86] R. W. Style, L. Isa, E. R. Dufresne, *Soft Matter* **2015**, *11*, 7412.

[87] K. Geisel, L. Isa, W. Richtering, *Langmuir* **2012**, *28*, 15770.

[88] S. Huang, K. Gawlitza, R. von Klitzing, L. Gilson, J. Nowak, S. Odenbach, W. Steffen, G. K. Auernhammer, *Langmuir* **2016**, *32*, 712.

[89] L. Scheidegger, M. Á. Fernández-Rodríguez, K. Geisel, M. Zanini, R. Elnathan, W. Richtering, L. Isa, *Phys. Chem. Chem. Phys.* **2017**, *19*, 8671.

[90] S. A. Vasudevan, A. Rauh, L. Barbera, M. Karg, L. Isa, *Langmuir* **2018**, *34*, 886.

[91] L. N. Arnaudov, O. J. Cayre, M. A. Cohen Stuart, S. D. Stoyanov, V. N. Paunov, *Phys. Chem. Chem. Phys.* **2010**, *12*, 328.

[92] A. Maestro, E. Guzmán, F. Ortega, R. G. Rubio, *Curr. Opin. Colloid Interface Sci.* **2014**, *19*, 355.

[93] V. N. Paunov, *Langmuir* **2003**, *19*, 7970.

[94] L. Isa, F. Lucas, R. Wepf, E. Reimhult, *Nat. Commun.* **2011**, *2*, 438.

[95] Y. Chai, A. Lukito, Y. Jiang, P. D. Ashby, T. P. Russell, *Nano Lett.* **2017**, *17*, 6453.

[96] M. Cui, C. Miesch, I. Kosif, H. Nie, P. Y. Kim, H. Kim, T. Emrick, T. P. Russell, *Nano Lett.* **2017**, *17*, 6855.

[97] G. Lin, X. Zhu, U. Anand, Q. Liu, J. Lu, Z. Aabdin, H. Su, U. Mirsaidov, *Nano Lett.* **2016**, *16*, 1092.

[98] P. Y. Kim, A. E. Ribbe, T. P. Russell, D. A. Hoagland, *ACS Nano* **2016**, *10*, 6257.

[99] K. Vondermassen, J. Bongers, A. Mueller, H. Versmold, *Langmuir* **1994**, *10*, 1351.

[100] C. R. Iacovella, R. E. Rogers, S. C. Glotzer, M. J. Solomon, *J. Chem. Phys.* **2010**, *133*, 164903.

[101] L. Costa, G. Li-Destri, N. H. Thomson, O. Konovalov, D. Pontoni, *Nano Lett.* **2016**, *16*, 5463.

[102] A. Huerre, F. Cacho-Nerin, V. Poulichet, C. E. Udoh, M. De Corato, V. Garbin, *Langmuir* **2018**, *34*, 1020.

[103] L. Costa, G. Li-Destri, N. H. Thomson, O. Konovalov, D. Pontoni, *Nano Lett.* **2016**, *16*, 5463.

[104] Z. Zhang, Y. Jiang, C. Huang, Y. Chai, E. Goldfine, F. Liu, W. Feng, J. Forth, T. E. Williams, P. D. Ashby, T. P. Russell, B. A. Helms, *Sci. Adv.* **2018**, *4*, eaap8045.

[105] C. Huang, Y. Y. Chai, Y. Jiang, J. Forth, P. D. Ashby, M. M. L. Arras, K. Hong, G. S. Smith, P. Yin, T. P. Russell, *Nano Lett.* **2018**, *18*, 2525.

[106] D. G. Schultz, X. M. Lin, D. Li, J. Gebhardt, M. Meron, P. J. Viccaro, B. Lin, *J. Phys. Chem. B* **2006**, *110*, 24522.

[107] S. Kubowicz, M. A. Hartmann, J. Daillant, M. K. Sanyal, V. V. Agrawal, C. Blot, O. Konovalov, H. Möhwald, *Langmuir* **2009**, *25*, 952.

[108] Y. Lin, A. Böker, H. Skaff, D. Cookson, A. D. Dinsmore, T. Emrick, T. P. Russell, *Langmuir* **2005**, *21*, 191.

[109] O. Marnette, E. Perez, F. Pincet, G. Bryant, *Colloids Surf. A* **2009**, *346*, 208.

[110] A. Donev, F. H. Stillinger, S. Torquato, *Phys. Rev. Lett.* **2005**, *95*, 090604.

[111] B. D. Lubachevsky, F. H. Stillinger, *J. Stat. Phys.* **1990**, *60*, 561.

[112] S. Torquato, F. H. Stillinger, *Rev. Mod. Phys.* **2010**, *82*, 2633. [113] B.-J. Lin, L.-J. Chen, *J. Chem. Phys.* **2007**, *126*, 034706.

[114] A. T. Gray, E. Mould, C. P. Royall, I. Williams, *J. Phys.: Condens. Matter* **2015**, *27*, 194108.

[115] M. P. Miklius, S. Hilgenfeldt, *Phys. Rev. Lett.* **2012**, *108*, 015502.

[116] S. Torquato, T. M. Truskett, P. G. Debenedetti, *Phys. Rev. Lett.* **2000**, *84*, 2064.

[117] A. Taloni, Y. Meroz, A. Huerta, *Phys. Rev. E* **2015**, *92*, 022131.

[118] M. Ozawa, T. Kuroiwa, A. Ikeda, K. Miyazaki, *Phys. Rev. Lett.* **2012**, *109*, 205701.

[119] S. Atkinson, F. H. Stillinger, S. Torquato, *Proc. Natl. Acad. Sci. USA* **2014**, *111*, 18436.

[120] T. M. Truskett, S. Torquato, S. Sastry, P. G. Debenedetti, F. H. Stillinger, *Phys. Rev. E* **1998**, *58*, 3083.

[121] C. A. Murray, W. O. Sprenger, R. A. Wenk, *Phys. Rev. B* **1990**, *42*, 688.

[122] S. Torquato, F. H. Stillinger, *Phys. Rev. E* **2003**, *68*, 041113.

[123] H. Zheng, S. A. Claridge, A. M. Minor, A. P. Alivisatos, U. Dahmen, *Nano Lett.* **2009**, *9*, 2460.

[124] M. J. Williamson, R. M. Tromp, P. M. Vereecken, R. Hull, F. M. Ross, *Nat. Mater.* **2003**, *2*, 532.

[125] N. de Jonge, F. M. Ross, *Nat. Nanotechnol.* **2011**, *6*, 695.

[126] J. D. Berry, M. J. Neeson, R. R. Dagastine, D. Y. C. Chan, R. F. Tabor, *J. Colloid Interface Sci.* **2015**, *454*, 226.

[127] C. Gu, L. Botto, *Soft Matter* **2016**, *12*, 705.

[128] S. Knoche, D. Vella, E. Aumaitre, P. Degen, H. Rehage, P. Cicuta, J. Kierfeld, *Langmuir* **2013**, *29*, 12463.

[129] K. D. Danov, R. D. Stanimirova, P. A. Kralchevsky, K. G. Marinova, N. A. Alexandrov, S. D. Stoyanov, T. B. J. Blijdenstein, E. G. Pelan, *J. Colloid Interface Sci.* **2015**, *440*, 168.

[130] J. Hegemann, S. Knoche, S. Egger, M. Kott, S. Demand, A. Unverfehrt, H. Rehage, J. Kierfeld, *J. Colloid Interface Sci.* **2018**, *513*, 549.

[131] R. F. Tabor, F. Grieser, R. R. Dagastine, D. Y. C. Chan, *J. Colloid Interface Sci.* **2012**, *371*, 1.

[132] J. Forth, A. Toor, T. P. Russell, unpublished.

[133] P. Cicuta, D. Vella, *Phys. Rev. Lett.* **2009**, *102*, 138302.

[134] S. Kutuzov, J. He, R. Tangirala, T. Emrick, T. P. Russell, A. Böker, *Phys. Chem. Chem. Phys.* **2007**, *9*, 6351.

[135] C. Huang, M. Cui, Z. Sun, F. Liu, B. A. Helms, T. P. Russell, *Langmuir* **2017**, *33*, 7994.

[136] Y. Zhang, S. Wang, J. Zhou, R. Zhao, G. Benz, S. Tcheimou, J. C. Meredith, S. H. Behrens, *Langmuir* **2017**, *33*, 4511.

[137] M. S. Manga, T. N. Hunter, O. J. Cayre, D. W. York, M. D. Reichert, S. L. Anna, L. M. Walker, R. A. Williams, S. R. Biggs, *Langmuir* **2016**, *32*, 4125.

[138] K. Du, E. Glogowski, T. Emrick, T. P. Russell, A. D. Dinsmore, *Langmuir* **2010**, *26*, 12518.

[139] N. Bizmark, M. A. Ioannidis, D. E. Henneke, *Langmuir* **2014**, *30*, 710.

[140] H. Fan, A. Striolo, *Phys. Rev. E: Stat. Nonlinear, Soft Matter Phys.* **2012**, *86*, 051610.

[141] X. Hua, M. A. Bevan, J. Frechette, *Langmuir* **2018**, *34*, 4830.

[142] X. Hua, M. A. Bevan, J. Frechette, *Langmuir* **2016**, *32*, 11341.

[143] S. Sundaram, J. K. Ferri, D. Vollhardt, K. J. Stebe, *Langmuir* **1998**, *14*, 1208.

[144] V. L. Kolev, K. D. Danov, P. A. Kralchevsky, G. Broze, A. Mehreteab, *Langmuir* **2002**, *18*, 9106.

[145] E. Vignati, R. Piazza, T. P. Lockhart, *Langmuir* **2003**, *19*, 6650.

[146] A. Drelich, F. Gomez, D. Clausse, I. Pezron, *Colloids Surf. A* **2010**, *365*, 171.

[147] P. F. Marina, C. Cheng, R. Sedev, A. Stocco, B. P. Binks, D. Wang, *Angew. Chem., Int. Ed.* **2018**, *57*, 9510.

[148] A. I. Abdel-Fattah, M. S. El-Genk, *J. Colloid Interface Sci.* **1998**, *202*, 417.

[149] A. I. Abdel-Fattah, M. S. El-Genk, *Adv. Colloid Interface Sci.* **1998**, *78*, 237.

[150] E. C. Mbamala, H. H. von Grünberg, *J. Phys.: Condens. Matter* **2002**, *14*, 4881.

[151] H. H. von Grünberg, E. C. Mbamala, *J. Phys.: Condens. Matter* **2001**, *13*, 4801.

[152] H. H. von Grünberg, *J. Phys.: Condens. Matter* **2000**, *12*, 6039.

[153] K. G. Marinova, R. G. Alargova, N. D. Denkov, O. D. Velev, D. N. Petsev, I. B. Ivanov, R. P. Borwankar, *Langmuir* **1996**, *12*, 2045.

[154] H.-J. Butt, *J. Colloid Interface Sci.* **1994**, *166*, 109.

[155] R. R. Dagastine, D. C. Prieve, L. R. White, *J. Colloid Interface Sci.* **2004**, *269*, 84.

[156] R. R. Dagastine, L. R. White, *J. Colloid Interface Sci.* **2002**, *247*, 310.

[157] D. Y. C. Chan, R. R. Dagastine, L. R. White, *J. Colloid Interface Sci.* **2001**, *236*, 141.

[158] J. H. J. Thijssen, A. B. Schofield, P. S. Clegg, *Soft Matter* **2011**, *7*, 7965.

[159] J. Forth, P. S. Clegg, *Langmuir* 6387, **2016**, *32*.

[160] D. J. French, P. Taylor, J. Fowler, P. S. Clegg, *J. Colloid Interface Sci.* **2015**, *441*, 30.

[161] O. J. Cayre, V. N. Paunov, *Langmuir* **2004**, *20*, 9594.

[162] A. Toor, B. A. Helms, T. P. Russell, *Nano Lett.* **2017**, *17*, 3119.

[163] X. Liu, S. Shi, Y. Li, J. Forth, D. Wang, T. P. Russell, *Angew. Chem.* **2017**, *129*, 12768.

[164] F. Jin, N. R. Gupta, K. J. Stebe, *Phys. Fluids* **2006**, *18*, 022103.

[165] F. Jin, J. K. Stebe, *Phys. Fluids* **2007**, *19*, 112103.

[166] V. Garbin, J. C. Crocker, K. J. Stebe, *Langmuir* **2012**, *28*, 1663.

[167] S. Baoukina, L. Monticelli, H. J. Risselada, S. J. Marrink, D. P. Tieleman, *Proc. Natl. Acad. Sci. USA* **2008**, *105*, 10803.

[168] A. Angelova, D. Vollhardt, R. Ionov, *J. Phys. Chem.* **1996**, *100*, 10710.

[169] S. Deutschländer, T. Horn, H. Löwen, G. Maret, P. Keim, *Phys. Rev. Lett.* **2013**, *111*, 098301.

[170] S. Deutschländer, A. M. Puertas, G. Maret, P. Keim, *Phys. Rev. Lett.* **2014**, *113*, 127801.

[171] S. Deutschla ̈nder, C. Boitard, G. Maret, P. Keim, *Phys. Rev. E* **2015**, *92*, 060302(R).

[172] C. P. Kelleher, R. E. Guerra, A. D. Hollingsworth, P. M. Chaikin, *Phys. Rev. E* **2017**, *95*, 022602.

[173] R. E. Guerra, C. P. Kelleher, A. D. Hollingsworth, P. M. Chaikin, *Nature* **2018**, *554*, 346.

[174] R. Aveyard, J. H. Clint, D. Nees, N. Quirke, *Langmuir* **2000**, *16*, 8820.

[175] V. Garbin, I. Jenkins, T. Sinno, J. C. Crocker, K. J. Stebe, *Phys. Rev. Lett.* **2015**, *114*, 108301.

[176] V. Pauchard, J. P. Rane, S. Banerjee, *Langmuir* **2014**, *30*, 12795.

[177] S. S. Datta, H. C. Shum, D. A. Weitz, *Langmuir* **2010**, *26*, 18612.

[178] Y. Lin, H. Skaff, A. Böker, A. D. Dinsmore, T. Emrick, T. P. Russell, *J. Am. Chem. Soc.* **2003**, *125*, 12690.

[179] J. T. Russell, Y. Lin, A. Böker, L. Su, P. Carl, H. Zettl, J. He, K. Sill, R. Tangirala, T. Emrick, K. Littrell, P. Thiyagarajan, D. Cookson, A. Fery, Q. Wang, T. P. Russell, *Angew. Chem., Int. Ed.* **2005**, *44*, 2420.

[180] L. Hobley, A. Ostrowski, F. V. Rao, K. M. Bromley, M. Porter, A. R. Prescott, C. E. Macphee, D. M. F. Van Aalten, N. R. Stanley-Wall, *Proc. Natl. Acad. Sci. USA* **2013**, *110*, 13600.

[181] R. J. Morris, M. Schor, R. M. C. Gillespie, A. S. Ferreira, L. Baldauf, C. Earl, A. Ostrowski, L. Hobley, K. M. Bromley, T. Sukhodub, S. Arnaouteli, N. R. Stanley-Wall, C. E. MacPhee, *Sci. Rep.* **2017**, *7*, 6730.

[182] B. C. Tripp, J. J. Magda, J. D. Andrade, *J. Colloid Interface Sci.* **1995**, *173*, 16.

[183] C. J. Beverung, C. J. Radke, H. W. U. Blanch, *Biophys. Chem.* **1999**, *81*, 59.

[184] K. M. Bromley, R. J. Morris, L. Hobley, G. Brandani, R. M. C. Gillespie, M. McCluskey, U. Zachariae, D. Marenduzzo, N. R. Stanley-Wall, C. E. MacPhee, *Proc. Natl. Acad. Sci. USA* **2015**, *112*, 5419.

[185] K. M. Bromley, C. E. MacPhee, *Interface Focus* **2017**, *7*, 20160124.

[186] L. M. C. Sagis, *Appl. Rheol.* **2010**, *20*, 24380.

[187] E. Hermans, J. Vermant, *Soft Matter* **2014**, *10*, 175.

[188] E. Hermans, M. Saad Bhamla, P. Kao, G. G. Fuller, J. Vermant, *Soft Matter* **2015**, *11*, 8048.

[189] M. Pepicelli, T. Verwijlen, T. A. Tervoort, J. Vermant, *Soft Matter* **2017**, *13*, 5977.

[190] P. J. Beltramo, M. Gupta, A. Alicke, I. Liascukiene, D. Z. Gunes, C. N. Baroud, J. Vermant, *Proc. Natl. Acad. Sci. USA* **2017**, *114*, 201705181.

[191] P. Erni, H. A. Jerri, K. Wong, A. Parker, *Soft Matter* **2012**, *8*, 6958.

[192] M. Maas, C. C. Ooi, G. G. Fuller, *Langmuir* **2010**, *26*, 17867.

[193] J. Forth, D. J. French, A. V. Gromov, S. King, S. Titmuss, K. M. Lord, M. J. Ridout, P. J. Wilde, P. S. Clegg, *Langmuir* **2015**, *31*, 9312.

[194] H. Xu, S. Melle, K. Golemanov, G. Fuller, *Langmuir* **2005**, *21*, 10016.

[195] M. Grauzinyte, J. Forth, K. A. Rumble, P. S. Clegg, M. Graužinyte, J. Forth, K. A. Rumble, P. S. Clegg, *Angew. Chem., Int. Ed.* **2015**, *54*, 1456.

[196] Q. Ma, Y. Song, G. Baier, C. Holtze, H. C. Shum, *J. Mater. Chem. B* **2016**, *4*, 1213.

[197] C. Huang, J. Forth, W. Wang, K. Hong, G. S. Smith, B. A. Helms, T. P. Russell, *Nat. Nanotechnol.* **2017**, *12*, 1060.

[198] S. Shi, X. Liu, Y. Li, X. Wu, D. Wang, J. Forth, T. P. Russell, *Adv. Mater.* **2018**, *30*, 1705800.

[199] J. Forth, X. Liu, J. Hasnain, A. Toor, K. Miszta, S. Shi, P. L. Geissler, T. Emrick, B. A. Helms, T. P. Russell, *Adv. Mater.* **2018**, *30*, 1707603.

[200] S. Bochner De Araujo, M. Merola, D. Vlassopoulos, G. G. Fuller, *Langmuir* **2017**, *33*, 10501.

[201] Z. A. Zell, A. Nowbahar, V. Mansard, L. G. Leal, S. S. Deshmukh, J. M. Mecca, C. J. Tucker, T. M. Squires, *Proc. Natl. Acad. Sci. USA* **2014**, *111*, 3677.

[202] R. Van Hooghten, V. E. Blair, A. Vananroye, A. B. Schofield, J. Vermant, J. H. J. Thijssen, *Langmuir* **2017**, *33*, 4107.

[203] J. Dupré De Baubigny, C. Trégouët, T. Salez, N. Pantoustier, P. Perrin, M. Reyssat, C. Monteux, *Sci. Rep.* **2017**, *7*, 1265.

[204] S. le Tirilly, C. Tregouet, M. Reyssat, S. Bone, C. Geffroy, G. G. Fuller, N. Pantoustier, P. Perrin, C. Monteux, *Langmuir* **2016**, *32*, 6089.

[205] S. Vandebril, A. Franck, G. G. Fuller, P. Moldenaers, J. Vermant, *Rheol. Acta* **2010**, *49*, 131.

[206] G. Kaufman, R. Boltyanskiy, S. Nejati, A. R. Thiam, M. Loewenberg, E. R. Dufresne, C. O. Osuji, *Lab Chip* **2014**, *14*, 3494.

[207] T. Verwijlen, L. Imperiali, J. Vermant, *Adv. Colloid Interface Sci.* **2014**, *206*, 428.

[208] D. Carvajal, E. J. Laprade, K. J. Henderson, K. R. Shull, *Soft Matter* **2011**, *7*, 10508.

[209] R. Aveyard, J. H. Clint, D. Nees, N. Quirke, *Langmuir* **2000**, *16*, 8820.

[210] E. S. Basheva, P. A. Kralchevsky, N. C. Christov, K. D. Danov, S. D. Stoyanov, T. B. J. Blijdenstein, H. J. Kim, E. G. Pelan, A. Lips, *Langmuir* **2011**, *27*, 2382.

[211] N. A. Alexandrov, K. G. Marinova, T. D. Gurkov, K. D. Danov, P. A. Kralchevsky, S. D. Stoyanov, T. B. J. Blijdenstein, L. N. Arnaudov, E. G. Pelan, A. Lips, *J. Colloid Interface Sci.* **2012**, *376*, 296.

[212] J. Zhang, R. J. Coulston, S. T. Jones, J. Geng, O. A. Scherman, C. Abell, *Science* **2012**, *335*, 690.

[213] A. R. Salmon, R. M. Parker, A. S. Groombridge, A. Maestro, R. J. Coulston, J. Hegemann, J. Kierfeld, O. A. Scherman, C. Abell, *Langmuir* **2016**, *32*, 10987.

[214] M. Cui, T. Emrick, T. P. Russell, *Science* **2013**, *342*, 460.

[215] S. Q. Choi, S. Steltenkamp, J. A. Zasadzinski, T. M. Squires, *Nat. Commun.* **2011**, *2*, 312.

[216] C. F. Brooks, G. G. Fuller, C. W. Frank, C. R. Robertson, *Langmuir* **1999**, *15*, 2450.

[217] S. Reynaert, C. F. Brooks, P. Moldenaers, J. Vermant, G. G. Fuller, *J. Rheol.* **2008**, *52*, 261.

[218] I. Buttinoni, Z. A. Zell, T. M. Squires, L. Isa, *Soft Matter* **2015**, *11*, 8313.

[219] I. Williams, T. M. Squires, *J. R. Soc., Interface* **2018**, *15*, 20170895.

[220] C.-C. Chang, A. Nowbahar, V. Mansard, I. Williams, J. Mecca, A. K. Schmitt, T. H. Kalantar, T. Kuo, T. M. Squires, *Langmuir* **2018**, *34*, 5409.

[221] F. Ravera, E. Santini, G. Loglio, M. Ferrari, L. Liggieri, *J. Phys. Chem. B* **2006**, *110*, 19543.

[222] F. Ravera, M. Ferrari, L. Liggieri, G. Loglio, E. Santini, A. Zanobini, *Colloids Surf. A* **2008**, *323*, 99.

[223] A. Maestro, E. Guzmán, E. Santini, F. Ravera, L. Liggieri, F. Ortega, R. G. Rubio, *Soft Matter* **2012**, *8*, 837.

[224] A. Maestro, E. Rio, W. Drenckhan, D. Langevin, A. Salonen, S. Anniina, *Soft Matter* **2014**, *10*, 6975.

[225] A. Maestro, O. S. Deshmukh, F. Mugele, D. Langevin, *Langmuir* **2015**, *31*, 6289.

[226] A. Maestro, A. Zaccone, *Nanoscale* **2017**, *9*, 18343.

[227] D. Zang, D. Langevin, B. P. Binks, B. Wei, *Phys. Rev. E* **2010**, *81*, 011604.

[228] D. Y. Zang, E. Rio, D. Langevin, B. Wei, B. P. Binks, *Eur. Phys. J. E* **2010**, *31*, 125.

[229] A. Toor, J. Forth, S. Bochner de Araujo, M. C. Merola, Y. Jiang, Y. Chai, P. D. Ashby, G. G. Fuller, T. P. Russell, unpublished, https://doi.org/10.1093/icb/icy006/4989945.

[230] S. Reynaert, P. Moldenaers, J. Vermant, *Phys. Chem. Chem. Phys.* **2007**, *9*, 6463.

[231] S. Roy, M. S. Tirumkudulu, *J. Rheol.* **2016**, *60*, 559.

[232] S. Roy, M. S. Tirumkudulu, *J. Rheol.* **2016**, *60*, 575.

[233] P. Sollich, F. Lequeux, P. Hébraud, M. E. Cates, *Phys. Rev. Lett.* **1997**, *78*, 2020.

[234] H. Zhang, K. Yu, O. J. Cayre, D. Harbottle, *Langmuir* **2016**, *32*, 13472.

[235] P. Cicuta, E. J. Stancik, G. G. Fuller, *Phys. Rev. Lett.* **2003**, *90*, 236101.

[236] I. Jasiuk, J. Chen, M. F. Thorpe, *Appl. Mech. Rev.* **1994**, *47*, S18.

[237] S. T. Milner, J.-F. Joanny, P. Pincus, *Europhys. Lett.* **1989**, *9*, 495.

[238] A. Lobkovsky, S. Gentges, H. Li, D. Morse, T. A. Witten, *Science* **1995**, *270*, 1482.

[239] A. J. Wood, *Physica A* **2002**, *313*, 83.

[240] H. Diamant, T. A. Witten, *Phys. Rev. Lett.* **2011**, *107*, 164302.

[241] V. Démery, B. Davidovitch, C. D. Santangelo, *Phys. Rev. E: Stat. Nonlinear, Soft Matter Phys.* **2014**, *90*, 042401.

[242] B. Davidovitch, R. D. Schroll, D. Vella, M. Adda-Bedia, E. A. Cerda, *Proc. Natl. Acad. Sci. USA* **2011**, *108*, 18227.

[243] D. Vella, J. Huang, N. Menon, T. P. Russell, B. Davidovitch, *Phys. Rev. Lett.* **2015**, *114*, 014301.

[244] K. Burton, J. H. Park, D. L. Taylor, *Mol. Biol. Cell* **1999**, *10*, 3745.

[245] N. J. Sniadecki, R. A. Desai, S. A. Ruiz, C. S. Chen, *Ann. Biomed. Eng.* **2006**, *34*, 59.

[246] L. Pocivavsek, R. Dellsy, A. Kern, S. Johnson, B. Lin, K. Y. C. Lee, E. Cerda, *Science* **2008**, *320*, 912.

[247] J. Huang, B. Davidovitch, C. D. Santangelo, T. P. Russell, N. Menon, *Phys. Rev. Lett.* **2010**, *105*, 2.

[248] M. Trejo, C. Douarche, V. Bailleux, C. Poulard, S. Mariot, C. Regeard, E. Raspaud, *Proc. Natl. Acad. Sci. USA* **2013**, *110*, 2011.

[249] J. Huang, M. Juszkiewicz, W. H. de Jeu, E. Cerda, T. Emrick, N. Menon, T. P. Russell, *Science* **2007**, *317*, 650.

[250] D. Vella, P. Aussillous, L. Mahadevan, *Europhys. Lett.* **2004**, *68*, 212.

[251] P. A. Kralchevsky, I. B. Ivanov, K. P. Ananthapadmanabhan, A. Lips, *Langmuir* **2005**, *21*, 50.

[252] T. S. Horozov, B. P. Binks, R. Aveyard, J. H. Clint, *Colloids Surf. A* **2006**, *282–283*, 377.

[253] B. D. Leahy, L. Pocivavsek, M. Meron, K. L. Lam, D. Salas, P. J. Viccaro, K. Y. C. Lee, B. Lin, *Phys. Rev. Lett.* **2010**, *105*, 058301.

[254] A. Tordesillas, D. Carey, A. B. Croll, J. Shi, B. Gurmessa, *Granular Matter* **2014**, *16*, 249.

[255] L. Pocivavsek, S. L. Frey, K. Krishan, K. Gavrilov, P. Ruchala, A. J. Waring, F. J. Walther, M. Dennin, T. A. Witten, K. Y. C. Lee, *Soft Matter* **2008**, *4*, 2019.

[256] E. Aumaitre, D. Vella, P. Cicuta, *Soft Matter* **2011**, *7*, 2530.

[257] K. E. Mueggenburg, X.-M. Lin, R. H. Goldsmith, H. M. Jaeger, *Nat. Mater.* **2007**, *6*, 656.

[258] S. S. You, R. Rashkov, P. Kanjanaboos, I. Calderon, M. Meron, H. M. Jaeger, B. Lin, *Langmuir* **2013**, *29*, 11751.

[259] S. Razavi, K. D. Cao, B. Lin, K. Y. C. Lee, R. S. Tu, I. Kretzschmar, *Langmuir* **2015**, *31*, 7764.

[260] S. D. Griesemer, S. S. You, P. Kanjanaboos, M. Calabro, H. M. Jaeger, S. A. Rice, B. Lin, *Soft Matter* **2017**, *13*, 3125.

[261] M. Zanini, C. Marschelke, S. E. Anachkov, E. Marini, A. Synytska, L. Isa, *Nat. Commun.* **2017**, *8*, 15701.

[262] M. Zanini, I. Lesov, E. Marini, C. P. Hsu, C. Marschelke, A. Synytska, S. E. Anachkov, L. Isa, *Langmuir* **2018**, *34*, 4861.

[263] H. Yang, T. Zhou, W. Zhang, *Angew. Chem., Int. Ed.* **2013**, *52*, 7455.

[264] H. Yang, L. Fu, L. Wei, J. Liang, B. P. Binks, *J. Am. Chem. Soc.* **2015**, *137*, 1362.

[265] M. Zhang, L. Wei, H. Chen, Z. Du, B. P. Binks, H. Yang, *J. Am. Chem. Soc.* **2016**, *138*, 10173.

[266] J. Huang, H. Yang, *Chem. Commun.* **2015**, *51*, 7333.

[267] H. Chen, H. Zou, Y. Hao, H. Yang, *ChemSusChem* **2017**, *10*, 1989.

[268] R. Hatti-Kaul, *Mol. Biotechnol.* **2001**, *19*, 269.

[269] C. D. Keating, *Acc. Chem. Res.* **2012**, *45*, 2114.

[270] J. A. Asenjo, B. A. Andrews, *J. Chromatogr. A* **2012**, *1238*, 1.

[271] S. Hardt, T. Hahn, *Lab Chip* **2012**, *12*, 434.

[272] J. Esquena, *Curr. Opin. Colloid Interface Sci.* **2016**, *25*, 109.

[273] F. Ruiz-Ruiz, J. Benavides, O. Aguilar, M. Rito-Palomares, *J. Chromatogr. A* **2012**, *1244*, 1.

[274] H. Tavana, A. Jovic, B. Mosadegh, Q. Y. Lee, X. Liu, K. E. Luker, G. D. Luker, S. J. Weiss, S. Takayama, *Nat. Mater.* **2009**, *8*, 736.

[275] J. P. Frampton, Z. Fan, A. Simon, D. Chen, C. X. Deng, S. Takayama, *Adv. Funct. Mater.* **2013**, *23*, 3420.

[276] M. W. Beijerinck, *Zentralbl. Bakteriol. Parasitenkd Infektionskrankh.* **1896**, *2*, 679.

[277] P. Å. Albertsson, *Nature* **1958**, *182*, 918.

[278] H. Tavana, K. Kaylan, T. Bersano-Begey, K. E. Luker, G. D. Luker, S. Takayama, *Adv. Funct. Mater.* **2011**, *21*, 2920.

[279] J. P. Frampton, B. M. Leung, E. L. Bingham, S. C. Lesher-Perez, J. D. Wang, H. T. Sarhan, M. E. H. El-Sayed, S. E. Feinberg, S. Takayama, *Adv. Funct. Mater.* **2015**, *25*, 1694.

[280] L. Eiden, C. Yamanishi, S. Takayama, J. F. Dishinger, *Anal. Chem.* **2016**, *88*, 11328.

[281] S. Kim, S. C. Lesher-Perez, B. C. Kim, C. Yamanishi, J. M. Labuz, B. M. Leung, S. Takayama, *Biofabrication* **2016**, *8*, 015021.

[282] Q. Ma, Y. Song, J. W. Kim, H. S. Choi, H. C. Shum, *ACS Macro Lett.* **2016**, *5*, 666.

[283] S. D. Hann, K. J. Stebe, D. Lee, *ACS Appl. Mater. Interfaces* **2017**, *9*, 25023.

[284] J. P. Douliez, N. Martin, T. Beneyton, J. C. Eloi, J. P. Chapel, L. Navailles, J. C. Baret, S. Mann, L. Bøven, L. Béven, *Angew. Chem., Int. Ed.* **2018**, *57*, 7780.

[285] H. Cheung Shum, J. Varnell, D. A. Weitz, *Biomicrofluidics* **2012**, *6*, 012808.

[286] A. Sauret, H. C. Shum, *Appl. Phys. Lett.* **2012**, *100*, 154106.

[287] Y. Song, A. Sauret, H. C. Shum, *Biomicrofluidics* **2013**, *7*, 061301.

[288] Y. Song, H. C. Shum, *Langmuir* **2012**, *28*, 12054.

[289] Y. Song, T. C. T. Michaels, Q. Ma, Z. Liu, H. Yuan, S. Takayama, T. P. J. Knowles, H. C. Shum, *Nat. Commun.* **2018**, *9*, 2110.

[290] Y. Song, U. Shimanovich, T. C. T. Michaels, Q. Ma, J. Li, T. P. J. Knowles, H. C. Shum, *Nat. Commun.* **2016**, *7*, 12934.

[291] J. R. Vieregg, M. Lueckheide, A. B. Marciel, L. Leon, A. J. Bologna, J. R. Rivera, M. V. Tirrell, *J. Am. Chem. Soc.* **2018**, *140*, 1632.

[292] L. Zhang, L. H. Cai, P. S. Lienemann, T. Rossow, I. Polenz, Q. Vallmajo-Martin, M. Ehrbar, H. Na, D. J. Mooney, D. A. Weitz, *Angew. Chem., Int. Ed.* **2016**, *55*, 13470.

[293] S. D. Hann, T. H. R. Niepa, K. J. Stebe, D. Lee, *ACS Appl. Mater. Interfaces* **2016**, *8*, 25603.

[294] M. Inam, J. R. Jones, M. M. Pérez-Madrigal, M. C. Arno, A. P. Dove, R. K. O'Reilly, *ACS Cent. Sci.* **2018**, *4*, 63.

[295] M. Klapper, S. Nenov, R. Haschick, K. Müller, K. Müllen, *Acc. Chem. Res.* **2008**, *41*, 1190.

[296] X. Lu, J. S. Katz, A. K. Schmitt, J. S. Moore, *J. Am. Chem. Soc.* **2018**, *140*, 3619.

[297] B. P. Finkle, H. D. Draper, J. H. Hildebrand, *J. Am. Chem. Soc.* **1923**, *45*, 2780.

[298] B. P. Binks, A. T. Tyowua, *Soft Matter* **2016**, *12*, 876.

[299] P. A. Kralchevsky, J. C. Eriksson, S. Ljunggren, *Adv. Colloid Interface Sci.* **1994**, *48*, 19.

[300] M. Zhang, R. Ettelaie, T. Yan, S. Zhang, F. Cheng, B. P. Binks, H. Yang, *J. Am. Chem. Soc.* **2017**, *139*, 17387.

[301] B. Rodier, A. De Leon, C. Hemmingsen, E. Pentzer, *ACS Macro Lett.* **2017**, *6*, 1201.

[302] A. M. Tawfeek, A. K. F. Dyab, H. A. Al-Lohedan, *J. Dispersion Sci. Technol.* **2014**, *35*, 265.

[303] B. J. Rodier, A. De Leon, C. Hemmingsen, E. Pentzer, *Polym. Chem.* **2018**, *9*, 1547.

[304] D. Cai, F. H. Richter, J. H. J. Thijssen, P. G. Bruce, P. S. Clegg, *Mater. Horiz.* **2018**, *5*, 499.

[305] Q. Luo, P. Wei, Q. Huang, B. Gurkan, E. B. Pentzer, *ACS Appl. Mater. Interfaces* **2018**, *10*, 16707.

[306] R. Bian, R. Lin, G. Wang, G. Lu, W. Zhi, S. Xiang, T. Wang, P. S. Clegg, D. Cai, W. Huang, *Nanoscale* **2018**, *10*, 3621.

[307] A. R. Mackie, A. P. Gunning, P. J. Wilde, V. J. Morris, *J. Colloid Interface Sci.* **1999**, *210*, 157.

[308] A. Mackie, A. Gunning, P. Wilde, V. Morris, *Langmuir* **2000**, *16*, 2242.

[309] Q. Lan, C. Liu, F. Yang, S. Liu, J. Xu, D. Sun, *J. Colloid Interface Sci.* **2007**, *310*, 260.

[310] P. Dommersnes, Z. Rozynek, A. Mikkelsen, R. Castberg, K. Kjerstad, K. Hersvik, J. Otto Fossum, *Nat. Commun.* **2013**, *4*, 2066.

[311] S. Melle, M. Lask, G. G. Fuller, *Langmuir* **2005**, *21*, 2158.

[312] Z. Sun, T. Feng, T. P. Russell, *Langmuir* **2013**, *29*, 13407.

[313] T. Feng, D. A. Hoagland, T. P. Russell, *Langmuir* **2014**, *30*, 1072.

[314] C. Huang, Z. Sun, M. Cui, F. Liu, B. A. Helms, T. P. Russell, *Adv. Mater.* **2016**, *28*, 6612.

[315] E. L. Rosen, R. Buonsanti, A. Llordes, A. M. Sawvel, D. J. Milliron, B. A. Helms, *Angew. Chem., Int. Ed.* **2012**, *51*, 684.

[316] P.-P. Fang, S. Chen, H. Deng, M. D. Scanlon, F. Gumy, H. J. Lee, D. Momotenko, V. Amstuts, F. Cortés-Salazar, C. M. Pereira, Z. Yang, H. H. Girault, D. Scanlon, P.-P. Fang, S. Chen, H. Deng, C. M. Pereira, Z. Yang, *ACS Nano* **2013**, *7*, 9241.

[317] Y. Montelongo, D. Sikdar, Y. Ma, A. J. S. Mcintosh, L. Velleman, A. R. Kucernak, J. B. Edel, A. A. Kornyshev, *Nat. Mater.* **2017**, *16*, 1127.

[318] M. E. Flatté, A. A. Kornyshev, M. Urbakh, *J. Phys.: Condens. Matter* **2008**, *20*, 073102.

[319] A. B. Subramaniam, M. Abkarian, L. Mahadevan, H. A. Stone,
Nature **2005**, *438*, 930.

[320] A. S. Utada, A. Fernandez-Nieves, H. A. Stone, D. A. Weitz,
Phys. Rev. Lett. **2007**, *99*, 094502.

[321] J. Eggers, E. Villermaux, *Rep. Prog. Phys.* **2008**, *71*, 036601.

[322] S. Tomotika, *Proc. R. Soc. London, Ser. A* **1935**, *150*, 322.

[323] T. R. Powers, D. Zhang, R. E. Goldstein, H. A. Stone, *Phys. Fluids*
1998, *10*, 1052.

[324] H. M. Princen, *Langmuir* **1986**, *2*, 519.

[325] T. G. Mason, J. Bibette, D. A. Weitz, *Phys. Rev. Lett.*
1995, *75*, 2051.

[326] Y. Zheng, Z. Yu, R. M. Parker, Y. Wu, C. Abell, O. A. Scherman, *Nat. Commun.* **2014**, *5*, 5772.

[327] Y. Zhang, A. McMullen, L. L. Pontani, X. He, R. Sha, N. C. Seeman,
J. Brujic, P. M. Chaikin, *Nat. Commun.* **2017**, *8*, 21.

[328] Z. Yang, J. Wei, Y. I. Sobolev, B. A. Grzybowski, *Nature*
2018, *553*, 313.

[329] G. Villar, A. D. Graham, H. Bayley, *Science* **2013**,
340, 48.

[330] G. Villar, A. J. Heron, H. Bayley, *Nat. Nanotechnol.*
2011, *6*, 803.

[331] M. A. Holden, D. Needham, H. Bayley, *J. Am. Chem. Soc.* **2007**,
129, 8650.

[332] Y. Elani, R. V. Law, O. Ces, *Nat. Commun.* **2014**, *5*, 5305.

[333] M. J. Booth, V. R. Schild, S. J. Box, H. Bayley, *Sci. Rep.* **2017**, *7*, 9315.

[334] Y. Elani, T. Trantidou, D. Wylie, L. Dekker, K. Polizzi, R. V. Law, O. Ces, *Sci. Rep.* **2018**, *8*, 4564.

[335] M. F. Haase, N. Sharifi-Mood, D. Lee, K. J. Stebe, *ACS Nano* **2016**,
10, 6338.

[336] M. F. Haase, K. J. Stebe, D. Lee, *Adv. Mater.* **2015**,
27, 7065.

[337] M. F. Haase, H. Jeon, N. Hough, J. H. Kim, K. J. Stebe, D. Lee,
Nat. Commun. **2017**, *8*, 1234.

[338] L. D. Zarzar, V. Sresht, E. M. Sletten, J. A. Kalow, D. Blankschtein,
T. M. Swager, *Nature* **2015**, *518*, 520.

[339] S. Nagelberg, L. D. Zarzar, N. Nicolas, K. Subramanian, J. A. Kalow,
V. Sresht, D. Blankschtein, G. Barbastathis, M. Kreysing,
T. M. Swager, M. Kolle, *Nat. Commun.* **2017**, *8*, 14673.

[340] G. J. T. T. Cooper, P. J. Kitson, R. Winter, M. Zagnoni, D. L. Long,
L. Cronin, *Angew. Chem., Int. Ed.* **2011**, *50*, 10373.

[341] L. Rodríguez-Arco, M. Li, S. Mann, *Nat. Mater.*
2017, *16*, 857.

[342] L. L. Pontani, J. Van Der Gucht, G. Salbreux, J. Heuvingh,
J. F. Joanny, C. Sykes, *Biophys. J.* **2009**, *96*, 192.

[343] F. C. Keber, E. Loiseau, T. Sanchez, S. J. DeCamp, L. Giomi,
M. J. Bowick, M. C. Marchetti, Z. Dogic, A. R. Bausch, *Science*
2014, *345*, 1135.

[344] T. Sanchez, D. T. N. Chen, S. J. Decamp, M. Heymann, Z. Dogic,
Nature **2012**, *491*, 431.

[345] K.-T. Wu, J. B. Hishamunda, D. T. N. Chen, S. J. DeCamp, Y.-W. Chang, A. Fernández-Nieves, S. Fraden, Z. Dogic, *Science* **2017**, *355*, eaal1979.

[346] G. H. Koenderink, Z. Dogic, F. Nakamura, P. M. Bendix,
F. C. MacKintosh, J. H. Hartwig, T. P. Stossel, D. A. Weitz, *Proc. Natl. Acad. Sci. USA* **2009**, *106*, 15192.

[347] S. Zhou, A. Sokolov, O. D. Lavrentovich, I. S. Aranson, *Proc. Natl. Acad. Sci. USA* **2014**, *111*, 1265.

[348] E. Loiseau, J. A. M. Schneider, F. C. Keber, C. Pelzl, G. Massiera, G. Salbreux, A. R. Bausch, *Sci. Adv.* **2016**, *2*, e1500465.

[349] Y. Elani, R. V. Law, O. Ces, *Phys. Chem. Chem. Phys.* **2015**, *17*, 15534.

[350] Y. Elani, S. Purushothaman, P. J. Booth, J. M. Seddon, N. J. Brooks,
R. V. Law, O. Ces, *Chem. Commun.* **2015**, *51*, 6976.

[351] Y. Elani, A. Gee, R. V. Law, O. Ces, *Chem. Sci.* **2013**,
4, 3332.

[352] C. L. Bergstrom, P. A. Beales, Y. Lv, T. K. Vanderlick, J. T. Groves,
Proc. Natl. Acad. Sci. USA **2013**, *110*, 6269.

[353] P. A. Beales, T. Kyle Vanderlick, *J. Phys. Chem. A*
2007, *111*, 12372.

[354] C. LoPresti, H. Lomas, M. Massignani, T. Smart, G. Battaglia,
J. Mater. Chem. **2009**, *19*, 3576.

[355] A. Joseph, C. Contini, D. Cecchin, S. Nyberg, L. Ruiz-Perez,
J. Gaitzsch, G. Fullstone, X. Tian, J. Azizi, J. Preston, G. Volpe,
G. Battaglia, *Sci. Adv.* **2017**, *3*, e1700362.

[356] L. Messager, J. R. Burns, J. Kim, D. Cecchin, J. Hindley,
A. L. B. Pyne, J. Gaitzsch, G. Battaglia, S. Howorka,
Angew. Chem., Int. Ed. **2016**, *55*, 11106.

[357] L. Wang, L. Chierico, D. Little, N. Patikarnmonthon, Z. Yang,
M. Azzouz, J. Madsen, S. P. Armes, G. Battaglia,
Angew. Chem., Int. Ed. **2012**, *51*, 11122.

[358] P. Dahiya, A. Debenedictis, T. J. Atherton, M. Caggioni,
S. W. Prescott, R. W. Hartel, P. T. Spicer, W. Hartel, P. T. Spicer,
Soft Matter **2017**, *13*, 2686.

[359] M. Caggioni, A. V. Bayles, J. Lenis, E. M. Furst, P. T. Spicer,
Soft Matter **2014**, *10*, 7647.

[360] M. Caggioni, J. Lenis, A. V. Bayles, E. M. Furst, P. T. Spicer,
Langmuir **2015**, *31*, 8558.

[361] T. A. Prileszky, E. M. Furst, *Chem. Mater.* **2016**, *28*, 3734.